Performance evaluation and resource allocation in millimeter waves device-to-device networks with beamforming

Yibo Quan

INSTITUT POLYTECHNIQUE DE PARIS

NNT : 2023IPPAT024

Thèse de doctorat

Performance evaluation and resource allocation in millimeter waves device-to-device networks with beamforming

Thèse de doctorat de l'Institut Polytechnique de Paris
préparée à Télécom Paris

École doctorale n°626 Institut Polytechnique de Paris (ED IP Paris)
Spécialité de doctorat : Informatique

Thèse présentée et soutenue à Palaiseau, le 6 Juillet 2023, par

YIBO QUAN

Composition du Jury :

Jean-Marie Gorce Professeur, INSA Lyon	Président / Examinateur
Anthony Busson Professeur, Université Lyon 1	Rapporteur
Laurent Clavier Professeur, IMT Nord Europe	Rapporteur
Ghaya Rekaya Ben Othman Professeur, Télécom Paris	Examinateur
Marceau Coupechoux Professeur, Télécom Paris	Directeur de thèse
Jean-Marc Kélif Ingénieur de Recherche, Orange Labs	Co-directeur de thèse

Contents

List of Figures

Acronyms

5G Fifth Generation. 1

AoA Angle of Arrival. 36, 51

AoD Angle of Departure. 36, 51

CCDF Complementary Cumulative Distribution Function. 15, 71

CDF Cumulative Distribution Function. 17, 64

CTMC Continuous-Time Markovain Chain. 34

D2D Device-to-Device. 1, 31

eMBB Enhanced Mobile Broadband. 1

FSPL Free Space Path Loss. 74

HPBW Half Power Beamwidth. 50

i.i.d. Independent and identically distributed. 12

IoT Internet of Things. 1

LOS Line-of-Sight. 2

mMTC Massive Machine-Type Communications. 1

mmWave Millimeter Wave. 2

NR New Radio. 1

OFDM Orthogonal Frequency-Division Multiplexing. 74

p.p. Point Process. 8

PDF Probability Density Function. 17, 37, 64

PGFL Probability Generating Funcational. 10, 12

PMF Probability Mass Function. 68, 98

PPP Poisson Point Process. 11

PSD Power Spectral Density. 64

QoS Quality-of-Service. 1

RCL Rate Conservative Law. 89

SINR Signal to Interference plus Noise Ratio. 61

ULA Uniform Linear Array. 2, 31

URLLC Ultra-Reliable Low Latency. 1

V2X Vehicles to Everything. 1

WLAN Wireless Local Area Network. 5

Acknowledgments

I would like to express my deepest gratitude to my advisors, Prof. Marceau Coupechoux and Dr. Jean-Marc Kélif, for their invaluable guidance throughout the entire journey of my highly cherished three years.

Without their constant support and encouragement, I would not have embarked on this adventure filled with learning and growth. Their expertise, patience, and dedication have been instrumental in shaping my academic career.

My sincere appreciation extends to the members of my thesis committee, Prof. Ghaya Rekaya, Prof. Jean-Marie Gorce, Prof. Laurent Clavier, and Prof. Anthony Busson, for their insightful feedback and valuable suggestions, which have greatly contributed to the refinement of my work.

I would also like to express my sincere gratitude to my colleagues at Orange and Telecom Paris, with whom I have shared knowledge and countless moments of laughter. Their camaraderie and collaboration have made the research environment a vibrant and enriching one.

Lastly, I extend my heartfelt thanks to my family and friends for their unwavering love, which serves as an eternal source of motivation in challenging myself and striving my goals.

Résumé en fançais

La communication de terminal à terminal (D2D) est une technologie clé pour les futurs réseaux sans fil. Elle permet aux appareils de communiquer directement, sans avoir besoin d'une infrastructure cellulaire, ce qui présente de nombreux avantages, tels que l'extension de la couverture, l'amélioration de la capacité et le délestage du réseau. Cela fait de D2D une technologie prometteuse pour les communications ultra-fiables à faible latence (URLLC). Cependant, elle doit surmonter les défis de l'interférence co-canal et de la bande passante limitée.

Pour résoudre ces problèmes, l'utilisation des ondes millimétriques (mmWave) s'avère efficace en raison de leur large bande passante. Néanmoins, les fréquences mmWave présentent une atténuation élevée, ce qui requiert l'utilisation de multiples antennes et la mise en place de la formation de faisceaux pour améliorer la force et la qualité du signal. Toutefois, lors de ce processus de formation de faisceaux, des erreurs de désalignement peuvent se produire, entraînant une dégradation des performances de transmission des données.

Pour relever ces défis, cette thèse porte sur l'analyse théorique des performances de la communication mmWave D2D. Les méthodes proposées permettent une évaluation rapide des performances des futurs réseaux avec communication mmWave D2D et d'identifier les paramètres critiques qui ont un impact significatif sur les performances, tels que la couverture, la latence et la fiabilité dans le contexte de l'URLLC. Les sections suivantes traitent du contenu de chaque chapitre.

Chapitre 1: Introduction

Ce chapitre présente les motivations de la thèse et le contexte des études sur les réseaux terminal-à-terminal en ondes millimétriques avec formation de faisceaux. Ensuite, nous exposons la structure du manuscrit ainsi que les contributions de la thèse. Le chapitre se conclut par la liste des publications liées à ces travaux.

La géométrie stochastique est largement utilisée pour évaluer la couverture, le débit et l'efficacité énergétique des réseaux sans fil en raison de sa flexibilité mathématique. Les études classiques utilisant cette méthode se concentrent principalement sur le calcul de la probabilité de couverture moyenne spatiale pour un utilisateur type. Toutefois, dans le contexte de l'URLLC, il est essentiel de prendre en compte la distribution des mesures de performance traditionnelles. Pour caractériser pleinement la distribution spatiale des performances de communication, il est possible de tirer parti de la meta-distribution.

La dynamique temporelle du réseau est un autre aspect crucial à étudier. Les approches traditionnelles pour étudier la dynamique des réseaux s'appuient sur la théorie des files d'attente, mais ces études, principalement inspirées par les réseaux câblés, modélisent le réseau avec de multiples serveurs dont les emplacements relatifs n'ont aucune influence sur leur comportement. Pour remédier à cette limitation, Sankararaman et Baccelli ont proposé en 2017 un modèle spatial de réseau sans fil de naissances et morts, qui modélise le réseau stochastique en fonction du processus ponctuel et prend en compte l'interaction entre les liens dans le temps en raison des variations du trafic.

Nous utilisons la géométrie stochastique et la théorie des files d'attente pour évaluer les variations spatiales et temporelles des performances de deux points de vue différents : les propriétés moyennes instantanées du réseau aléatoire et les propriétés d'ergodicité globale d'un réseau dynamique avec des demandes de service aléatoires.

Chapitr 2: Fondements mathématiques et réseaux

Ce chapitre donne un aperçu des outils mathématiques et des technologies de communication sans fil explorés dans cette thèse. Le chapitre commence par une introduction à la géométrie stochastique, abordant des sujets tels que le processus ponctuel et la théorie de Palm. Nous examinons ensuite plusieurs applications de la géométrie stochastique pour la modélisation des réseaux sans fil, notamment la caractérisation de la couverture et l'analyse de la méta-distribution. De plus, nous abordons le processus de naissance-mort spatial en tant que modèle de réseau dynamique. Dans une deuxième partie du chapitre consacrée aux fondements sur les réseaux, nous introduisons le cadre des réseaux D2D, ainsi que les technologies des ondes millimétriques et du beamforming. Un modèle analogique de formation de faisceau fondé sur un réseau linéaire d'antennes (ULA) est présenté dans cette par-

tie. Le diagramme de puissance de ce modèle de formation de faisceau est montré en fonction de l'angle de rayonnement et du nombre d'antennes.

Chapitre 3: Réseau D2D spatio-temporel sans fil avec formation de faisceaux

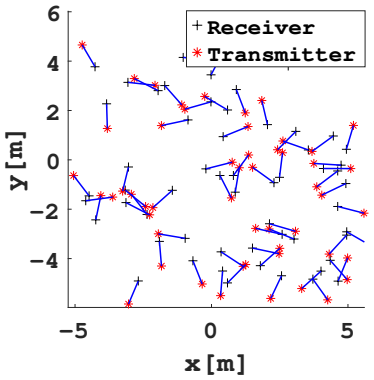

Figure 1: Réseau de Poisson bipolaire.

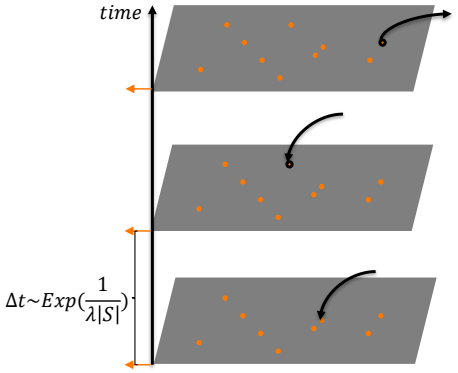

Figure 2: Le processus de naissance-mort spatial.

Dans ce chapitre, nous étudions l'impact de la formation de faisceaux sur un réseau de communication D2D dynamique, où les émetteurs et les récepteurs adoptent la formation de faisceaux à l'aide de l'ULA. Le réseau est dynamique car il y a des arrivées aléatoires de nouveaux dispositifs D2D. Les instants d'arrivée des paires émetteur-récepteur sont modélisés comme un processus de Poisson stationnaire. Les positions auxquelles les paires émetteur-récepteur arrivent suivent un processus de Poisson illustré par la Figure 1, qui est un réseau de Poisson bipolaire. En outre, les utilisateurs qui terminent leurs communications quittent immédiatement le réseau. De cette manière, un modèle spatio-temporel continu pour le réseau sans fil est établi, voir la Figure 2. Sankararaman et Baccelli analysent la condition de stabilité spatiale d'un réseau sans fil à une seule antenne avec naissances et morts en utilisant les outils des calculs de Palm et du principe de conversation des flux de Miyazawa. Un taux d'arrivée critique, λ_c, est introduit dans leurs travaux pour ce type de réseau sans tenir compte de la formation de faisceaux. Nous étendons leurs résultats en introduisant des réseaux d'antennes directionnelles pour les utilisateurs D2D. Une expression analytique du taux d'arrivée critique λ_c^{BF} est donnée en fonc-

tion du nombre d'antennes. Comme le montre la Figure 3, le nombre moyen de dispositifs, appelé intensité β, converge vers une limite en fonction du temps lorsque le taux d'arrivée est inférieur à λ_c^{BF}. Lorsque le taux d'arrivée est supérieur à λ_c^{BF}, le réseau n'admet pas de régime stationnaire et β augmente sans limite.

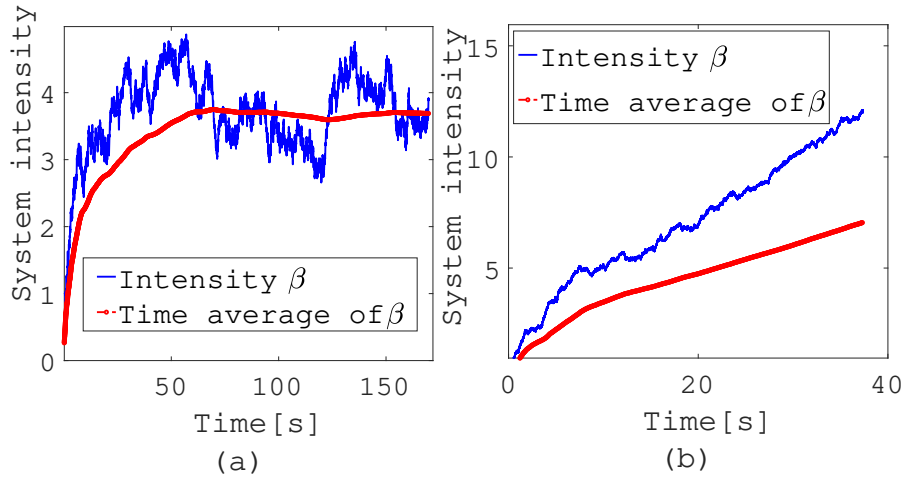

Figure 3: Intensité β en fonction du temps. (a) taux d'arrivée inférieur à λ_c^{BF}; (b) taux d'arrivée supérieur à λ_c^{BF}, lorsque le nombre d'antennes est de 4.

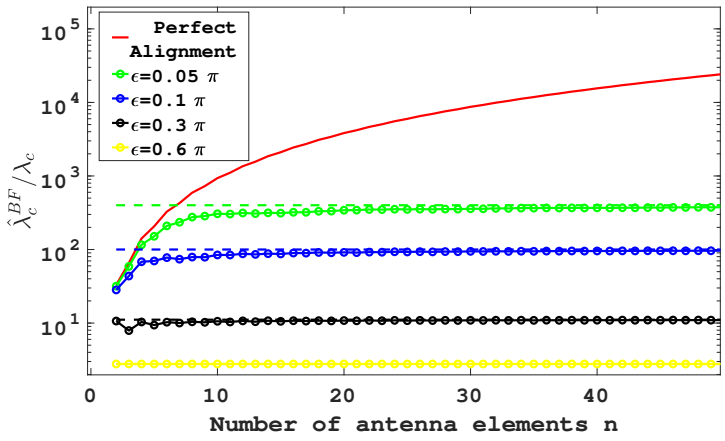

Figure 4: λ_c^{BF}/λ_c pour un réseau avec un alignement parfait (courbe rouge) ; $\hat{\lambda}_c^{BF}/\lambda_c$ en fonction de n pour un réseau avec différents niveaux d'erreur uniforme d'alignement du faisceau (courbes avec marques circulaires) ; limites supérieures de $\hat{\lambda}_c^{BF}/\lambda_c$ pour différentes régions d'erreur d'alignement ϵ (lignes en pointillés).

Comme les faisceaux sont étroits, leur désalignement peut réduire considérablement les performances du réseau. L'évaluation de l'impact du désalignement est donc réalisée en supposant une distribution statistique des erreurs d'alignement. Dans nos études, nous proposons une expression analytique du taux d'arrivée critique, $\hat{\lambda}_c^{BF}$

dans l'hypothèse d'une erreur d'alignement uniforme ou gaussienne tronquée. Nos résultats analytiques et numériques démontrent que dans le cas d'un alignement parfait du faisceau, le taux d'arrivée critique, λ_c^{BF}, peut croître indéfiniment avec un nombre croissant d'éléments d'antenne. Toutefois, lorsque l'alignement du faisceau est imparfait, le taux d'arrivée critique, $\hat{\lambda}_c^{BF}$, ne présente plus d'augmentation illimitée. La Figure 4 montre le rapport entre le taux d'arrivée critique, $\hat{\lambda}_c^{BF}$, avec un défaut d'alignement uniforme et le taux d'arrivée critique sans la formation de faisceaux, λ_c, en fonction du nombre d'antennes n. Des expressions closes des limites supérieures des taux d'arrivée critiques sont données pour les modèles de désalignement gaussien tronqué et uniforme.

Chapitre 4: Meta-distribution des débits pour le réseau D2D à ondes millimétriques

Dans ce chapitre, nous nous concentrons sur l'étude des propriétés instantanées de la communication D2D dans le spectre des ondes millimétriques, en mettant particulièrement l'accent sur la diversité de la couverture et de la fiabilité entre les différentes liaisons. Comme pour le modèle dynamique, le réseau est modélisé comme un réseau bipolaire de Poisson. Les émetteurs et les récepteurs des utilisateurs sont équipés d'antennes directionnelles et adoptent la formation de faisceaux. Nous définissons la fiabilité comme la probabilité de transmission réussie d'un paquet de données dans un délai donné, qui peut être quantifiée par la probabilité de couverture du débit. Les premières études sur le D2D se concentrent sur la probabilité de couverture moyenne parmi tous les utilisateurs. Or, les conditions de couverture et de fiabilité varient d'un utilisateur à l'autre et d'un endroit à l'autre. La probabilité de couverture conditionnelle est donc proposée pour caractériser spécifiquement la distribution du taux de transmission pour un utilisateur type dans un réseau :

$$P_s(\eta) \triangleq \mathbb{P}(\mathcal{R} > \eta | \Phi^T, \Phi^R) \tag{1}$$

où $\mathcal{R}$ est le taux de transmission, η est le seuil de taux, Φ^T et Φ^R sont les processus ponctuels par rapport aux positions des émetteurs et des récepteurs. Dans le contexte de l'URLLC, nous souhaitons également connaître la proportion d'utilisateurs qui satisfont aux exigences de fiabilité. La meta-distribution est donc définie comme la distribution spatiale de la probabilité de couverture conditionnelle comme suit :

$$\bar{F}_{P_s(\eta)}(\epsilon) \triangleq \mathbb{P}^!(P_s(\eta) > \epsilon), \qquad \epsilon \in [0,1], \theta \in \mathbb{R}^+. \tag{2}$$

où ϵ est le seuil de fiabilité et $\mathbb{P}^!$ fait référence à la probabilité de Palm pour l'utilisateur type.

En considérant l'hypothèse d'un désalignement gaussien tronqué, nous dérivons des expressions calculables des moments de la probabilité conditionnelle de couverture du débit en fonction du nombre d'éléments d'antenne. L'approximation bêta de la meta-distribution du débit est obtenue sur la base du premier et du deuxième moment. Les simulations numériques confirment nos résultats analytiques. Elles montrent que les performances de couverture peuvent se détériorer de manière significative en raison d'un mauvais alignement. En outre, nous constatons que l'augmentation du nombre d'antennes n'améliore pas nécessairement la couverture ou la fiabilité. Les dispositifs dotés d'un plus grand nombre d'antennes sont plus sensibles aux erreurs d'alignement. Nous mettons en évidence l'existence d'un nombre optimal d'antennes qui maximise la probabilité de couverture du débit (moyen) et qui dépend de l'ampleur de l'erreur, voir Figure 5.

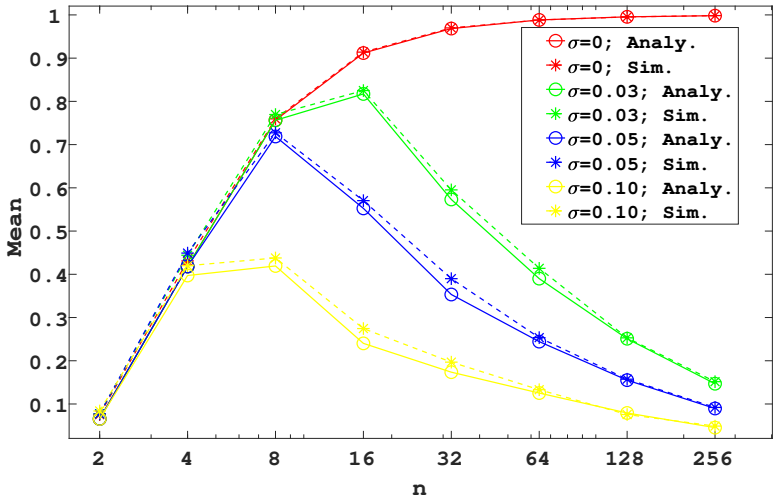

Figure 5: Moyenne de $P_s(\eta)$ en fonction du nombre d'antennes n pour différents écarts d'erreur d'alignement ϵ.

En outre, il existe un nombre optimal d'antennes qui maximise le nombre d'utilisateurs satisfaisant aux contraintes de fiabilité. Cette valeur optimale est fonction du seuil de fiabilité, voir Figure 6.

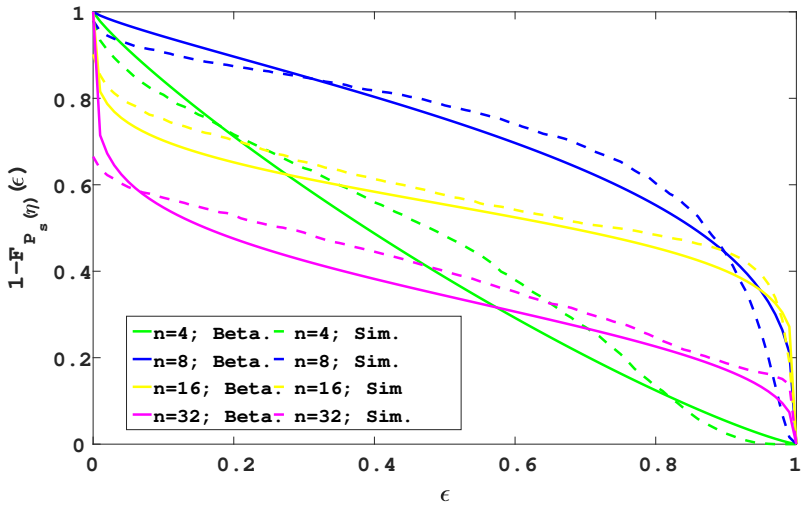

Figure 6: Meta distribution avec désalignement.

Chapitre 5: Gestion des faisceaux pour les réseaux mmWave URLLC D2D

Dans le chapitre précédent, nous avons étudié les effets du désalignement des faisceaux sur la meta-distribution des débits dans les réseaux D2D à ondes millimétriques. Nos résultats ont révélé une dégradation significative de la couverture en cas de désalignement. Cependant, le désalignement n'a été modélisé que de manière statistique, sans que ses sources spécifiques ne soient discutées. L'alignement des faisceaux est une étape cruciale dans le réseau d'accès radio moderne pour l'accès initial et la synchronisation. Pour réaliser la formation de faisceaux d'ondes millimétriques, le balayage exhaustif des faisceaux est largement utilisé comme méthode de formation de faisceaux basée sur un livre de codes dans divers systèmes de communication sans fil. Dans ce chapitre, nous approfondissons cette question en examinant l'alignement des faisceaux induit par le codebook d'apprentissage des faisceaux. Plus précisément, nous étudions un réseau D2D sur ondes millimétriques dédié à l'URLLC, dans lequel les utilisateurs emploient des antennes multiples pour réaliser la formation de faisceaux. Le processus de transmission des paquets est divisé en deux phases : une phase d'apprentissage du faisceau, au cours de laquelle un balayage exhaustif du faisceau est adopté, et une phase de transmission des données, illustrées par la Figure 7.

Ce chapitre étudie la distribution de l'erreur de désalignement résultant d'une phase d'apprentissage imparfaite, due à la résolution finie des livres de codes et

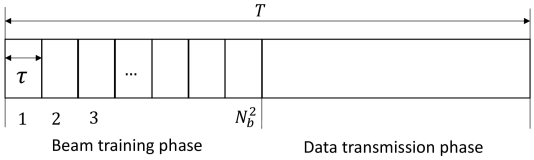

Figure 7: L'intervalle de temps d'une durée de T comprend : (i) une phase d'apprentissage du faisceau, qui consiste en N_b^2 mini-créneaux d'une durée de τ ; (ii) une phase de transmission des données.

à la variation rapide du canal. Pour la phase d'apprentissage du faisceau, nous proposons des formules closes pour la fonction de de distribution discrète conjointe des gains d'antenne à l'émetteur et au récepteur résultant du processus de balayage du faisceau, en supposant n'importe quelle distribution générique d'évanouissement rapide, y compris Nakagami-M et n'importe quelle résolution de livre de codes. Pour la phase de transmission des données, des expressions de forme close pour tous les moments de la probabilité de couverture conditionnelle du débit sont dérivées, et la meta-distribution est approximée à l'aide de l'approximation bêta. L'étude évalue les performances globales du réseau par le biais de la meta-distribution du débit effectif présentée ci-dessous, qui tient compte des ressources dédiées à l'apprentissage et des erreurs de désalignement des faisceaux.

$$\bar{F}_{\tilde{P}_c(\tilde{\eta})}(\epsilon) \triangleq \mathbb{P}^!(\tilde{P}_c(\tilde{\eta}) > \epsilon), \qquad \epsilon \in [0,1], \tilde{\eta} \in \mathbb{R}^+. \tag{3}$$

où $\tilde{P}_c(\tilde{\eta})$ est la probabilité de couverture conditionnelle du débit effectif présentée comme suit:

$$\tilde{P}_c(\tilde{\eta}) = \mathbb{P}\left(\widetilde{\mathcal{R}} > \tilde{\eta} | \Phi^T, \Phi^R\right) \tag{4}$$

où $\tilde{\eta}$ est le seuil de débit effectif et $\widetilde{\mathcal{R}}$ est le débit effectif réalisable défini comme suit :

$$\widetilde{\mathcal{R}} = \left(1 - \frac{N_b^2 \tau}{T}\right)^+ \mathcal{R} \tag{5}$$

où $\mathcal{R}$ est le débit de transmission, T est la durée de l'intervalle de temps et $N_b^2\tau$ est la durée de la phase d'apprentissage du faisceau. Cette meta-distribution se réfère à la proportion d'utilisateurs qui peuvent terminer de manière fiable la transmission dans le temps imparti. Elle nous permet d'obtenir des garanties statistiques de latence pour les communications URLLC.

Grâce à des expériences numériques, nous mettons en évidence les compromis entre la quantité de ressources dédiées à l'apprentissage et celles dédiées à la transmissions de données d'une part et entre le nombre d'antennes et les erreurs de désalignement d'autre part. Nous sommes en mesure d'optimiser la taille du livre de codes et le nombre d'antennes. À notre connaissance, ces compromis n'ont pas été étudiés dans la littérature en utilisant la meta-distribution tout en tenant compte de la résolution du livre de codes. Il est préférable d'avoir moins d'antennes lorsqu'un délai très court est nécessaire avec une grande fiabilité. En revanche, le gain potentiel de nombreuses antennes peut être exploité lorsque la contrainte de délai est relâchée, voir la Figure 8.

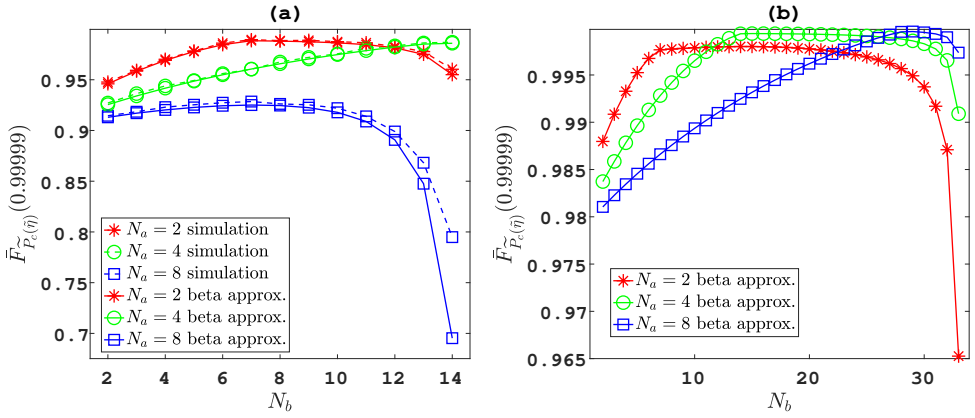

Figure 8: Proportion de dispositifs ayant une probabilité de couverture du débit conditionnel effectif supérieure au seuil de fiabilité 99.999% en fonction du nombre de faisceaux pour $T = 1$ ms (a) et $T = 5$ ms (b).

Chapitre 6: Conclusion et travaux futurs

Ce chapitre conclut le travail et présente des extensions potentielles des travaux réalisés dans cette thèse. Par exemple :

- Pour le cas stationnaire, la méthode actuelle de balayage des faisceaux prend beaucoup de temps. Les travaux futurs pourront améliorer le modèle en envisageant des méthodes de formation de faisceaux plus souples et plus générales, telles que la recherche hiérarchique de faisceaux. La formation de faisceaux dans nos travaux actuels est un cas analogique simple basé sur le réseau phasé, qui n'est pas optimal lorsque la propagation n'est pas en ligne de vue. Nous espérons étudier les performances au niveau du réseau avec des techniques

de formation de faisceaux plus avancées, telles que la formation de faisceaux hybrides. Des méthodes de formation de faisceaux plus adaptatives et plus efficaces doivent être examinées pour des techniques multi-antennes plus avancées.

- Pour le cas dynamique, on sait que la configuration de l'emplacement des appareils à un instant donné suit un processus ponctuel stationnaire si le taux d'arrivée de nouveaux utilisateurs n'est pas trop élevé. Mais il ne s'agit pas d'un processus ponctuel de Poisson puisqu'il existe des grappes dans ce processus ponctuel. L'idée initiale selon laquelle les appareils adoptent la formation de faisceaux est qu'elle peut augmenter la puissance de chaque utilisateur. L'impact de la formation de faisceaux sur la distribution des appareils reste une question intéressante à laquelle il faut répondre. Les performances de couverture de ce réseau dans un état stable devraient être étudiées. Idéalement, nous espérons trouver la distribution spatiale du temps de séjour attendu dans un état stable.

- Nous devrions tenir compte davantage du temps de cohérence dans nos études futures. D'une part, le spectre élevé est confronté à un effet Doppler important et le temps de cohérence du canal est court. D'autre part, le temps de cohérence du canal peut être réduit lorsque la formation de faisceaux est utilisée. Pour tenir pleinement compte de cet effet, nous devons prendre en considération la cohérence spatiale et le temps de cohérence du faisceau, qui indiquent l'intervalle général ou le temps moyen pour conserver le même niveau de gain de formation de faisceau. En tenant compte du temps de cohérence, la formation de faisceau doit être ajustée comme le suivi de faisceau et l'effet du désalignement doit être reconsidéré en conséquence.

À long terme, l'étude des effets de la mobilité des utilisateurs sur les performances d'alignement et de couverture du réseau nécessiterait des études plus complexes. Le réseau du futur sera un vaste système dynamique caractérisé par une mobilité intense. Cependant, dans un scénario plus réaliste, le mouvement des utilisateurs de D2D est limité par des contraintes physiques telles que les rues et l'architecture. Le processus Poisson linéaire semble donc être un modèle idéal pour caractériser les trajectoires des appareils. Il serait intéressant d'appliquer ce modèle dans d'autres études.

Chapter 1

Introduction

1.1 Context and motivation

Fifth Generation New Radio (5G NR) proposes three main prospects for the future network: enhanced mobile broadband (eMBB), ultra-reliable low latency communications (URLLC), and massive machine-type communication (mMTC) [1]. It is expected that mobile users can experience high data rates of up to 20 Gbits/s, low latency of 1ms with 99.999% reliability, and up to one million connections per square kilometer, especially for the applications such as the industrial internet of things (IoT) and vehicles to everything (V2X) [2]. However, given the ever-increasing growth of the cellular users and wide range of IoT devices, 5G may not meet the future demands of high reliability and high density of communications, given that the future network is foreseen to be an ultra large scale dynamic complex system. In this context, device-to-device communication (D2D) is emerging as a promising technology to address the explosion of demands for high data rate services. D2D has garnered significant attention as a means of improving the quality of service (QoS) for proximity services, offering potential improvements in latency, reliability, throughput, and energy consumption. Moreover, D2D can help to reduce the load on the network by extending cellular coverage [3].

D2D allows direct communication between nearby devices. Indeed, part of the traffic is directly assigned to "devices" without requiring the use of the resources of base stations. Moreover, a device can relay communication between a base station and another device located outside its coverage area, which can play essential roles in emergency situations where part of the infrastructure is destroyed. Therefore, D2D communication can help to meet the stringent requirements of the future

5G radio network. However, employing D2D communication suffers from high interference and insufficient bandwidth. However, D2D communications suffer from unpredictable interference as D2D transmitters can be active anywhere around every receiver with little control from the network. A fundamental challenge of D2D networks is thus the management of co-channel interference. Moreover, the demand for higher data rates, lower latency and higher reliability requires more and more bandwidth. Exploiting the millimeter wave (mmWave) bands seems to be a suitable solution for these problems [4]–[7]. Millimeter wave D2D communication is a technology that uses high-frequency radio waves in the range $30 - 300$ GHz for direct communication between devices. Compared to sub-6 GHz bands usually adopted for cellular communications, mmWaves offer very large bandwidths, allowing fast and reliable transmissions [8]. High carrier frequencies are however characterized by a very short coherence time and a predominant Line-of-Sight (LOS) propagation with high attenuation [9]. In order to overcome these challenging propagation conditions, it is necessary to equip devices with multiple antennas and to perform beamforming to enhance the signal strength and quality [10].

The use of the multi-antenna technique for wireless communication has by now been widely studied for many decades. The concept of "beamforming" refers to a technique where the power gain of antenna arrays is focused in the desired directions. As a result, this technique can reduce interference and improve throughput performance. The energy efficiency can also be improved since the power is focused. In LOS propagation, classical beamforming has a well-defined beam shape, with relatively narrow main lobe pointed into a desired physical direction, for example, towards the objective user device. There are several papers in the literature showing the great potential of beamforming for D2D communications for reducing interference and improving network throughput, see e.g. [11], [12]. Among these works, a classical antenna configuration, namely the uniform linear array (ULA)[13], is widely adopted as a platform as an antenna array geometry to perform beamforming. In this thesis, we also consider ULA to improve the network performance. Those aforementioned technologies of 5G will be discussed in chapter 2 associated with its general background on motivations and challenges.

In order to have a quick evaluation of the performance of future networks with mmWave D2D communication, and to identify critical parameters that significantly impact the performance, such as coverage, latency, and reliability in the context of URLLC, it is is essential to have analytical methods for evaluating performance.

Coverage for devices in the network is mainly determined by channel conditions and network topology, which necessitate analytical or numerical approximations of device positions. Regarding latency, it can be defined in various ways and at different layers of communication protocols of the protocol stack. One simple definition of latency is the delay experienced by a data packet from the point it enters a given protocol layer at the transmitter to the point it exits the same layer at the receiver [14]. The protocol design for resource utilization and transmission schemes, along with the dynamic changes in coverage that take place for each link over time, can both affect latency. In the context of URLLC, the definition of reliability is coupled to the latency requirement. One way to define the reliability is to calculate the probability that the latency does not exceed a given deadline [14]. We will see that this definition is similar to that of the coverage probability. To analyze the performance of these systems, it is necessary to consider both spatial and temporal variations.

Stochastic geometry is widely used to evaluate the coverage, throughput, and energy efficiency of wireless networks due to its mathematical flexibility [15], [16]. In this approach, devices or base stations are modeled as a point process, and performance parameters such as the transmission rate can be regarded as the marks of each point. Spatial averages of marks of a stationary planar point process can be evaluated as expectations under the Palm probability. Classical studies using this method mainly focus on calculating the average coverage probability for a typical user using Palm calculus [17]. However, in the context of URLLC, it is essential to consider the distribution of traditional performance metrics to understand, for example, the proportion of users meeting reliability requirements as defined in [2]. To fully characterize the spatial distribution of communication reliability, the meta-distribution can be leveraged [18]. In chapter 2, we provide a brief introduction to stochastic geometry and to the concept of meta-distribution.

As previously mentioned, while studies focusing at a given time instant on spatial averages are informative, it is important to also consider temporal dynamics. Traditional approaches to study network dynamics leverage queuing theory, but these studies, primarily inspired by wired networks, model the network with multiple servers whose relative locations have no influence on their behavior [19]. To address this limitation, the spatial birth-death wireless network model has been proposed, which models the stochastic network as a function of the point process and takes into account the interaction between links across time due to traffic variations [20].

This model is based on the spatial birth-death process [21], in which users arrive to the plane as a homogeneous Poisson rain and are each marked with a random service time. At any given time, the service rate of each user is related to the configuration of the point process. Chapter 2 provides a presentation of the spatial birth-death process.

1.2 Contribution of the thesis

In this thesis, we evaluate several performance indicators of D2D communication in a radio network by considering the impact of beamforming. Generally speaking, we try to tackle this problem through two different points of view: Instantaneous average properties of the random network and the global ergodicity properties of a dynamical network with random service requests.

We consider a dynamic D2D communication model where transmitters and receivers have multiple antennas and adopt beamforming for the dynamic case. The network is dynamic since there are random arrivals of new D2D devices. Moreover, the users who finish the communications leave the network immediately. In this way, a continuous spatio-temporal model for the wireless network is established, which combines a spatial stochastic point process and a dynamic birth-death process. The application of this model to the D2D network was firstly studied by Sankararaman and Baccelli in 2017 [20]. In this thesis, we extend the result of Sankararaman and Baccelli on the stability condition to D2D networks where users are equipped with directional antennas arrays. We use an analog beamforming model based on a ULA [22]. By applying such a beamforming technique, the point process is no longer isotropic but can still remain in a stationary state under certain constraints. Our task is to study the impact of beamforming for the stability region of this dynamic network. In addition, the shape of beam is related to the number of antennas in a ULA. More antennas can bring stronger beams but reduce the beam width. Since the beams are narrow, the beam misalignment can dramatically reduce the performance of the network. Thus the evaluation of the impacts of misalignment is performed. The works related to this part is presented in chapter 3.

For the instantaneous properties, we are interested in understanding the diversity of link reliability across different links at a given time in the mmWave D2D network, under the stationary state. Similar to the dynamic case, our study considers D2D transmitters and receivers with multiple antennas that adopt beamforming.

We define reliability as the probability of successful transmission of a data packet within a given time period, which can be quantified by the rate coverage probability. We derive mathematical approximations for the meta-distribution of this reliability metric. The impacts of beamforming are investigated by considering imperfect beam alignment. Similar to the dynamic case, we evaluate the effects of misalignment by assuming a statistical alignment error. Our results show that beam misalignment can degrade the average coverage of the network and reduce the proportion of reliable communication links. Additionally, we find that increasing the number of antennas may not necessarily improve coverage or reliability. Links with more antennas are more sensitive to alignment errors. We highlight the existence of an optimal number of antennas that maximizes the (average) rate coverage probability which depends on the error magnitude. We also show that there is an optimal number of antennas maximizing the number of users satisfying a reliability requirement. This optimal number is dependent on the required reliability. The work related to this part is presented in chapter 4.

In addition to studying the statistical assumption of alignment errors, we are also interested in the causes of beam misalignment. Beam alignment is a crucial step in the modern radio access network for initial access and synchronization. To achieve millimeter wave beamforming, exhaustive beam sweeping is widely used as a beam training method in various wireless communication systems such as wireless local area network (WLAN), 5G cellular network, and sidelink communication. Our studies demonstrate that misalignment may occur during the beam sweeping process, primarily due to the limited resolution of beamforming codebooks and channel variations. Furthermore, our findings show that there is a trade-off between training overhead and data transmission reliability. We derive the meta-distribution of the effective rate as a statistical latency guarantee for URLLC communications, considering both the training overhead and misalignment. The results indicate that there exist optimal numbers of antennas and beam sweeping schemes for URLLC communications. Chapter 5 presents our studies on these topics.

1.3 Structure of the thesis

The remaining chapters of this thesis are structured as follows. Chapter 2 provides a review of the mathematical foundations and wireless network backgrounds relevant to the research. Chapter 3 investigates the stability of a spatio-temporal D2D net-

work with imperfect beam alignment. Chapter 4 focuses on the meta-distribution analysis of the D2D network with imperfect beam alignment. In chapter 5, we extend the study to include misalignment induced during the beam sweeping process. Finally, chapter 6 concludes the thesis and provides some insights into future research directions.

1.4 List of publications

Journal Paper:

- Yibo QUAN, Marceau COUPECHOUX and Jean-Marc KELIF, "Rate Meta-Distribution in Millimeter Wave URLLC Device-to-Device Networks with Beam Misalignment ", submitted to IEEE TWC.

Conference papaers:

- Yibo QUAN, Jean-Marc KELIF and Marceau COUPECHOUX, "Spatio-Temporal Wireless D2D Network With Beamforming", ICC 2021 - IEEE International Conference on Communications, 2021, pp. 1-6, doi: 10.1109/ICC42927.2021.9500356.
- Yibo QUAN, Marceau COUPECHOUX and Jean-Marc KELIF, "Spatio-Temporal Wireless D2D Network With Imperfect Beam Alignment", WCNC 2022 - IEEE Wireless Communications and Networking Conference, 2022, pp.2346-2351, doi: 10.1109/WCNC51071.2022.9771938.
- Yibo QUAN, Marceau COUPECHOUX and Jean-Marc KELIF, "Rate Meta-distribution in mmW D2D Networks with Beam Misalignment", GLOBECOM 2022 - IEEE Global Communications Conference, 2022, pp. 1825-1830, doi: 10.1109/GLOBECOM48099.2022.10001302.

Chapter 2

Mathematical foundations and network backgrounds

This chapter provides an overview of the mathematical tools and wireless communication technologies that are explored in this thesis. The chapter begins with an introduction to stochastic geometry, covering topics such as the point process and the Palm theory. We then examine several applications of stochastic geometry for wireless network modeling, including coverage characterization and meta-distribution analysis. Additionally, we discuss the spatial birth-death process as a dynamic network model. In a second part of the chapter dedicated to the background in Networks, we introduce the framework of D2D networks, as well as millimeter wave and beamforming technologies.

2.1 Short introduction to stochastic geometry

Stochastic geometry is a powerful tool to study the randomness properties of spatial patterns. This method can help us explore the geometrical patterns of many things in our natural world. Furthermore, it is widely used in academic domains like astronomy, life science, computer, network science, etc. [16], [23]. In wireless networking, stochastic geometry is applied to study the geometrical topology of the network, including the locations of transmitters, receivers, and sources of interference, which play a crucial role in radio communication. Whether we need to make dimensioning decisions or evaluate the quality of service, knowledge of the transmitter locations is essential. One of the core objects of this domain is to construct the statistical models for the random point processes and investigate their properties. This section provides a brief review of the mathematical theory of stochastic geometry.

2.1.1 Point process

Basic definitions

A spatial point process (p.p.) Φ is a random, finite or countably-infinite collection of points residing in some measurable space, usually the Euclidean space $\mathbb{R}^d$, without accumulation points [15]. Take the two dimensional Euclidean space $\mathbb{R}^2$ as an example, we can define a configuration of $\mathbb{R}^2$ as follows:

Definition 1. *(Configuration of $\mathbb{R}^2$) A configuration of $\mathbb{R}^2$ is a locally finite set of points of $E \subset \mathbb{R}^2$.*

For example $\mathbb{N}$ is a configuration of $\mathbb{R}^2$ but $\{\frac{1}{n} : n \in \mathbb{N}^*\}$ is not because it is not locally finite at 0. Then we can denote a set of configurations of $E \subset \mathbb{R}^2$ as Γ_E. A configuration, denoted as ξ, is an element of Γ_E. It can either be expressed as a set $\xi = \{x_1, x_2, x_3...\}$, or a measure $\xi = \sum_{x\in\xi} \delta_x$, where δ is the Dirac measure. For any function $f : E \to \mathbb{R}$, we can denote

$$f(\xi) = \sum_{x\in\xi} f(x) = \int f \mathrm{d}\xi \tag{2.1}$$

If $A \subset E$, $\xi(A)$ is the number of point of ξ in A.

Definition 2. *(Point process in $\mathbb{R}^2$) A point process Φ on $E \subset \mathbb{R}^2$ is a random variable whose values are in space Γ_E.*

In another word, a point process can be regarded as a random variable taking values from locally finite configurations of points, or equivalently, a counting measure. Considering a more general notation of random measures, the following notations and definitions concerning the point process theory are introduced in [24].

Definition 3. *(Counting measure [24]) A counting measure μ is a locally finite measure taking values in $\{0, 1, 2, ..., \infty\}$ on $(\mathbb{G}, \mathcal{B}(\mathbb{G}))$, where $(\mathbb{G}, \mathcal{T})$ is a topological space which is locally compact, second countable (i.e.,its topology $\mathcal{T}$ has a countable basis), and Hausdorff (i.e., distinct points have disjoint neighborhoods), abbreviated by l.c.s.h. and $\mathcal{B}(G)$ is its associated Borel $\sigma-$algebra.*

It is convenient to express Φ by using the Dirac measure $\Phi = \sum_i \delta_{x_i}$, where δ_{x_i} is the Dirac measure at x.

Definition 4. *(Point process in general space [24]) Let $\mathbb{G}$ be a l.c.s.h space. Let $\mathbb{M}(\mathbb{G})$ be a set of counting measures on $(\mathbb{G}, \mathcal{B}(\mathbb{G}))$. Let $(\Omega, \mathcal{F}, \mathbb{P})$ be a probability space. A point process (p.p.) is a measurable mapping*

$$\Phi : (\Omega, \mathcal{F}, \mathbb{P}) \to (\mathbb{M}(\mathbb{G}), \mathcal{M}(\mathbb{G})) \tag{2.2}$$

The distribution of Φ is denoted as $\mathbb{P}_\Phi := \mathbb{P} \circ \Phi^{-1}$.

For all $B \in \mathcal{B}(\mathbb{G})$, $\Phi(B)$ is a random variable whose value can be understood as the number of points in B.

Characterizations of a point process

A random measure can be characterized by different ways. We introduce hereafter three basic metrics for a point process: mean measure, the Laplace transform and the void probability.

Definition 5. *(Mean measure) The mean measure of a point process Φ defined in $\mathbb{G}$ is a measure defined on $(\mathbb{G}, \mathcal{B}(\mathbb{G}))$, such that*

$$M_\Phi(B) = \mathbb{E}[\Phi(B)], \qquad B \in \mathcal{B}(\mathbb{G}) \tag{2.3}$$

Definition 6. *(Laplace functional) For all measurable functions $f : \mathbb{G} \to \mathbb{R}_+$, the Laplace transform of f on a point process Φ is defined as follows:*

$$\mathcal{L}_\Phi(f) = \mathbb{E}\left[\exp\left(-\int_{\mathbb{G}} f \, d\Phi\right)\right] = \mathbb{E}\left[\exp\left(-\sum_{x \in \Phi} f(x)\right)\right] \tag{2.4}$$

It is important to study the Laplace transform of a point process because it can characterize completely the distribution of the process.

Lemma 1. *The probability distribution of a point process is fully characterized by its Laplace transform:*

$$\mathcal{L}_{\Phi}(f) = \mathcal{L}_{\Phi'}(f) \longleftrightarrow \Phi \overset{law}{=} \Phi' \tag{2.5}$$

That is to say, once the Laplace transform of any measurable function are the same for two point processes, these point processes should have the same law. Then, we can define the probability generating functional for a point process as the Laplace transform.

Definition 7. *(Probability generating functional (PGFL) [24]) Let $\mathbb{G}$ be a l.s.c.h. space, for any measurable function $f : \mathbb{G} \to [0, 1]$. The probability generating function $\mathcal{G}(\Phi)$ of a point process Φ is defined as follows:*

$$\mathcal{G}_{\Phi}(f) = \mathcal{L}_{\Phi}(-\log f) = \mathbb{E}\left[\exp\left(\int_{\mathbb{G}} \log f \, d\Phi\right)\right] \tag{2.6}$$

Note that the right side of the formula is the expectation of the products of f:

$$\mathbb{E}\left[\exp\left(\int_{\mathbb{G}} \log f \, d\Phi\right)\right] = \mathbb{E}\left[\prod_{x\in\Phi} f(x)\right] \tag{2.7}$$

Definition 8. *(Void probability) The void probability for a point process Φ is defined as:*

$$v(B) = \mathbb{P}(\Phi(B) = 0), \qquad B \in \mathcal{B}(\mathbb{G})$$

Properties of a point process

Definition 9. *(Simple point process [23]) A point process is said to be simple if all points are isolated. Mathematically, a counting measure is said to be simple if $\mu(\{x\}) \leq 1, \forall x \in \mathbb{G}$. A point process Φ is simple if*

$$\mathbb{P}(x \in \mathbb{G}, \Phi(\{x\}) \leq 1) = 1$$

Definition 10. *(Stationary point process [23]) A point process on $\mathbb{R}^d$ is said to be stationary when its distribution is invariant under translation, that is $\Phi = \sum_{k\in\mathbb{Z}} \delta_{X_k}$ and $S_t\Phi = \sum_{k\in\mathbb{Z}} \delta_{X_k - t}$ have the same distribution for all $t \in \mathbb{R}^d$.*

Definition 11. *(Isotropic point process [23]) A point process on $\mathbb{R}^d$ is said to be isotropic when its distribution is invariant under rotation, that is $\Phi = \sum_{k\in\mathbb{Z}} \delta_{X_k}$ and $\boldsymbol{r}\Phi = \sum_{k\in\mathbb{Z}} \delta_{\boldsymbol{r}X_k}$ have the same distribution, where $\boldsymbol{r}$ is a rotation about the origin.*

Corollary 1. *A point process is said to be motion-invariant if it is both stationary and isotropic [23].*

Theorem 2. *(Campbell's averaging formula [24]) For a point process Φ on a l.c.s.h. space $\mathbb{G}$ with mean measure M_Φ, let $f : \mathbb{G} \to \mathbb{C}$ be a function that is either a non-negative or integrable with respect to M_Φ, that is in $L^1_{\mathbb{C}}(M_\Phi, \mathbb{G})$ space. Then $\int_{\mathbb{G}} f\, d\Phi$ is a well defined variable and we have the following relation:*

$$\mathbb{E}[\int_{\mathbb{G}} f\, d\Phi] = \int_{\mathbb{G}} f\, dM_\Phi \tag{2.8}$$

If the intensity function exists for a point process Φ defined on $\mathbb{R}^d$, the Campbell's formula is equivalent to [23]:

$$\mathbb{E}[\sum_{x\in\Phi} f(x)] = \int_{\mathbb{R}^d} f(x)\lambda(x)\mathrm{d}x \tag{2.9}$$

2.1.2 Poisson point process

Definition 12. *(Poisson point process (PPP)[15]) Let Λ be a locally finite non-null measure on $\mathbb{R}^d$. A Poisson point process with intensity measure Λ defined on $(\mathbb{R}^d, \mathcal{B})$ is a point process such that:*

- *For all compact set $B \subset \mathcal{B}$, $\Phi(B)$ has a Poisson distribution with mean $\Lambda(B)$. If Λ admits a density λ, that is:*

$$\mathbb{P}(\Phi(B) = k) = \exp\left(-\int_B \lambda(x)\, dx\right) \frac{(\int_B \lambda(x)\, dx)^k}{k!} \tag{2.10}$$

- *For disjoint Borel sets $B_1, ..., B_k \in \mathcal{B}$, $\Phi(B_1), ..., \Phi(B_k)$ are independent random variables.*

The second condition is known as complete independence. We then characterize the Poisson point process by the Laplace functional and the void function.

Proposition 3. *(Poisson point process Laplace functional) Let Φ be a PPP on $\mathbb{R}^d$ with intensity Λ.*

$$\mathcal{L}(\Phi)(f) = \exp\left(-\int_{\mathbb{R}^d} (1 - e^{-f})\, d\Lambda\right) \tag{2.11}$$

Corollary 2. *The PGFL of a Poisson point process Φ can be expressed as:*

$$\mathcal{G}_{\Phi}(f) = \prod_{x \in \Phi} f(x) = \exp\left(- \int_{\mathbb{R}^d} (1 - f) d\Lambda \right) \tag{2.12}$$

Proposition 4. *(Poisson point process void function) The void probability for a Poisson point process with intensity Λ is as follows:*

$$v(B) = e^{-\Lambda(B)}, \quad \forall B \in \mathcal{B} \tag{2.13}$$

Definition 13. *(Homogeneous Poisson point process) If Φ is a Poisson point process with intensity measure Λ, and $\Lambda(dx) = \lambda \times dx$ where $\lambda \in \mathbb{R}_+$. Then Φ is said to be a homogeneous Poisson point process with intensity λ.*

The characteristic λ is clearly invariant under rotation and translation. Therefore the homogeneous Poisson point process must be stationary and isotropic.

2.1.3 Superposition, thinning and marking

Definition 14. *(Superposition [24]) Let $\Phi_0, \Phi_1, ...$ be a sequence of point process defined on $\mathbb{R}^d$ on the same probability space. The superposition of point process refers to the sum of several point process $\Phi = \sum_k \Phi_k$.*

Lemma 5. *For a superposition $\Phi = \sum_k \Phi_k$ defined on $\mathbb{R}^d$, let $B_0, B_1, ...$ be a sequence of relatively compact open sets whose union covers $\mathbb{R}^d$. When $\Phi_0, \Phi_1, ...$ are independent and $\sum_k \mathbb{E}[\Phi_k(\cdot)]$ is locally finite on $\mathbb{R}^d$, the superposition Φ is a point process if and only if*

$$\sum_k \mathbb{P}(\Phi_k(B_j) \neq 0) < \infty \tag{2.14}$$

Proposition 6. *Let $\Phi_0, \Phi_1, ...$ be a sequence of independent Poisson point process with intensity measures $\Lambda_0, \Lambda_1, ...$, the superposition $\Phi = \sum_k \Phi_k$ is a Poisson point process with intensity $\Lambda = \sum_k \Lambda_k$ if and only if the latter is locally finite.*

Definition 15. *(Thinning) The thinning of point process refers to erasing some points within a point process randomly. The thinning of a point process $\Phi = \sum_k \delta_{X_k}$ with a retention function $p : \mathbb{R}^d \to [0, 1]$ is a point process given by:*

$$\Phi^p = \sum_k \mathbb{1}\{U_k < p(X_k)\} \delta_{X_k} \tag{2.15}$$

where $U_0, U_1, ..$ is a sequence of Independent and identically distributed (i.i.d.) random variables uniformly distributed in $[0, 1]$.

Proposition 7. *The thinning of Poisson point process of intensity measure* Λ *with retention probability* p *is a Poisson point process of intensity measure* $p\Lambda$*:*

$$(p\Lambda)(A) = \int_A p(x)\Lambda(dx) \tag{2.16}$$

Definition 16. *(Marked point process) Marking a point process refers to the fact of adding a specific characteristics, or marks belonging to a certain measurable space, to each point in the point process. A marked point process is a point measure*

$$\tilde{\Phi} = \sum_i \delta(x_i, m_i) \tag{2.17}$$

where $\delta(x, m)$ *is a Dirac measure on the Cartesian product* $\mathbb{R}^d \times \mathbb{R}^l$*.*

The space of their realizations is denoted as $\tilde{M}$. Particularly, the marked point process $\tilde{\Phi}(A \times \mathbb{R}^l)$ is finite for any bounded set $A \subset \mathbb{R}^d$.

Definition 17. *(Independently marked point process) A marked point process is said to be independently marked if the marks are mutually independent and are only conditionally to the points attached to in* Φ*:*

$$\mathbb{P}(m_i \in \cdot | \Phi) = \mathbb{P}(m_i \in \cdot | x) = F_x(dm) \tag{2.18}$$

where $F_\cdot(\cdot)$ *is a probability kernel. If* $F_\cdot(\cdot)$ *does not depend on* x*, it is called the mark distribution and the point process is called an i.i.d. marked point process.*

2.1.4 Palm theory

Palm's probability or Palm's measure in point process theory is the probability of an event given that the point process contains a point at a place. It also formalizes the notion of the "typical point" of the process. We can informally interpret a typical point as the point randomly selected among the points with the same chance. Here we present the definition based on the Radon–Nikodym theorem [15].

Definition 18. *(Reduced Campbell measure) The reduced Campbell measure of* Φ *is the measure*

$$C^!(B \times \Gamma) = \mathbb{E}\left[\int_B \mathbb{1}(\Phi - \delta_x \in \Gamma)\Phi(dx)\right], \qquad \forall B \subset \mathbb{R}^d \tag{2.19}$$

on $\mathbb{R}^d \times \mathbb{M}$*, where* $\mathbb{M}$ *is the set of point measures.*

The reduced Campbell measure is a complement of the mean measure M_Φ. By removing a particular point from Φ, the resulting configuration satisfies proper Γ. To be more rigorous, $C^!(\cdot \times \Gamma)$ is absolute continuous with respect to $M_\Phi(\cdot)$ for each Γ. Thus we can outline the relationship between $C^!(\cdot \times \Gamma)$ and $M_\Phi(\cdot)$ by the Radon–Nikodym derivative.

Proposition 8. *(Reduced Palm distribution)*

$$C^!(B \times \Gamma) = \int_B \mathbb{P}_x^!(\Gamma) M_\Phi(dx), \quad \forall B \subset \mathbb{R}^d \tag{2.20}$$

The function $\mathbb{P}_x^! = \mathbb{P}_x^!(\Gamma)$ depends on the removed set Γ. The probability $\mathbb{P}_x^!$ can be regarded as a probability distribution on $\mathbb{M}$ for each given x, if $M_\Phi(\cdot)$ is locally finite. And $\mathbb{P}_x^!$ is called the reduced Palm distribution of Φ given that there is a point at x.

Theorem 9. *(Reduced Campbell-Little-Mercke Formula) For all non-negative functions defined on $\mathbb{R}^d \times \mathbb{M}$*

$$\mathbb{E}\left[\int_{\mathbb{R}^d} f(x, \Phi - \epsilon_x)\Phi(dx)\right] = \int_{\mathbb{R}^d}\int_{\mathbb{M}} f(x,\mu)\mathbb{P}_x^!(d\mu)M_\Phi(dx) \tag{2.21}$$

$$= \int_{\mathbb{R}^d} \mathbb{E}[f(\Phi_x^!, x)]M_\Phi(dx) \tag{2.22}$$

$$= \int_{\mathbb{R}^d} \mathbb{E}_x^![f(\Phi, x)]M_\Phi(dx) \tag{2.23}$$

where $\Phi_x^! := \Phi - \delta_x$ and $\mathbb{E}_x^!$ is the expectation with respect to the reduced Palm distribution $\mathbb{P}_x^!$

Remind that for the Poisson point process, the mean measure is denoted as the intensity measure $M_\Phi = \Lambda$.

Theorem 10. *(Slivnyak–Mecke Theorem) Let Φ be a Poisson point process with intensity measure Λ, for $\Lambda-$almost all $x \in \mathbb{R}^d$*

$$\mathbb{P}_x^! = \mathbb{P} \tag{2.24}$$

That is to say, the reduced Palm distribution is identical to the original distribution of a Poisson point process. Therefore, $\Phi_x^!$ and Φ has the same Laplace transform characteristic for Poisson point process.

The reduced Palm distribution $\mathbb{P}_x^!$ can be easily extended to the Palm distribution $\mathbb{P}_x^!$ by considering $\Phi_x = \Phi + \delta_x$. Then Φ_x, $\Phi_x^!$ and Φ have the same distribution for Poisson point process.

2.2 SINR Coverage and meta-distribution

A classical application of stochastic geometry to the wireless network is to evaluate the coverage of a communication. Mathematically, the coverage probability, or the success probability over a typical link, is defined as the complementary cumulative distribution function (CCDF) of the SINR [18], i.e.:

$$p_s(\eta) \triangleq \mathbb{P}(\text{SINR} > \eta) \tag{2.25}$$

where η is a SINR threshold. Traditionally the value of this probability is calculated by spatial averaging, which is valid for the ergodic point process. Take a Poisson point process, for instance, we set a point at the origin, then, according to the Mecke Theorem 10, the Palm distribution is the same as its original distribution. Then we account for the frequency that the SINR of this typical point is larger than η by changing the point configuration in each iteration. Of course, we can also do the same operations for all the points, and then we calculate the average value among different points. However, the calculated value of p_s can only provide a global information about the coverage, that is, the percentage of success transmission devices we can find after each experiment. Nevertheless, if we take an individual view on different links, the coverage performance can differ significantly. Thus the meta distribution is proposed as a spatial distribution of the success probability for different links. Before the definition of meta distribution, we introduce the conditioned coverage probability.

Definition 19. *(Conditional coverage probability) Let Φ be a given point process, the conditional coverage probability for a typical link is defined as:*

$$P_s(\eta) \triangleq \mathbb{P}(SINR > \eta|\Phi) \tag{2.26}$$

Since Φ is a random point process, the probability $P_s(\eta)$ which depends on Φ is also a random variable, whose mean is the success probability $p_s(\eta)$.

Then the so-called meta-distribution is defined as the distribution of the conditioned coverage probability $P_s(\eta)$.

Definition 20. *(SINR Meta-distribution) Given a point process Φ, the SINR meta-distribution of a typical link is defined as the complementary CCDF of the conditioned coverage probability $P_s(\eta)$:*

$$\bar{F}_{P_s}(\epsilon, \eta) \triangleq \mathbb{P}^!(P_s(\eta) > \epsilon), \qquad \epsilon \in [0, 1], \eta \in \mathbb{R}^+. \tag{2.27}$$

Where $\mathbb{P}^!$ denotes the Palm measure of Φ, given that there is an active transmitter at the prescribed location. The classic success transmission probability p_s is the spatial average of the conditioned probability:

$$p_s(\eta) = \mathbb{E}^![P_s(\eta)] = \int_0^1 \bar{F}_{P_s}(\epsilon)\mathrm{d}\epsilon \tag{2.28}$$

And the b-th moment of $P_s(\eta)$ is denoted as $M_b(\eta)$, i.e.

$$M_b(\eta) \triangleq \mathbb{E}^![P_s(\eta)^b] = \int_0^1 b\epsilon^{b-1}\bar{F}_{P_s}(\epsilon)\mathrm{d}\epsilon \tag{2.29}$$

2.2.1 Calculation of meta-distribution

It is not easy to calculate the distribution of P_s directly. There are some alternative approaches to establish the meta distribution from the moments that reveal the high-order statistics properties of the conditional success probability. This type of problems that tries to obtain the distribution of a random variable from its moments can be called Hausdorff moment problem [25]. Here is a brief summary for the recently developed approaches of the calculation of the meta distribution.

Gil-Pelaez theorem

The exact expression of meta-distribution can be obtained based on the Gil-Pelaez theorem [18], [26].

Theorem 11. *(Gil-Pelaez theorem) For a univariate random variable X*

$$\bar{F}_X(x) = \mathbb{E}[\mathbb{1}_{\{X\leq x\}}] = \frac{1}{2} - \frac{1}{\pi}\int_0^\infty \frac{Im(e^{-jtx}\varphi_X(t))}{t}dt \tag{2.30}$$

where $j^2 = -1$. $Im(\cdot)$ denotes the imaginary part. $\varphi_X(t)$ is the characteristic function of X.

Let $X = \ln P_s(\eta)$, the characteristic function of X is expressed as follows:

$$\varphi_X(t) = \mathbb{E}[e^{jtX}] = \mathbb{E}[P_s(\eta)^{jt}] = M_{jt}, \qquad t \in \mathbb{R}.$$

Then the meta distribution $\bar{F}_{P_s(\theta)}(\epsilon)$ has an expression has follows:

$$\bar{F}_{P_s(\eta)}(\epsilon) = \mathbb{E}[\mathbb{1}_{\{\ln P_s(\eta)\leq \ln(\epsilon)\}}] = \frac{1}{2} - \frac{1}{\pi}\int_0^\infty \frac{Im(e^{-jt\ln(\epsilon)}M_{jt})}{t}\mathrm{d}t \tag{2.31}$$

Beta approximation

In practice, the expression above based on the Gil-Pelaez theorem is hard to be implemented by numerical method. Because this formula often involves the integration of complex value functions with complete oscillations. The beta-distribution based approximation is used in [18] to approximate the meta distribution by mapping the first and second moments.

The PDF of a beta distributed random variable X with mean μ is:

$$f_X(x) = \frac{x^{\alpha-1}(1-x)^{\beta-1}}{B(\alpha,\beta)} \tag{2.32}$$

Where $B(\cdot,\cdot)$ is a Beta function. The CDF of a Beta-distribution is expressed as the regularized incomplete beta function $I_x(\alpha,\beta)$:

$$I_x(\alpha,\beta) = \frac{\int_0^x t^{\alpha-1}(1-t)^{\beta-1}}{B(\alpha,\beta)} \tag{2.33}$$

A Beta distribution can be fully characterized by its mean and variance, which are expressed as follows:

$$\mathbb{E}(X) = \frac{\alpha}{\alpha+\beta} \tag{2.34}$$

$$\mathbb{E}(X^2) = \frac{\alpha+1}{\alpha+\beta+1}\mathbb{E}(X) \tag{2.35}$$

By matching the mean and variance of the Beta distribution with $M_1(\eta)$ and $M_2(\eta)$ of the conditioned coverage probability, we can calculate the two parameters α and β as follows:

$$\alpha = \frac{M_1 M_2 - M_1^2}{M_1^2 - M_2} \tag{2.36}$$

$$\beta = \frac{(1-M_1)(M_2-M_1)}{M_1^2 - M_2} \tag{2.37}$$

Thus the approximation of $\bar{F}_{P_s(\eta)}(\epsilon)$ follows:

$$\bar{F}_{P_s(\eta)}(\epsilon) \simeq 1 - I_x\left(\frac{M_1 M_2 - M_1^2}{M_1^2 - M_2}, \frac{(1-M_1)(M_2-M_1)}{M_1^2 - M_2}\right) \tag{2.38}$$

In most cases this beta approximation has very excellent accuracy and is widely used in most studies about meta-distribution.

Binomial mixtures approach

Reference [27] proposed an approach that utilizes binomial mixtures to obtain a piecewise approximation of the meta-distribution based on the integer moments $M_j = \mathbb{E}[P_s(\eta)^j]$, where $j \in \mathbb{N}^*$. The exact meta-distribution can be obtained by taking the limit of this approximation as follows:

$$\bar{F}_{P_s(\eta)}(\epsilon) = 1 - \lim_{i\to\infty} \sum_{k=0}^{\lfloor i\eta \rfloor} \sum_{j=k}^{i} \binom{i}{j}\binom{j}{k}(-1)^{j-k} M_j \tag{2.39}$$

Reference [27] stated that based on this approach, the meta distribution can be easily calculated by a simple linear transform of the integer moment vector $(M_j)_{j=0}^{i}$. By adjusting the value of i on can get his aimed accuracy.

Fourier-Jacobi approach

Reference [28] introduced the use of Fourier-Jacobi expansion to express the meta-distribution as an infinite sum of shifted Jacobi polynomials. This approach offers improved accuracy compared to the simple beta approximation method, although the convergence of the latter requires further investigation [27].

Euler sum approach

Reference [29] presents an efficient approach that utilizes the trapezoidal integration rule and Euler sum method to approximate the meta distribution as a finite sum of imaginary moments. With this approach, the meta distribution can be expressed as follows:

$$\bar{F}_{P_s(\eta)}(\epsilon) \simeq \frac{2^{-Q}\exp^{(A/2)}}{\ln^2(\epsilon)} \sum_{q=0}^{Q} \binom{Q}{q} \sum_{n=0}^{N+q} \frac{(-1)^n}{\beta_n} \mathrm{Re}\left[\frac{M_{-s_n/\ln(\epsilon)}}{s_n}\right] \tag{2.40}$$

where the triplet (A, N, Q) are positive integers which can be used to adjust the estimation accuracy. The parameter $\beta_0 = 2$ and $\beta - n = 1$ for $n \in \{1, 2, ..., N + Q\}$. The value $s_n = \frac{A+j2\pi n}{2}$ where $j = \sqrt{-1}$ and $n \in \{0, 1, 2..., N + Q\}$.The estimation error can be controlled within $e - 10$ by well choosing the parameters (A, N, Q).

2.3 Spatial birth-death process

The classical birth-death process [30] is a particular case of continuous-time Markov process, where the state is defined as the number of individuals alive, and the transitions are of only two types: "births" which increase the state by one and "deaths"

which decrease the state by one. The transition rate depends on the number of individuals alive. In a more general sense, the state space can be a point process that we define at the beginning of this chapter, and the configuration of the point process decides the birth rate or death rate. This kind of process is named as spatial birth-death process by Preston in 1975 [21], [31].

Given a metric space $S \subset \mathbb{R}^d$, we consider a point process Φ defined on $(S, \mathcal{B}(S))$, with underlying probability space $(\Omega, \mathcal{F}, \mathbb{P})$. Let $(\mathbb{M}(S), \mathcal{M}(S))$ be a set of counting measures on S. The state space of our process is a subset of $\mathbb{M}(S)$. Note that $(\Omega, \mathcal{F}, \mathbb{P})$ is a complete probability space for both the point process Φ and our birth-death process. A spatial birth-and-death process is a continuous time Markov chain with state space the set of all configurations of Φ. For $n \geq 0$, let $(\mathbb{M}(S)_n, \mathcal{M}(S)_n)$ be the measurable space of all configurations of n points in $S \subset \mathbb{R}^d$. Thus $\mathbb{M}(S) = \cup_{n=0}^{\infty} \mathbb{M}(S)_n$ is the set of all configurations with any number of points in S.

Consider now a continuous time homogeneous Markov chain $\{\Phi(t)\}$ with state space $\mathbb{M}(S)$ defined as follows. If $\Phi(t) = \varphi \in \mathbb{M}(S)_n$ at time t, then after a period of waiting time, $\Phi(t)$ can make a transition only to $\mathbb{M}(S)_{n-1}$ (if there is a death) or to $\mathbb{M}(S)_{n+1}$ (if there is a birth). The intensity function of new arrivals in state φ is denoted $\beta(\varphi)$, where $\beta : \mathbb{M}(S) \to \mathbb{R}_+$ and the death rate is denoted $\delta(\varphi)$, where $\delta : \mathbb{M}(S) \to \mathbb{R}_+$ (with $\delta(0) = 0$). The intensity of the jumps for process $\Phi(t)$ is $\alpha(\varphi) = \beta(\varphi) + \delta(\varphi)$. Note that $\Phi(t)$ is a jump process in the sense that it is constant by parts, right continuous and jumps from one state to another at every transition.

The homogeneous Markov chain $\Phi(t)$ is characterized by the birth and death rates and by a transition kernel $K : \mathbb{M}(S) \times \mathcal{M}(S) \to [0, 1]$, where $K(\varphi, F)$ is the probability to transit to the Borel measurable set $F \subset \mathcal{M}(S)$ starting from state $\varphi \in \mathbb{M}(S)$ at the next transition (or jump). When $\varphi \in \mathbb{M}(S)_n$ we can decompose the kernel in two functions $K_\beta^{(n)}$ and $K_\delta^{(n)}$ defined as follows:

$$K_\beta^{(n)}(\varphi, F) = P\left[\Phi(t+\tau) \in F | \Phi(t) = \varphi, \Phi(t+\tau) \in \mathbb{M}(S)_{n+1}\right] \quad (2.41)$$

$$K_\delta^{(n)}(\varphi, F) = P\left[\Phi(t+\tau) \in F | \Phi(t) = \varphi, \Phi(t+\tau) \in \mathbb{M}(S)_{n-1}\right] \quad (2.42)$$

so that:

$$K(\varphi, F) = \frac{\beta(\varphi)}{\alpha(\varphi)} K_\beta^{(n)}(\varphi, F) + \frac{\delta(\varphi)}{\alpha(x)} K_\delta^{(n)}(\varphi, F) \quad (2.43)$$

The process constructed in the previous section exists uniquely if and only if the Kolmogorov backward equations have a unique solution. Let $Q_t(\varphi, F)$ for $\varphi \in \mathbb{M}(S)$

and $F \in \mathcal{F}$ be the transition function of the process Φ, i.e.,

$$Q_t(\varphi, F) = P[\Phi(t) \in F | \Phi(0) = \varphi]. \tag{2.44}$$

i.e., the probability of being in F at t knowing that the initial configuration is φ. Q_t should be distinguished from K in the sense that Q_t characterizes the transition after t, while K is the transition kernel after a jump. Then Q_t is the solution of Kolmogorov's backward equations:

$$\begin{aligned} &\frac{\partial}{\partial t} Q_t(\varphi, F) = -\{\beta(\varphi) + \delta(\varphi)\} Q_t(\varphi, F) \\ &+ \beta(\varphi) \int Q_t(y, F) K_\beta^{(n)}(x, \mathrm{d}y) + \delta(\varphi) \int Q_t(y, F) K_\delta^{(n)}(x, \mathrm{d}y) \end{aligned} \tag{2.45}$$

Preston noted that the equation may not possess a unique solution, as the lack of uniqueness arises from the potential occurrence of an infinite number of jumps within a finite time with positive probability. However, a specific solution known as the minimum solution exists, where transitions from one state to another are achieved after an infinite number of jumps.

2.4 Device-to-device communication

2.4.1 Framework and standard development

Device-to-device communication enables direct communication between devices without relying on a central network node or base station. In other words, devices communicate with each other directly in a peer-to-peer fashion [32], [33]. This approach is also known as sidelink communication, which differs from traditional downlink and uplink communications.

D2D communication was initially introduced as part of Long-Term Evolution (LTE) by the 3rd Generation Partnership Project (3GPP) in 3GPP Release 12, and has since been developed as part of both the LTE and 5G standards. The LTE standard includes a feature called Proximity Services (ProSe), which allows D2D users to discover other devices in close proximity and communicate with them directly within a cellular network [34]. ProSe has been enhanced in subsequent releases to support features such as multicast and group communications.

In addition to ProSe, the 3GPP has developed a sidelink technology called LTE-V2X in Release 14, which was further enhanced in Release 15 to support LTE Vehicle-to-Everything (LTE-V2X). This technology uses the sidelink radio interface to enable direct communication between vehicles and other devices [35]. With the introduction of 5G New Radio, the 3GPP has developed a new D2D communication technology called 5G NR V2X under Release 16. This technology uses the sidelink to enable high-speed, low-latency communication between devices [36], and supports various use cases such as road safety, traffic efficiency, and infotainment.

5G sidelink builds on the foundation of LTE sidelink and offers many improvements, including lower latency, wider bandwidth, and higher reliability. 5G NR supports Sidelink since Release 16, and enhanced sidelink capabilities were included in Release 17 to provide superior resource allocation, improved power savings, and extended coverage. In recent standard developments for sidelink, device relay has played a key role in extending coverage and improving performance efficiency.

2.4.2 Classification of D2D communication

D2D communication can be implemented in different modes, as illustrated in Figure 2.1. In outband mode, D2D communication uses an unlicensed band outside the cellular spectrum. This avoids interference from the cellular band and is more

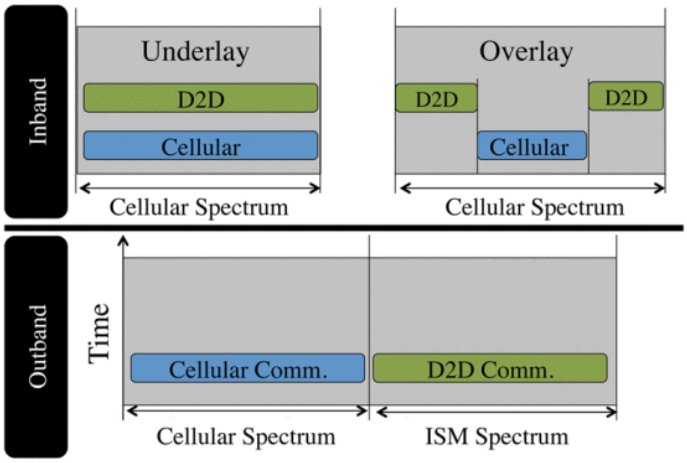

Figure 2.1: Classification of D2D communication. (Figure is from [32]).

suitable for wireless applications in the unlicensed band, such as Internet of Things (IoT). In inband mode, the D2D users and the cellular users share the same spectrum resource. The advantage of inband mode is that it can improve the spectrum efficiency, though interference management remains a problem to be solved. Specifically, one way to employ the inband D2D is the so-called "Overlay D2D", where the licensed spectrum is divided into non-overlapping portions allocated to the D2D users or cellular users. Another method of inband D2D is to underlay the D2D communication with cellular communication, where D2D users and cellular users compete to utilize the same spectrum band. Thus a more robust resource orchestration is needed to guarantee the quality of service of both cellular and D2D users [32]. An important consideration for the application of D2D communication is mode selection, which involves deciding whether to use the traditional cellular mode involving the base station or to operate in the D2D mode. Additionally, determining whether to use D2D communication as inband or outband, and whether to employ underlay or overlay techniques, presents a challenge that requires further investigation. D2D communication in different modes adds varying levels of complexity to network management. In particular, interference management is a significant challenge that must be addressed in such studies. The studies in this thesis focus on the outband mode of D2D communication.

2.4.3 D2D use cases

D2D communication has several potential applications, especially in mobile networks, where it can be used for peer-to-peer direct communication or as a relay in

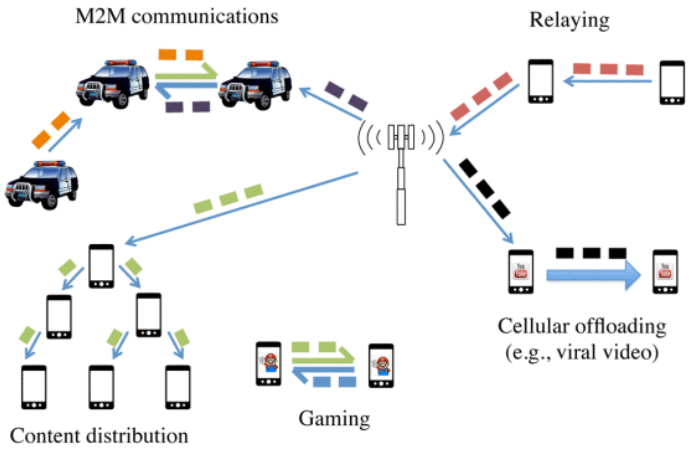

Figure 2.2: D2D applications (Figure is from [32]).

cellular, vehicular, or IoT networks. Below are some examples of D2D applications:

- Proximity-based services (cellular offloading): D2D communication can enable proximity-based services, including location-based advertising, social networking, and mobile gaming. In this scenario, devices are within the communication range of the base station and are using the licensed spectrum for D2D communication. This can help with traffic offloading for the cellular network [33].

- Provision of Emergency Services: This type of application scenario occurs when a user is out of network coverage. D2D communication can provide direct communication for emergency personnel, allowing for faster response times and better coordination during emergencies. The device can establish a D2D link with a device in proximity and relay its transmission to the cellular network.

- Content sharing: D2D communication can facilitate efficient content sharing between devices within a local area network, such as sharing photos, videos, and music files. With D2D communication, users can receive content directly from the base station and relay it to other nearby users, reducing the burden on the cellular network and improving the speed of content sharing. This direct communication between devices can help to reduce latency, resulting in faster and more reliable content delivery.

- Vehicle-to-vehicle (V2V) communication: V2V communication is a critical application of D2D communication in the context of 5G NR V2X communi-

cation. It enables vehicles to communicate directly with each other, sharing information and coordinating movements to avoid collisions. D2D communication allows vehicles to establish direct communication links, resulting in faster communication, lower latency, and better reliability compared to communication through the cellular network. This technology can help improve road safety and traffic efficiency by enabling real-time communication between vehicles [36].

2.5 Millimeter wave communication

Millimeter-wave is a portion of the electromagnetic spectrum with frequencies ranging from 30 GHz to 300 GHz. It is a frequency band much higher than the traditional cellular frequency bands, which typically operate in the sub-6 GHz frequency range. MmWaves have unique characteristics that make them attractive for wireless communication, such as their large bandwidth and ability to support very high data rates. The international telecommunication union (ITU) has designated frequency bands around 60 GHz in different parts of the world. Within the spectrum of millimeter wave, there are several commonly used bands [37]:

- K_a band : $26.5 - 40$ Ghz
- Q band : $33 - 50$ Ghz
- V band : $50 - 70$ Ghz
- W band : $75 - 110$ Ghz
- D band : $110 - 170$ Ghz

These licensed spectrums support bandwidths of up to 400 MHz. In the case of mmWave communication, certain fundamental characteristics arise due to significantly shorter wavelengths compared to the sub-6 GHz band. For example, at 28 GHz, the wavelength measures 10.7 mm, at 60 GHz it is 5 mm, and at 300 GHz, it is 1 mm. The short wavelengths of mmWave offer significant potential for adaptive mmWave antenna arrays with high gain and compact dimensions, provided that the distance between antenna elements exceeds half the wavelength. Typically, the physical size of an antenna is proportional to the wavelength. It is thus possible to use multiple antennas on the device.

A frequently discussed challenge in mmWave communication is severe propagation attenuation caused by millimeter waves. Due to their small wavelength, they are easily absorbed by rain and the atmosphere. It is crucial to study the mmWave channel propagation characteristics for developing 5G wireless communication systems. Large-scale path loss is used to model communication systems across varying distances and frequencies. One common path-loss model is the close-in (CI) free space reference distance model [38], which is a log-distance path loss model shown as follows:

$$PL(f,d)[dB] = FSPL(f,1m)[dB] + 10\alpha \log_{10}(d) + \chi_\sigma \tag{2.46}$$

where α denotes the path-loss exponent,f denotes the frequency, $FSPL(f,1m) = 20\log_{10}(\frac{4\pi f}{c}))$ denotes the free space path-loss in dB at a reference distance 1 m, and c is the speed of light. The path-loss exponent at 28 GHz in urban microcell environment is around 2.3 along the LOS path and is around 2.0 at 73 GHz [39].

Channel coherence time is another significant statistical parameter that describes the time-varying nature of the channel. It represents the duration during which the channel impulse response is considered to remain relatively unchanged [9]. According to Clarke's model power angular spectrum, the channel coherence time is inversely proportional to the maximum Doppler frequency, denoted as f_d, which is determined by the frequency and the velocity of motion, given by $f_d = \frac{vf}{c}$. Consequently, the Doppler effect is more pronounced in high-frequency spectrum, leading to a considerably short coherence time. For example, assuming a speed of 10 km/h, the channel coherence time at 28 GHz is about 0.482 ms [9]. When the frequency is 71 GHz, the coherence time drops to 0.19 ms. These values are much shorter than a typical slot duration of 1 ms.

Overall, it is necessary to consider the specific characteristics of mmWave technology when studying the network performance of mmWave networks.

2.6 Beamforming

The basic idea of beamforming involves manipulating the phase and amplitude of the signal transmitted by an array of antennas to create a beam or pattern of radiation in a specific direction. This enables mmWave signals to be transmitted and received with higher gain, signal-to-noise ratio, and resistance to interference and blockage. The beam shape can be either static or dynamically varying. In cellular networks,

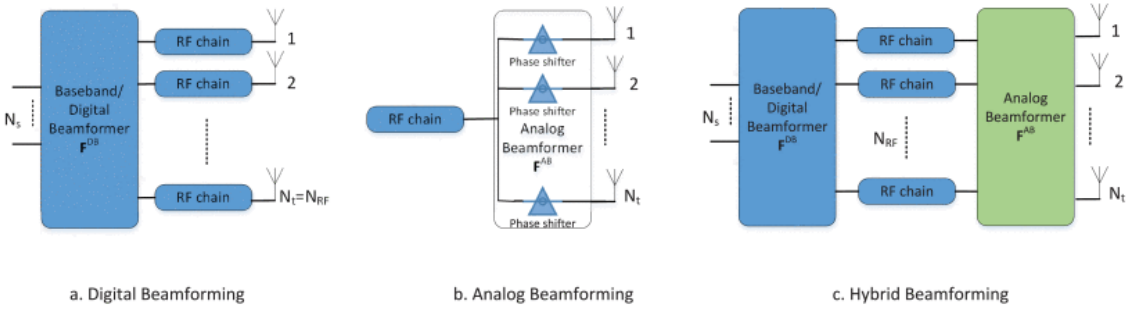

Figure 2.3: Beamforming architectures: (a) Digital beamforming, (b) Analog beamforming, (c) Hybrid beamforming. (Figure is from [41])

static beamforming is commonly used with a narrow main beam in the vertical domain and a wide sector coverage in the horizontal domain to serve multiple users simultaneously, known as multi-user beamforming. On the other hand, dynamic beamforming provides more flexibility in tailoring the beam shape to suit different scenarios, taking into account the mobility of objects and channel variations [13].

In analogue beamforming, several antenna elements are connected via phase shifters to a single radio-frequency chain, in which only the phase of the signals can be adjusted at each antenna element to form a single beam. The codebook of beamformers, usually constructed based on digital Fourier transform, shapes a beam whose main lobe points at the target user. Analogue beamforming is one of the simplest methods to implement beamforming, and it can be implemented at both transmitter and receiver sides with low cost and low complexity. In mmWave propagation, the multipath scenario is less prominent compared to sub-6G spectrum communication, resulting in less diversity gain to exploit. Therefore, analogue beamforming is well-suited for line-of-sight (LOS) scenarios in mmWave communication.

However, under the context of more complicated channel conditions with multiple paths, analogue beamforming is no more optimal. Digital beamforming [40] has more flexibility. The amplitude and phase variation is done in the baseband by digital precoding and each antenna element of the array is equipped with an radio-frequency chain that can multiply a weight to its signal. Therefore, multiple streams can be sent simultaneously, and there is no more typical beam shape under this context. It also involves the possibility to have different beams for different parts of a frequency carrier [13]. In contrast to analogue beamforming, digital beamforming suffers from a higher implementation complexity.

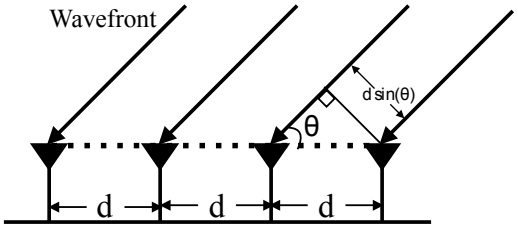

Figure 2.4: Uniform linear array structure.

In order to combine the economic advantage of analogue beamforming and the flexibility of digital beamforming, hybrid beamforming is proposed [42]. Such beamforming has fewer radio-frequency chains than digital beamforming, where a phase-shifter connects different radio-frequency chains and antenna elements. To sum up, hybrid beamforming aims at balancing the complexity vs. performance tradeoff between digital beamforming and analogue beamforming.

2.6.1 Uniform linear array

A uniform linear array (ULA) is a type of antenna array where a number of individual antennas are placed in a straight line with equal spacing between adjacent elements. Each element of the array receives signals with slightly different phase shifts, resulting in a focused radiation pattern in a particular direction. A ULA is commonly used in applications such as radar systems, direction finding, and wireless communication systems, where high directional gain and spatial selectivity are required. The performance of a ULA depends on the spacing between the antennas, the frequency of operation, and the number of elements in the array. By adjusting the phase and amplitude of the signals, a beam can be formed that is focused in a specific direction, maximizing the signal strength in that direction while minimizing it in other directions. Thus, a ULA is an ideal array geometry for beamforming due to its inherent structure and the ability to manipulate the signals received by each element in the array.

As shown in Figure 2.4, for each one-diemensional array, n antenna elements are aligned along a straight line and are uniformly spaced with distance d. Considering the arrays at the transmitter side first, in the direction θ with respect to the axis of the ULA, the far-field pattern f_a^T of the array is the sum of n plane waves emitted

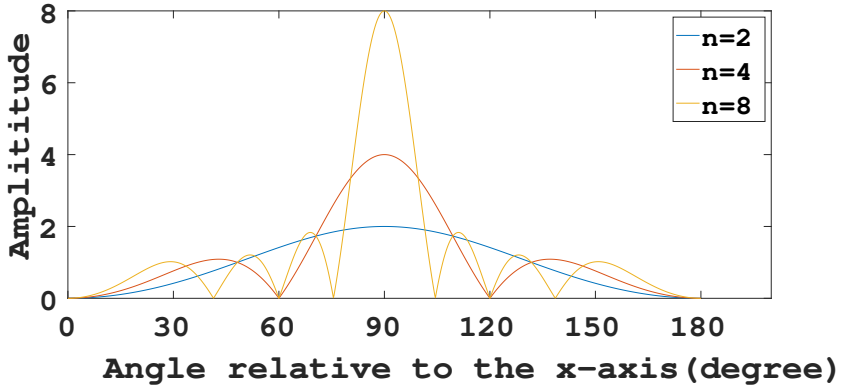

Figure 2.5: Power pattern of ULA.

by each element:

$$f_a^T(\theta) = \frac{1}{\sqrt{n}} f_e(\theta) \sum_{i=1}^{n} a_i e^{j((i-1)kd\cos\theta)} \tag{2.47}$$

where $f_e(\theta)$ is the field pattern at every antenna element; $k = 2\pi/\lambda$ where λ is the wavelength and a_i is a phase offset applied at antenna element i. The term $1/\sqrt{n}$ is a normalization factor to account for the power split among the n antenna elements. Choosing $a_i = e^{-j((i-1)kd\cos\theta_0^T)}$ as a beam steering vector, where θ_0^T is the boresight direction of the ULA. Then the power gain $g_a^T(\theta, \theta_0^T) = |f_a^T(\theta)|^2$ is given by:

$$g_a^T(\theta, \theta_0^T) = \frac{1}{n} g_e(\theta) \left| \frac{\sin(nk\frac{d}{2}(\cos\theta - \cos\theta_0^T))}{\sin(k\frac{d}{2}(\cos\theta - \cos\theta_0^T))} \right|^2 \tag{2.48}$$

where $g_e(\theta)$ is the power pattern of an antenna element. The maximum array factor gain for the transmitter is achieved for $\theta = \theta_0^T$ [43]. Thus, the maximum gain of the transmitters antenna is $g_a^T(\theta_0^T, \theta_0^T) = g_e n$.

Now for the receiver antenna, there is no need to divide the power into n parts. So the power of the received signal is given by:

$$g_a^R(\theta, \theta_0^R) = g_e(\theta) \left| \frac{\sin(nk\frac{d}{2}(\cos\theta - \cos\theta_0^R))}{\sin(k\frac{d}{2}(\cos\theta - \cos\theta_0^R))} \right|^2 \tag{2.49}$$

Similarly, the maximum array factor gain is achieved for $\theta = \theta_0^R$. Then, the maximum gain is $g_a^R(\theta_0^R, \theta_0^R) = g_e n^2$.

Figure 2.5 displays the power pattern of a transmitter, expressed by formula (2.48), for varying numbers of antenna elements. In Figure 2.6, this pattern is presented in polar coordinates. The figure demonstrates that as the number of antennas increases, the maximum power of the ULA also increases, but the main

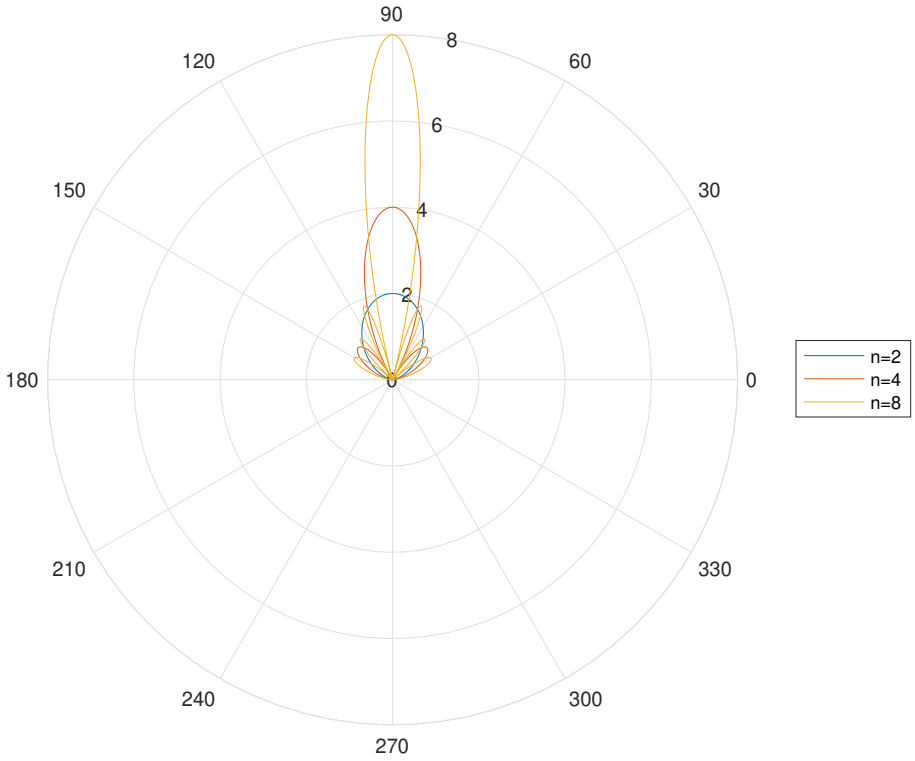

Figure 2.6: Power pattern of ULA in polar coordinate.

beam becomes narrower. This change can lead to better signal quality and reduced interference in wireless systems.

Chapter 3

Spatio-temporal wireless D2D network With beamforming

In this chapter, we investigate the beam misalignment impacts of a dynamic D2D communication network, where both transmitters and receivers adopt beamforming by using ULA. A time continuous dynamic model is adopted for this analysis. We use tools of stochastic geometry and the Miyazawa rate conversation law to analyse the stability condition of such a network. An analytical expression of the critical arrival rate is given under a uniform or truncated Gaussian alignment error assumption. Our analytical and numerical findings demonstrate that in the case of perfect beam alignment, the critical arrival rate can grow indefinitely with an increasing number of antenna elements. However, when the beam alignment is imperfect, the critical arrival rate no longer exhibits an unbounded increase. Closed-form expressions of the upper bounds for critical arrival rates are given for both the uniform and the truncated Gaussian misalignment models.

3.1 Introduction

Device-to-device communications emerge as a promising technology to improve the spectral efficiency of next generation cellular networks. Since it allows direct communication between nearby devices, this technique is the basis of new proximity based services. As the number of D2D transmissions increases, it becomes more and more difficult to meet stringent quality of service requirements, such as those foreseen for URLLC in 5G.

A solution to improve the networks performance is beamforming. Several papers in the literature show the great potential of beamforming for D2D communications for reducing interference and improving network throughput, see e.g. [11][12]. It is still an open issue to study the randomness of large scale networks with D2D communication, when there are massive access of random located users using beamforming with various communication demands.

Since the main lobe of the beam usually is narrow, it is evident that the misalignment error can cause significant impacts on the performance of the network. However, due to the estimation errors of the directions and other hardware limitations, the beam alignment error cannot be neglected. Paper [5] shows that for a Poisson bipolar network, the beam alignment error can significantly impact the throughput and the coverage. Similar works are done to evaluate the coverage and rate performance of D2D or cellular networks in the presence of beam alignment error [44], [45]. Besides the flat-top antenna power pattern model proposed in [46], paper [5] also models the directional antenna pattern using a cosine function in order to obtain a more accurate array power pattern. A uniform beam alignment error model and a Gaussian beam alignment error model are studied in [5], [44].

Most existing works that study the QoS of D2D communication focus on the analysis of rate and coverage [6], [47]. These works study the average performance of the network, given a static configuration of device locations. The methods of stochastic geometry are applied in these studies. Some works study more dynamic cases [48] [49], where each device has a dynamic queue of packets to transmit. In these works, networks are modeled as classical queue interacting problems [50], where time is slotted and thus considered as discrete. A weakness of this model lies in the constant number of users throughout time. In a more realistic network model, users arrive at random locations, at random time instants, with a random amount of data to be transmitted and leave the network when the transmission is over.

Thus, a spatial birth-death wireless network [20] is proposed to model this network as a continuous-time spatial birth-death process [21], which is briefly introduced in chapter 2. The stability condition of a a spatial birth-death wireless network is given in [20] without considering the application of beamforming.

3.2 Contributions

Here, we extend the results of [20] to D2D networks equipped with directional antenna arrays and the impacts of imperfect beam alignment is considered. Our contributions can be summarized as follows:

- We propose a beamforming model for D2D communications based on the ULA model, which is tractable from a stochastic geometry point of view.
- We propose a uniform beam alignment model and a truncated Gaussian beam alignment model for continuous-time spatial birth-death D2D networks.
- We derive new critical arrival rates for this D2D network as a function of the number of antenna elements by considering the aforementioned beam alignment models. For each beam alignment error model, a closed-form expression of the critical arrival rate's upper bound is given.
- Our analytical and numerical results show that beamforming extends the stability region of D2D networks and the critical arrival rate is increasing with the number of antennas.
- Our analytical and numerical results also show that the beam misalignment reduces the stability region of D2D networks with beamforming. Although we confirm that the critical rate is an increasing function of the number of antennas, we highlight an upper bound which depends on the antenna alignment error amplitude.

In the rest of this chapter, we introduce the system models in section 3.3. Section 3.4 presents the stability criteria. Section 3.5 derives upper bounds of the critical arrival rate. The numerical results are shown in section 3.6. Section 3.7 concludes the chapter.

3.3 System Model

3.3.1 Spatial birth-death process

Chapter 2 has given a general introduction to the spatial birth-death process. Here, we present its application to model a dynamic wireless network. The spatial birth-death process is a generalized birth-death process that considers the spatial locations of the individuals. Specifically, the birth rate and the death rate of the process depend on the spatial configuration of the individuals at each time instant. Consider a 2-dimension Poisson bipolar network, as shown in Figure 3.1 [18], where the transmitter-receiver D2D user pairs live in a two-dimensional Euclidean plane $\mathbf{S}$, $\mathbf{S} \subset \mathbb{R}^2$. Each transmitter has a file of random size to transmit to its associated receiver. This network is categorized as a birth-death process since the time instants at which it appears and leaves the network are random for each pair. We use the Poisson process with arrival rate $\lambda|\mathbf{S}|$ to model the 'birth' (or arrival) time instants of the transmitter-receiver pairs, where $\lambda \in \mathbb{R}^+$ is the arrival rate per unit of area.

Once a pair appears in the network, it starts the file transmission. For all the pairs, the file size is assumed to be an i.i.d. random variable following an exponential law of mean L bits. The transmission rate of each pair is dynamic following the Shannon rate, where the interference comes from other active pairs. When the transmission is finished, the pair leaves the network immediately. The sojourn time, denoted by W_s, is defined as the time interval from the 'birth' to the 'death' of each D2D pair. Moreover, the appearing positions of the transmitter-receiver pairs also form a homogeneous Poisson point process. We assume that the transmitter devices are uniformly distributed on the disks centered around the receivers of radius r, where r is supposed to be a constant in our studies.

The spatial birth-death process is known to be a continuous-time Markovain chain (CTMC) [21], whose states are the position configurations of the pairs. At each time instant t, the positions of pairs can be interpreted as a marked point process $\Phi_t = \sum_{i=1}^{N_t} \delta(x_i, y_i)$, where $N_t = \Phi_t(\mathbf{S})$ is the number of active pairs in the plane at time t; x_i denotes the position of the i-th active receiver; the mark y_i denotes the transmitter location of the i-th pair; $\delta(\cdot)$ is the Dirac measure. Thus the process $\Phi_t(\mathbf{S})$ is a classical birth-death process defined as a counting measure.

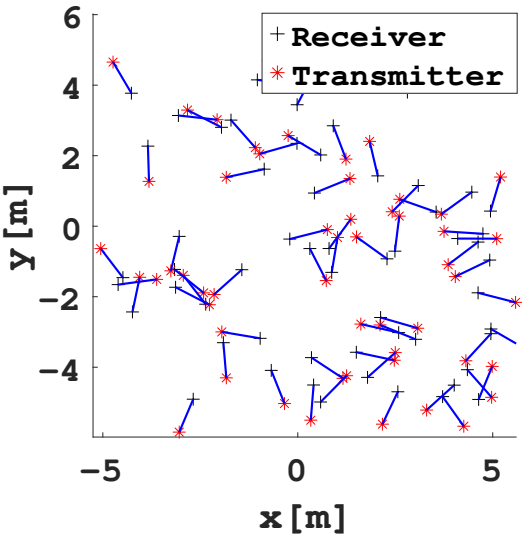

Figure 3.1: Poisson bipolar network

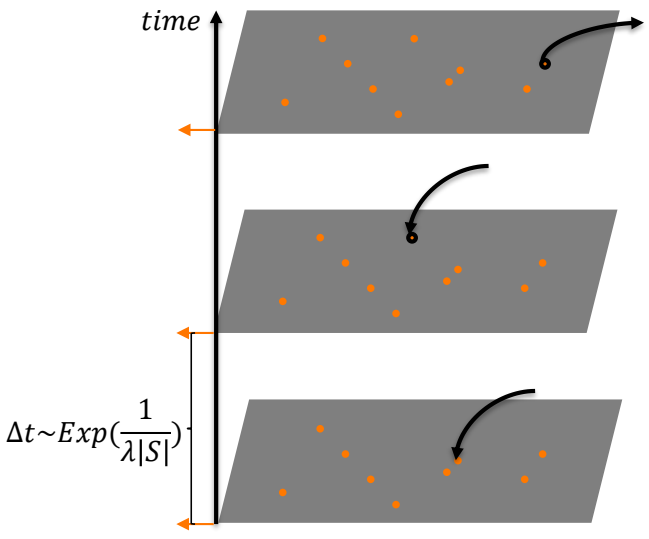

Figure 3.2: Arrivals and departures of transmitter-receiver pairs in a spatial birth-death wireless network.

3.3.2 Beamforming

We consider a point-to-point system in free-space with LOS propagation. Both the transmitter and the receiver sides are equipped with 1-dimensional ULA. For each array, n antenna elements are aligned along a straight line and are uniformly spaced with distance d. The model of ULA has been presented in chapter 2. Here we recall its power patterns. Considering the arrays at the transmitter side first, in the direction θ with respect to the axis of ULA, the power gain $g_a^T(\theta, \theta_0^T) = |f_a^T(\theta)|^2$ is given by:

$$g_a^T(\theta, \theta_0^T) = \frac{1}{n} g_e(\theta) \left| \frac{\sin(nk\frac{d}{2}(\cos\theta - \cos\theta_0^T))}{\sin(k\frac{d}{2}(\cos\theta - \cos\theta_0^T))} \right|^2 \tag{3.1}$$

where $g_e(\theta)$ is the antenna power pattern. If we assume a rectangular patch antenna, the antenna radiation pattern is hemispheric and has a directivity of 2 [22]. Hence, we now assume $d = \lambda/2$ and the power pattern of an antenna element g_e is defined as follows:

$$g_e(\theta) = \begin{cases} 2, & \theta \in [0, \pi] \\ 0, & \text{otherwise} \end{cases} \tag{3.2}$$

The maximum array factor gain for the transmitter is achieved for $\theta = \theta_0^T$ [43]. Thus, the maximum gain of the transmitters antenna is $g_a^T(\theta_0^T, \theta_0^T) = 2n$. For the receiver antenna, the power of the received signal is given by:

$$g_a^R(\theta, \theta_0^R) = g_e(\theta) \left| \frac{\sin(nk\frac{d}{2}(\cos\theta - \cos\theta_0^R))}{\sin(k\frac{d}{2}(\cos\theta - \cos\theta_0^R))} \right|^2 \tag{3.3}$$

We use the same value of g_e as in (3.2). Then, the maximum gain is $g_a^R(\theta_0^R, \theta_0^R) = 2n^2$.

3.3.3 Beam alignment error distribution

We now align the direction of the array's maximum radiation at the transmitter side to the direction of its associated receiver by setting θ_0^T to be the angle of departure (AoD) ξ with respect to the array's axis. At the receiver side, we set $\theta_0^R = \psi$ to align the main beam of the receiver towards its transmitter, where ψ is the angle of arrival (AoA) with respect to the axis of ULA. To simplify the calculation, we suppose that all the antenna arrays are set to be broadside array antennas, where $\theta_0^T = \theta_0^R = \pi/2$. Devices then try to adjust their directions so that the axes of the corresponding antenna arrays are parallel to each other and the main lobes are aligned with each

other. However, due to potential errors in the estimation of AoD and AoA, the main antenna lobes may not be perfectly aligned (see Figure 3.3, where the BAE is denoted as e). Hence, we assume that ξ and ψ are two random variables with the same mean of $\pi/2$. In other words, we suppose that there are estimation errors for the exact directions of the devices. The center of the error regions is the main beam directions of the concerned devices. Moreover, the alignment error distribution is supposed to be identical not only for both transmitter and receiver sides but also for all the device pairs. This assumption is reasonable since all the devices are i.i.d. distributed with similar environmental conditions in the network.

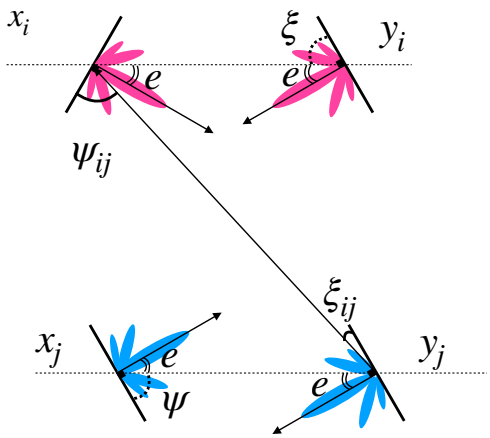

Figure 3.3: Two D2D transmitter-receiver pairs at $[x_i, y_i]$ and $[x_j, y_j]$. For each receiver/transmitter, ψ/ξ represents the AoA/AoD of the plane wave from/to the corresponding transmitter/receiver, which has an error difference e with its maximum radiation direction (broadside direction in the figure). ψ_{ij}/ξ_{ij} is the direction of interfering transmitter/receiver.

Denote the probability density function (PDF) of ξ as f_ξ and the PDF of ψ as f_ψ. Then the mean of transmitter's antenna gain in the direction ξ is:

$$\mathbb{E}[g_a^T(\xi, \theta_0^T)] = \int_{-\pi}^{\pi} g_a^T(x, \theta_0^T) f_\xi(x) \mathrm{d}x \tag{3.4}$$

The mean of the receiver's antenna gain at the direction ψ is:

$$\mathbb{E}[g_a^R(\psi, \theta_0^R)] = \int_{-\pi}^{\pi} g_a^R(x, \theta_0^R) f_\psi(x) \mathrm{d}x \tag{3.5}$$

Two beam alignment error distributions are studied in this paper, namely the uniform distribution and the truncated Gaussian distribution.

Uniform beam alignment error

We assume that the error occurs with the same likelihood in a certain error region. This model is used where only some prior information about the error limits are known. Thus we have $\xi \sim U(\theta_0^T - \epsilon, \theta_0^T + \epsilon)$ and $\psi \sim U(\theta_0^R - \epsilon, \theta_0^R + \epsilon)$, where ϵ is the error limit.

Truncated Gaussian beam alignment error

According to the central limit theorem, the Gaussian distribution can properly estimate the beam errors induced by multiple independent sources. We assume that the errors have a span from $-\pi$ to π. The PDF of ξ can be expressed by using the truncated Gaussian distribution [51]:

$$f_\xi(x) = \frac{1}{\sqrt{2\pi}\sigma} \frac{\exp(-\frac{1}{2}(\frac{x-\theta_0^T}{\sigma})^2)}{erf(\frac{\pi}{\sqrt{2}\sigma})}, x \in [\theta_0^T - \pi, \theta_0^T + \pi] \tag{3.6}$$

Similarly, we have $f_\psi(x)$ of the same form:

$$f_\psi(x) = \frac{1}{\sqrt{2\pi}\sigma} \frac{\exp(-\frac{1}{2}(\frac{x-\theta_0^R}{\sigma})^2)}{erf(\frac{\pi}{\sqrt{2}\sigma})}, x \in [\theta_0^R - \pi, \theta_0^R + \pi] \tag{3.7}$$

where $erf(\cdot)$ is the Gaussian error function defined as $erf(x) = \frac{2}{\sqrt{\pi}} \int_0^x e^{-t^2} \mathrm{d}t$.

3.3.4 Transmission rate

Consider a Line-of-Sight propagation environment with no multi-path fading. We denote the path-gain function as $\ell(\cdot) : \mathbb{R} \to \mathbb{R}$. All the transmitter devices use the same frequency and have the same transmission power P. Let G_{ij}^T denote the antenna gain of a transmitter located at y_j, in the direction of a receiver located at x_i. The corresponding antenna gain of the receiver at x_i for the same path is denoted as G_{ij}^R. As shown in Figure 3.3, for a plane wave departing from y_j towards x_i, the AoD and the AoA with respect to the axis of ULA are denoted as ξ_{ij} and ψ_{ij}, respectively. Hence we have $G_{ij}^T = g_a^T(\xi_{ij}, \theta_0^T)$ and $G_{ij}^R = g_a^R(\psi_{ij}, \theta_0^R)$. Thus the interference at a receiver located at x_i can be written:

$$I^{BF}(x_i, \Phi_t) = \sum_{[x_j, y_j] \in \Phi_t, i \neq j} G_{ij}^T G_{ij}^R P \ell(\|x_i - y_j\|) \tag{3.8}$$

Let B denotes the bandwidth and $\mathcal{N}_0$ denotes the noise power density. The expression of the transmission rate for a pair at $[x_i, y_i]$ is:

$$R^{BF}(x_i, \Phi_t) = W \log_2 \left(1 + P \frac{G_{ii}^R G_{ii}^T \ell(r)}{\mathcal{N}_0 W + I^{BF}(x_i, \Phi_t)}\right) \tag{3.9}$$

Note that $G_{ii}^T = g_a^T(\xi, \theta_0^T)$ and $G_{ii}^R = g_a^R(\psi, \theta_0^R)$.

3.4 Stability criterion

Since a spatial birth-death process can be characterized as a Markov chain, it is crucial to know whether it has a stationary regime. The critical arrival rate λ_c is defined as the threshold of arrival rate such that the spatial birth-death process Φ_t is stable if and only if $\lambda < \lambda_c$. In [20], a closed-form expression of the critical rate is given for the network that we describe in section 3.3.1 without beamforming:

$$\lambda_c = \frac{W\ell(r)}{\ln(2)La}, \tag{3.10}$$

where $a = \int_{\mathbf{S}} \ell(\|x\|)dx$. In other words, all the users in such a network can finish their file transmissions within the limit time interval, if and only if $\lambda < \lambda_c$. Otherwise, the system is unstable, and the number of active pairs tends to infinity. In this work, we extend the stability criteria to the network under the beamforming paradigm in section 3.3.2, and calculate the critical arrival rate for the case with or without beam misalignment.

Proposition 12. *The critical arrival rate under the beamforming paradigm in section 3.3.2 for the case without beam misalignment is given as follows:*

$$\lambda_c^{BF}(n) \quad = \quad \frac{G_{max}^R G_{max}^T W\ell(r)}{\ln(2)L\mathbb{E}[a^{BF}]} \tag{3.11}$$

where $G_{max}^R = 2n^2$ and $G_{max}^T = 2n$. $\mathbb{E}[a^{BF}]$ is the integral over $\mathbf{S}$ of the path-gain function amplified with BF:

$$\mathbb{E}[a^{BF}] = \frac{a}{4\pi^2}\int_{-\pi}^{\pi} g_a^T(\theta, \theta_0^T)d\theta \int_{-\pi}^{\pi} g_a^R(\eta, \theta_0^R)d\eta \tag{3.12}$$

Proposition 13. *For the network with the beam misalignment, the new critical arrival rate can be expressed as follows:*

$$\hat{\lambda}_c^{BF}(n) \quad = \quad \frac{\mathbb{E}[g_a^T(\xi, \theta_0^T)]\mathbb{E}[g_a^R(\psi, \theta_0^R)]W\ell(r)}{\ln(2)L\mathbb{E}[a^{BF}]} \tag{3.13}$$

where $\mathbb{E}[g_a^T(\xi, \theta_0^T)]$ and $\mathbb{E}[g_a^R(\psi, \theta_0^R)]$ are given by (3.4) and (3.5), which are functions of n.

Theorem 14. *Assuming the ULA model with n antenna elements, when there is no beam alignment error, the spatial birth-death process Φ_t admits no stationary regime if $\lambda > \lambda_c^{BF}(n)$. When there is beam alignment error, the spatial birth-death process Φ_t admits no stationary regime if $\lambda > \hat{\lambda}_c^{BF}(n)$.*

Proof: See Appendix A.

3.5 Performance analysis

According to formula (3.11), the critical arrival rate rises as a function of the number of antenna elements n if there is no beam alignment error. For the extreme case, λ_c^{BF} can increase to infinity when n tends to infinity. In contrast to this result, we will show that the critical arrival rate $\hat{\lambda}_c^{BF}$ can no longer increase without limit, considering the imperfect beam alignment.

3.5.1 Uniform beam alignment error

When the error is limited in a region $[-\epsilon, \epsilon]$ and $\theta_0^T = \theta_0^R = \frac{\pi}{2}$, the critical arrival rate can be expressed as follows:

$$\hat{\lambda}_c^{BF}(n) = \begin{cases} \dfrac{\pi^2\lambda_c}{\epsilon^2}\left(\dfrac{\int_{\pi/2-\epsilon}^{\pi/2+\epsilon}\left|\frac{\sin(\frac{1}{2}n\pi\cos\theta)}{\sin(\frac{1}{2}\pi\cos\theta)}\right|^2 \mathrm{d}\theta}{\int_0^{\pi}\left|\frac{\sin(\frac{1}{2}n\pi\cos\theta)}{\sin(\frac{1}{2}\pi\cos\theta)}\right|^2 \mathrm{d}\theta}\right)^2, & \epsilon \le \pi/2 \\ \dfrac{\pi^2\lambda_c}{\epsilon^2}, \quad \epsilon > \pi/2 \end{cases} \tag{3.14}$$

Since the part in the brackets is less than 1, the critical arrival rate λ_c^{BF} has an upper bound:

$$\hat{\lambda}_c^{BF}(n) \le \frac{\pi^2\lambda_c}{\epsilon^2} \tag{3.15}$$

3.5.2 Truncated Gaussian beam alignment error

When the errors have distributions given by (3.7) and (3.8), the critical arrival rate can be expressed as follows:

$$\hat{\lambda}_c^{BF}(n) = \frac{2\pi\lambda_c}{\sigma^2 erf^2(\frac{\pi}{\sqrt{2}\sigma})} \times \left(\frac{\int_0^{\pi}\left|\frac{\sin(\frac{1}{2}n\pi\cos\theta)}{\sin(\frac{1}{2}\pi\cos\theta)}\right|^2 \exp(-\frac{1}{2}(\frac{\theta-\frac{\pi}{2}}{\sigma})^2)\mathrm{d}\theta}{\int_0^{\pi}\left|\frac{\sin(\frac{1}{2}n\pi\cos\theta)}{\sin(\frac{1}{2}\pi\cos\theta)}\right|^2 \mathrm{d}\theta}\right)^2 \tag{3.16}$$

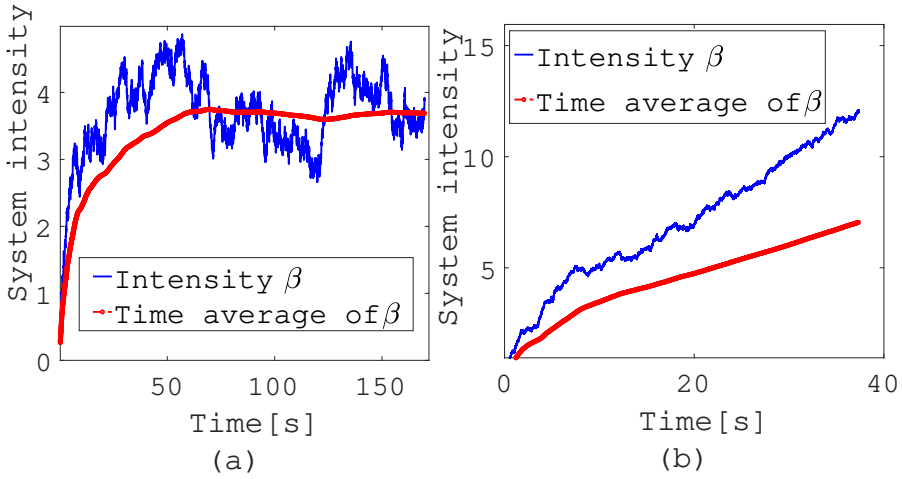

Figure 3.4: β as a function of time when $\lambda = 32\lambda_c$ (a), and when $\lambda = 38\lambda_c$ (b), where $n = 4$, $\lambda_c^{BF} = 35.35\lambda_c$.

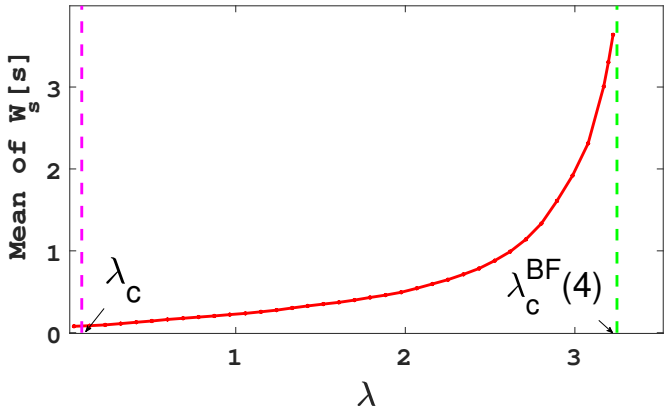

Figure 3.5: Average of sojourn time W_s as a function of λ with $n = 4$.

Since the exponential coefficient in the brackets is non-negative and less than 1, $\hat{\lambda}_c^{BF}$ has an upper bound as follows:

$$\hat{\lambda}_c^{BF}(n) \leq \frac{2\pi\lambda_c}{\sigma^2 erf^2(\frac{\pi}{\sqrt{2}\sigma})} \tag{3.17}$$

3.6 Numerical results

In this section, we numerically illustrate our theoretical results. Our simulator works on a square plane $\mathbf{S} = [-Q, Q]^2, Q \in \mathbb{R}^+$. As explained in section 3.3.1, there are two types of events in a spatial birth-death process: arrivals of new device pairs and departures of pairs that have finished their transmissions. The configuration of Φ_t only changes when these two events arise, so do the transmission rates of the device pairs. The 'birth' events follow a Poisson process of rate $\lambda|\mathbf{S}|$, so the inter-arrival

time t_a follows the exponential law of mean $\frac{1}{\lambda|\mathbf{S}|}$ in seconds. The time interval t_d from time t to the next 'death' is estimated as the minimum delay that any pair finishes its file transmission using the transmission rate imposed by Φ_t. So the mechanism of the simulator states that, after each 'birth' event, we compare t_a and t_d. Once t_a is less than t_d, we add a new device pair at a random position in $\mathbf{S}$. Otherwise, we delete the pair that finishes its transmission. We then update the transmission rates, the remaining file sizes, and the time interval to the next 'birth' or 'death'. The total number of active pairs $\Phi_t(\mathbf{S})$ and the time t are recorded when these events occur. For each pair, we adopt (3.10) to calculate the transmission rate. The AoDs ξ and AoAs ψ are set to be random variables whose means are θ_0^T and θ_0^R ($\theta_0^T = \theta_0^R = \pi/2$).

We simulate the birth-death process Φ_t in forward time, based on the system model described in section 3.3.1. In order to avoid border effects, the network area is transformed in a torus. If Φ_t is stable then it admits a stationary regime Φ_0. We denote β the intensity of this spatial point process Φ_0. The value of β can be estimated by observing the value $\mathbb{E}[\frac{\Phi^0(\mathbf{S})}{\|S\|}]$. We can thus observe the sample path of the intensity function $\beta(t) = \frac{\Phi_t(\mathbf{S})}{\|\mathbf{S}\|}$, which is a time series. If the time average value of $\beta(t)$ converges to be a constant, the process Φ_t is ergodic and has a unique stationary regime. This is known to be the first order property of the stationary point process [52].

The form of the path-loss function $\ell(\cdot)$ should be carefully chosen to keep the value of $a = \int_{x\in\mathbf{S}} \ell(\|x\|)dx$ bounded. In our simulation we take a bounded path-loss model $\ell(r) = (1+r)^{-4}$. The network plane $\mathbf{S}$ is considered to be a square centered at the origin. The length of $\mathbf{S}$ is $2Q$ and $Q = 10$ meters in our simulation. The pair distance r is chosen as 1 meter. The average file size is $L = 1$ Mbits. Other parameters are the bandwidth $W = 1$ MHz, the noise power $W\mathcal{N}_0 = -100$ dBm, and the transmission power $P = 20$ dBm.

3.6.1 Impact of beamforming without misalignment

We first consider the D2D network with perfect aligned beamforming. In Figure 3.4, we show a case where the number of antenna elements is $n = 4$. According to (3.11), we get $\lambda_c^{BF} \approx 35.35\lambda_c$. In Figure 3.4 (a), we set $\lambda = 32\lambda_c$. The blue curve shows the intensity function $\beta(t)$, and the red curve is its time average trajectory expressed as $\bar{\beta}(t) = \frac{\int_0^t \beta(t)}{t}$. It illustrates clearly that Φ_t admits a stationary regime, since $\bar{\beta}(t)$

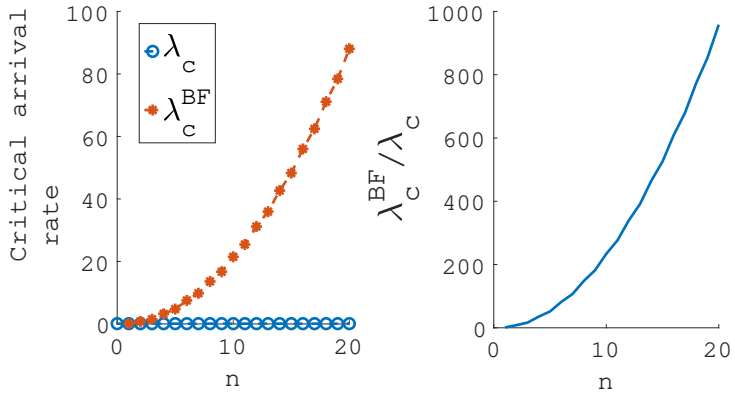

Figure 3.6: Critical arrival rates $\lambda_c^{BF}(n)$, λ_c and $\lambda_c^{BF}(n)/\lambda_c$ as a function of n.

reaches a limit. When the arrival rate exceeds $\lambda_c^{BF}(n)$, like in Figure 3.4 (b), where $\lambda = 38\lambda_c$, the Markov chain is not time ergodic and $\beta(t)$ grows indefinitely. This is due to the fact that the increase of arrivals causes more interference in the network which reduces the total network throughput, to such extent that the load exceeds the network capacity.

Another approach to verify the stability of the process is to study the sojourn time W_s. According to the little law, $\beta = W_s\lambda$ when this system queue is stable. This means that W_s should be bounded to keep β bounded. The average of W_s taken among all the pairs in one realisation is shown in Figure 3.5. The average of W_s goes to be infinity when the arrival rate gets close to $\lambda_c^{BF}(n)$, which verifies our stability condition.

The impact of beamforming is significant in terms of the expansion of the stability region. In Figure 3.6, we show $\lambda_c^{BF}(n)$ and λ_c as functions of the number of antenna elements n, where λ_c is a constant. The value of $\lambda_c^{BF}(n)$ increases dramatically when n increases, since (3.11) is an increasing function of n.

3.6.2 Impact of beam misalignment

In Figure 3.7, we show $\beta(t)$ as a function of time (blue curves), and the moving average of $\beta(t)$ (red curves), where the uniform beam alignment error is taken into account. It is shown in Figure 3.7(a) that $\beta(t)$ doesn't grow indefinitely to infinity when λ is less than $\hat{\lambda}_c^{BF}$, which illustrates that Φ_t is stable. Figure 3.7(b) shows that the population of active pairs in the plane and β tends to infinity when $\lambda > \hat{\lambda}_c^{BF}$. Thus, we confirm the result of Theorem 14 and the expression of $\hat{\lambda}_c^{BF}$ in (3.14). In the same way, we confirm the expression of the critical arrival rate $\hat{\lambda}_c^{BF}$ given in (3.16)

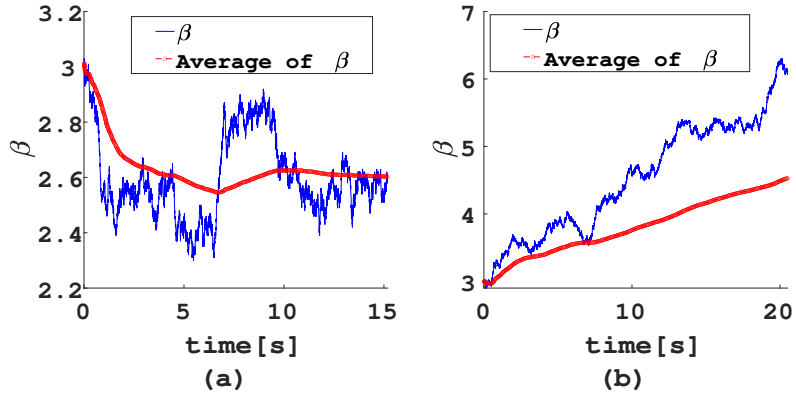

Figure 3.7: System intensity β as a function of time for network with Uniform beam alignment error. (a) $\lambda = 0.9\hat{\lambda}_c^{BF}$; (b) $\lambda = 1.1\hat{\lambda}_c^{BF}$, where $\epsilon = 0.2\pi$, $n = 4$, $\hat{\lambda}_c^{BF} = 1.8258$ ($\lambda_c^{BF} = 12.9721$ without misalignment).

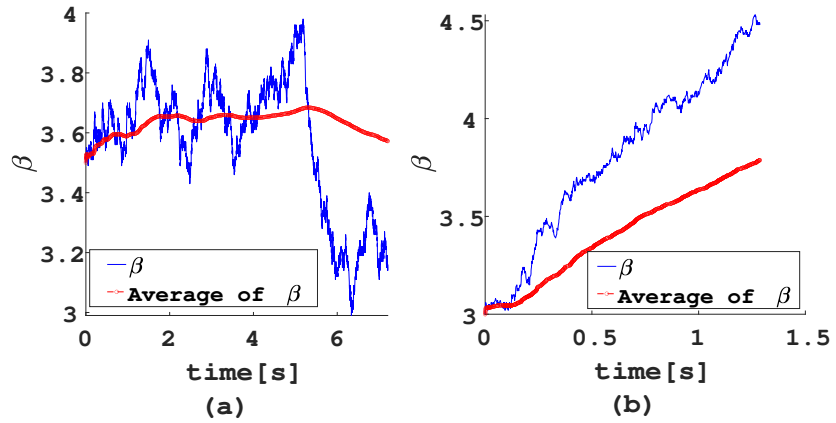

Figure 3.8: System intensity β as a function of time for network with truncated Gaussian beam alignment error. (a) $\lambda = 0.9\hat{\lambda}_c^{BF}$; (b) $\lambda = 1.1\hat{\lambda}_c^{BF}$, where $\sigma = 0.3$, $n = 4$, $\hat{\lambda}_c^{BF} = 3.7737$ ($\lambda_c^{BF} = 12.9721$ without misalignment).

by Figure 3.8, under the assumption of a truncated Gaussian beam alignment error.

Figures 3.9 and 3.10 show the ratio between the critical arrival rate with beamforming $\hat{\lambda}_c^{BF}$ and without beamforming λ_c for the uniform and truncated Gaussian beam alignment error models, respectively. The solid red curve assumes a perfect alignment of beams; it increases and tends to infinity as the number of antenna elements increases to infinity. This is because when n increases, the maximum antenna array gain increases and, as the beam becomes thinner, interference is reduced. When a beam alignment error is assumed, the ratio is still increasing, but it is also upper bounded by and tends toward a value that depends on the magnitude of the error. The larger the extent of the error, the lower the upper limit. Suppose the

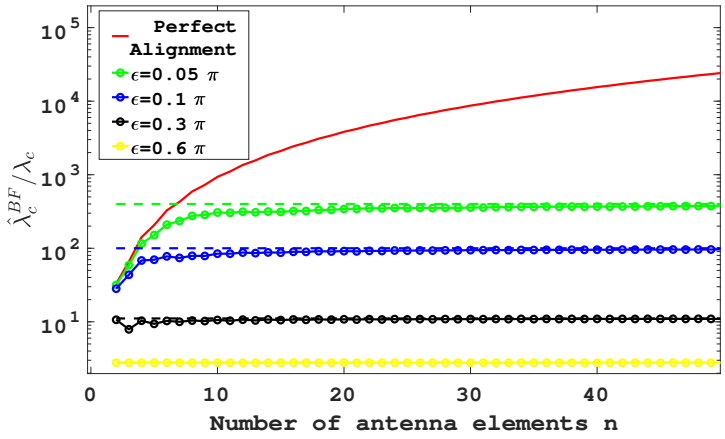

Figure 3.9: λ_c^{BF}/λ_c for network with perfect alignment (red curve); $\hat{\lambda}_c^{BF}/\lambda_c$ as a function of n for network with Uniform beam alignment error (curves with circle marks); Upper bounds of $\hat{\lambda}_c^{BF}/\lambda_c$ for different error regions ϵ (dotted lines).

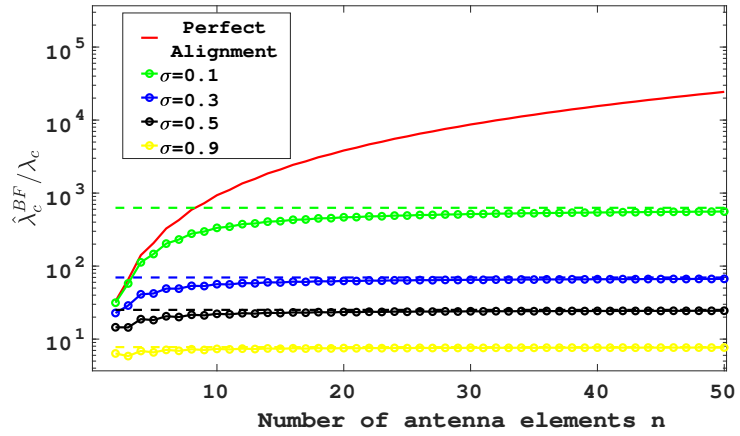

Figure 3.10: λ_c^{BF}/λ_c for network with perfect alignment (red curve); $\hat{\lambda}_c^{BF}/\lambda_c$ as a function of n for network with Gaussian beam alignment error (curves with circle marks); Upper bounds of $\hat{\lambda}_c^{BF}/\lambda_c$ for different normal deviations σ (dotted lines).

error is too high (typically when $\epsilon > \frac{\pi}{2}$), beamforming performance is close to the performance with omnidirectional antennas. We observe that when n increases, even a small misalignment error degrades the performance significantly. This is due to the fact that beams are becoming thinner and thinner as n increases, and a small angle variation implies a drop in the antenna gain. We conclude that the spatial multiplexing gain of ULA is limited when the beam alignment is not perfect.

Figure 3.11 illustrates that under the context of uniform misalignment, $\hat{\lambda}_c^{BF}$ decreases when we extend the size of the error region. When $\epsilon = \pi$, the difference between the broadside direction and the AoD/AoA of the associated device can be any value between $[0, 2\pi]$. The arrival rate that the system can support is the same

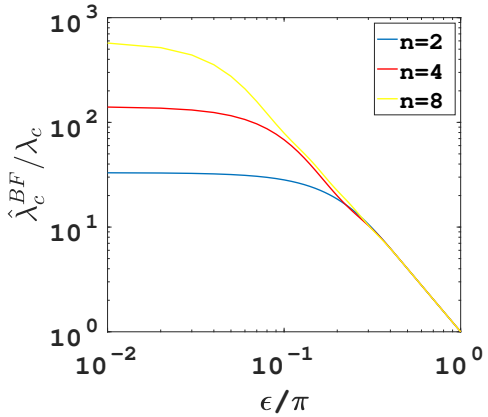

Figure 3.11: $\hat{\lambda}_c^{BF}/\lambda_c$ as a function of ϵ/π for network with Uniform beam alignment error.

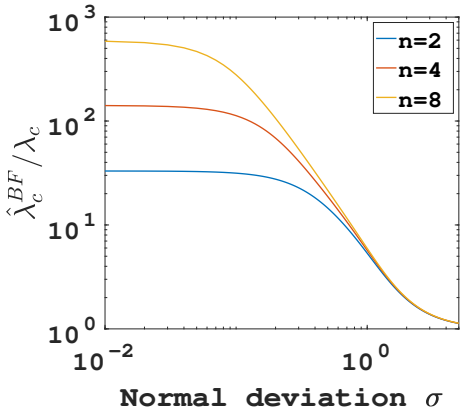

Figure 3.12: $\hat{\lambda}_c^{BF}/\lambda_c$ as a function of σ for network with Gaussian beam alignment error.

as with a single antenna system in this case ($\hat{\lambda}_c^{BF}/\lambda_c$ tends to 1). For the Gaussian misalignment, the impact of normal deviation σ is studied in Figure 3.12. When σ is very large, the beamforming pattern can no longer aggregate the power to the directions of devices. The critical arrival rate with ULA decreases towards λ_c with a single antenna as a function of σ.

3.7 Conclusion

This chapter studies the impacts of misalignment for a spatial wireless D2D network equipped with ULA. Both the uniform beam alignment error model and the truncated Gaussian beam alignment error model are studied. The network is modeled as a spatial birth-death process, which combines stochastic geometry ideas and the queuing theory methods. Our main contribution is to establish the closed-form expression for the network's critical arrival rate as a function of the number of antenna arrays, considering the earlier misalignment models. For each misalignment model, we derive an upper bound of the critical arrival rate. The critical arrival rate cannot exceed these upper bounds even though the number of antenna elements increases. The numerical results show that these upper bounds match properly when the number of antenna elements is large enough.

Chapter 4

Rate meta-distribution for mmWave D2D network

In chapter 3, we examined the dynamic D2D communication model with beamforming. In this chapter, our focus shifts to investigating the instantaneous properties of D2D communication in the mmWave spectrum, specifically emphasizing coverage and reliability diversity across various links. Similar to the dynamic model, the transmitter and receiver sides of users are equipped with directional antennas and adopt beamforming. By considering the truncated Gaussian misalignment assumption introduced in chapter 3, we derive computationally tractable expressions of the conditional rate coverage probability's moments as a function of the number of antenna elements. The beta approximation of the rate meta-distribution is obtained based on the first and the second moment. The numerical simulations confirm our analytical results. They show that the coverage performance can deteriorate significantly due to misalignment. Furthermore, an optimal number of antenna elements must be chosen to get the best coverage. In addition, there exists an optimal number of antennas which maximizes the number of users who satisfy the reliability constraints. This optimal value is a function of the reliability threshold.

4.1 Introduction

Stochastic geometry is a widely used mathematical tool for evaluating the coverage and rate performance of wireless networks, see e.g. [16]. While early studies on D2D focus on the average coverage probability among all users [17], it is essential in the context of URLLC to consider the distribution of the traditional performance metrics, to know for example the proportion of users meeting reliability requirements, as defined for example in [2]. To fully characterize the spatial distribution of communication reliability, The meta-distribution for D2D communication has thus been proposed [18]. Initial results have been then extended in the literature. For example, the meta-distribution of the underlay D2D communication in a cellular network is studied in [47]. In [46] and [6], the meta-distribution for mmWave D2D networks are derived, where only the D2D transmitters are equipped with multiple antennas.

In the existing works that study the meta-distribution of the mmWave D2D network, the beam alignment is however supposed to be ideal. The maximum array gain is achieved by steering the main beam in the desired direction during the beam training period. However, in practice, a small misalignment error may provoke severe performance deterioration, which is confirmed by the existing works that study the coverage performance of cellular network [53]. It has also been shown in D2D networks [54], [55] in terms of coverage probability. Thus the beam alignment error cannot be neglected and there is no existing work studying the meta-distribution in conjunction with this type of error.

4.2 Contributions

The contribution of this chapter is summarized as follows:

- We provide a closed-form and computationally tractable formula for all the moments of the conditional rate coverage probability in D2D networks with perfect beamforming and antennas at both the transmitter and the receiver (see Theorem 15). We extend this result to the case of imperfect beamforming by considering a Gaussian misalignment model (see Theorem 16). The rate meta-distribution is then approximated using the beta approximation.
- The simulations results show the accuracy of the analytical analysis and show that the beta approximation provides a good estimate of the meta-distribution.

They show that the coverage performance can deteriorate significantly due to misalignment.

- We highlight the existence of an optimal number of antennas that maximizes the (average) rate coverage probability which depends on the error magnitude. We also show that there is an optimal number of antennas maximizing the number of users satisfying a reliability requirement. This optimal number is dependent on the required reliability.

In the rest of this chapter, we introduce the system model in section 4.3. Section 4.4 presents the analytical study of the rate meta-distribution. The numerical results are shown in section 4.5. Section 4.6 concludes the chapter.

4.3 System model

We study the mmWave D2D network by considering the classical bipolar network model [18]. The transmitter-receiver pairs are randomly located in a 2-dimensional space and perform point-to-point data transmissions. The D2D transmitters form a homogeneous PPP Φ^T with intensity λ. Without loss of generality, we assume that each transmitter has a dedicated D2D receiver uniformly located on the circle around the transmitter, with a constant radius r. We denote the point process associated with the receivers by Φ^R. A typical receiver is assumed to be at the origin and attempts to receive the data from the corresponding transmitter. According to the Slivnyak theorem, the statistical characteristics do not change for a PPP if we add a point in a particular position [16].

4.3.1 Beamforming

To compensate for the visible mmWave propagation loss, ULA is used at both transmitter and receiver ends. For each pair, the transmit and receive beams are required to be aligned toward each other. For the sake of mathematical tractability, we simplify the actual antenna pattern by the sectorized gain pattern based on the realistic pattern of ULA introduced in chapter 2. The power pattern g_e is the same as in (3.2). This model consists of a main beam and a side beam as shown in Figure 4.1. The main beam gain is precisely the real maximum gain of ULA. The side beam gain is calculated without changing the average radiation intensity.

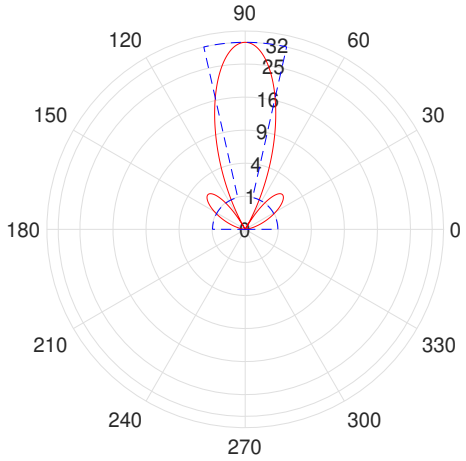

Figure 4.1: ULA power pattern (solid line) and sectorized beamforming pattern (dotted line).

Both transmitter and receiver antenna arrays have the same half power beamwidth (HPBW) ω, which corresponds to the angular aperture of the main beam. For a ULA with n antenna elements, the HPBW can be expressed as a function of n as follows:

$$\omega(n) \quad = \quad 2\left(\frac{\pi}{2} - \arccos\frac{2.784}{n\pi}\right) \tag{4.1}$$

Let G^T_{max} and G^T_{min} represent the antenna gains of the main and side beams at transmitter's side. Respectively, we use G^R_{max} and G^R_{min} to denote the antenna gain of the main and side beams at receiver's side. Specifically, we have

$$\begin{cases} G^T_{max} = 2n \\ G^T_{min} = \rho(n) \\ G^R_{max} = 2n^2 \\ G^R_{min} = n\rho(n) \end{cases} \tag{4.2}$$

Here ρ is a function of n as shown in (4.3):

$$\rho(n) \quad = \quad \frac{\int_0^{\pi} \frac{2}{n} \left|\frac{\sin(\frac{1}{2}n\pi\cos\theta)}{\sin(\frac{1}{2}\pi\cos\theta)}\right|^2 d\theta - 2n\omega(n)}{\pi - \omega(n)} \tag{4.3}$$

To sum up, the array gain of a transmitter can be expressed as follows:

$$g^T_a(\theta, \theta^T_0) = \begin{cases} G^T_{max}, & 0 \le |\theta - \theta^T_0| \le \omega/2 \\ G^T_{min}, & \omega/2 \le |\theta - \theta^T_0| \le \pi/2 \\ 0, & \text{otherwise} \end{cases} \tag{4.4}$$

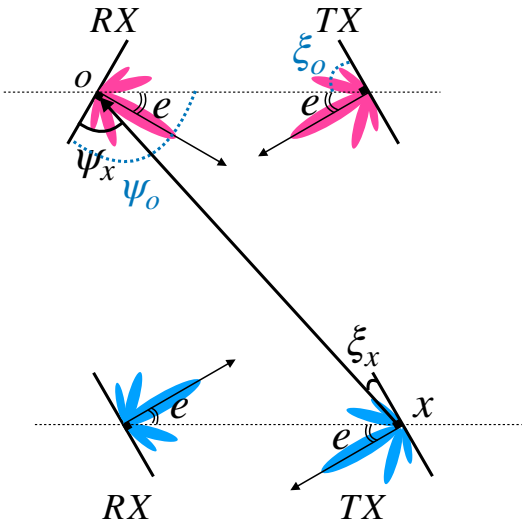

Figure 4.2: Two D2D transmitter-receiver pairs (blue and rose) with misalignment.

where θ is the AoD of the plane wave with respect to the linear array's axis. We denote θ_0^T as the boresight direction of the transmitter array (main lobe direction), which is decided by the beamformer. Respectively, the array gain of a receiver $g_a^R(\theta, \theta_0^R)$ has a main lobe of gain G_{max}^R within the same HPBW around its boresight direction θ_0^R, and a sidelobe of gain G_{min}^R. The proof of (4.1)-(4.3) are presented in Appendix C.

4.3.2 Misalignment model

Consider a typical receiver device at origin O. Then ψ_o is the AoA of the plane wave from its corresponding transmitter regarding the receiver antenna array's axis. Moreover, ξ_o is the AoD to the transmitter array's axis. We choose $\theta_0^T = \theta_0^R = \pi/2$ to ensure that the antenna arrays are broadside antennas (boresight direction is perpendicular to the axis). Ideally, the transmitter and receiver should be face-to-face to align their main lobes of beams to each other. That is to say $\psi_o = \xi_o = \pi/2$. Nevertheless, the alignment is often not perfect in reality, so there is an alignment error e as shown in Figure 4.2. Thus ψ_o and ξ_o can be modelled as random variables whose means are θ_0^R and θ_0^T. According to the central limit theorem, the truncated Gaussian distribution is a properly estimation of the alignment errors induced by multiple independent sources. We assume that the errors have a span from $-\pi$ to π. The PDF of ξ_o or ψ_o can thus be expressed by using the truncated Gaussian

distribution [51]:

$$f_\xi(x) = \frac{1}{\sqrt{2\pi}\sigma} \frac{\exp(-\frac{1}{2}(\frac{x-\theta_0^T}{\sigma})^2)}{erf(\frac{\pi}{\sqrt{2}\sigma})}, x \in [\theta_0^T - \pi, \theta_0^T + \pi] \tag{4.5}$$

4.3.3 Channel model

For a typical active receiver located at the origin O and its corresponding transmitter at x_o, the total antenna gain of this link is:

$$G_o(\xi_o, \psi_o) = g_a^R(\psi_o, \theta_0^R) g_a^T(\xi_o, \theta_0^T) \tag{4.6}$$

Consider a link between a receiver located at origin O and an interfering transmitter located at x. As shown in 4.2, ψ_x is the AoA with respect to receiver's array axis, and ξ_x is the AoD with respect to transmitter's array axis. Then the antenna gain of this link can be expressed as follows:

$$G_x(\xi_x, \psi_x) = g_a^R(\psi_x, \theta_0^R) g_a^T(\xi_x, \theta_0^T) \tag{4.7}$$

We are interested in the Shannon rate $\mathcal{R}$:

$$\mathcal{R} = W \log_2(1 + \frac{P h_{x_o} G_o(\xi_o, \psi_o) \ell(r)}{\sum_{x \in \Phi \setminus x_o} P h_x G_x(\xi_x, \psi_x) \ell(|x|) + \mathcal{N}_0 W}) \tag{4.8}$$

where $\ell(\cdot)$ is the path gain function: $\ell(x) = x^{-\alpha}$. The small-scale fading coefficient associated with the link from the transmitter at x to the receiver at origin is denoted by h_x, which has an exponential distribution with unit mean (Rayleigh fading). Moreover, all users transmit with the same power P. The noise power is $\mathcal{N}_0 W$, where $\mathcal{N}_0$ and W are the noise power spectral density and the bandwidth, respectively.

4.4 Meta distribution

The meta-distribution defined in [18] describes the spatial distribution of the devices' communications' reliability. Similar to the definition in [56], we define the rate meta-distribution as a two-parameter distribution function as follows:

$$\bar{F}_{P_s(\eta)}(\epsilon) \triangleq \mathbb{P}^!(P_s(\eta) > \epsilon), \qquad \epsilon \in [0, 1], \eta \in \mathbb{R}^+. \tag{4.9}$$

where $P_s(\eta)$ is the conditional rate coverage probability or the conditional success probability:

$$P_s(\eta) \triangleq \mathbb{P}(\mathcal{R} > \eta | \Phi^T, \Phi^R) \tag{4.10}$$

The classical coverage probability is its mean. The notation $\mathbb{P}^!$ denotes the Palm measure of $\{\Phi^T, \Phi^R\}$, given that there is an active receiver at the prescribed location. During a long period, users may experience different communication conditions. Thus the conditional rate coverage probability describes the temporal success probability of a certain user. We call the threshold ϵ as the reliability threshold of the network. It is assumed that the communication is reliable if the probability of the user getting a rate higher than η is larger than ϵ. Then the rate meta-distribution $\bar{F}_{P_s(\eta)}(\epsilon)$ is designed to characterize the spatial distribution of reliability.

4.4.1 Moments of the conditional rate coverage probability

Theorem 15. *Consider a D2D network with the BF model introduced in Section 4.3. If the beam alignment is perfect, the b-th moment of the conditional rate coverage probability $M_b(\eta)$ has the following expression:*

$$M_b(\eta) = \exp\left(-b\eta' \frac{\mathcal{N}_0 W}{P G_o(\xi_o, \psi_o)}\right) \exp(-\lambda Q_b(\eta)) \tag{4.11}$$

where $\eta' = \frac{2^{\frac{\eta}{W}}-1}{\ell(R)}$, and $Q_b(\eta)$ is a function of b and η:

$$\begin{aligned} Q_b(\eta) = \lim_{T\to\infty} \frac{T^\delta \delta \pi}{4} \sum_{n=1}^{\infty} \binom{b}{n} (-1)^{n+1} B(\delta, 1) \\ \times \Bigg(p^2 {}_2F_1(n, \delta, \delta+1, \frac{-G_o(\xi_o,\psi_o)T}{G_1\eta'}) \\ + 2p(1-p) {}_2F_1(n, \delta, \delta+1, \frac{-G_o(\xi_o,\psi_o)T}{G_2\eta'}) \\ + (1-p)^2 {}_2F_1(n, \delta, \delta+1, \frac{-G_o(\xi_o,\psi_o)T}{G_3\eta'}) \Bigg) \end{aligned} \tag{4.12}$$

where $p = \omega/\pi$, $\delta = 2/\alpha$, $G_1 = 4n^3$, $G_2 = 2n^2\rho$ and $G_3 = n\rho^2$. Function $B(\cdot,\cdot)$ is the Beta function and ${}_2F_1(\cdot)$ is the hyper-geometric function.

Proof. The proof is a special case of the proof of Theorem 16. □

4.4.2 Impact of misalignment

We define the matching probability as p_{ma}, which refers to the case where ξ_o (respectively ψ_o) is within the HPBW around θ_0^T (respectively θ_0^R):

$$p_{ma} = \int_{\theta_0^T - \frac{\omega}{2}}^{\theta_0^T + \frac{\omega}{2}} f_{\xi_o} \mathrm{d}\xi_o \tag{4.13}$$

The effective probability p_{ef} specifies the probability that ξ_o or ψ_o is within $[0, \pi]$:

$$p_{ef} = \int_{\theta_0^T - \frac{\pi}{2}}^{\theta_0^T + \frac{\pi}{2}} f_{\xi_o} \mathrm{d}\xi_o \tag{4.14}$$

With these notations, we have the following result:

Theorem 16. *With beam misalignment, the b-th moment of the conditional rate coverage probability has the following expression:*

$$\begin{aligned} M_b = {} & p_{ma}^2 \exp\left(-b\eta' \frac{\mathcal{N}_0 W}{P G_1}\right) \exp\left(-\lambda Q_b(G_1, \eta)\right) \\ & + 2p_{ma}(p_{ef} - p_{ma}) \exp\left(-b\eta' \frac{\mathcal{N}_0 W}{P G_2}\right) \exp\left(-\lambda Q_b(G_2, \eta)\right) \\ & + (p_{ef} - p_{ma})^2 \exp\left(-b\eta' \frac{\mathcal{N}_0 W}{P G_3}\right) \exp\left(-\lambda Q_b(G_3, \eta)\right) \end{aligned} \tag{4.15}$$

where $Q_b(G_o, \eta)$ has the same expression as the right hand side of the formula (4.12).

Proof. See Appendix D. □

4.4.3 Beta approximation

The numerical computation of the exact rate meta-distribution by using Gil-Pélaez theorem [18] is often difficult. An alternative solution is to approximate it with a Beta-distribution [18] by matching the first and the second moment as follows:

$$\bar{F}_{P_s(\eta)}(\epsilon) = 1 - I_\epsilon\left(\frac{M_1 M_2 - M_1^2}{M_1^2 - M_2}, \frac{(1 - M_1)(M_2 - M_1)}{M_1^2 - M_2}\right) \tag{4.16}$$

where $I_\epsilon(\cdot)$ is the regularized incomplete beta function [46].

4.5 Numerical results

At the beginning of the simulation, a specific configuration of the network is decided by randomly choosing the locations of the devices, where the location for each transmitter is uniformly chosen in the plane, and the position of its corresponding receiver is uniformly chosen on a circle of radius R around it. Assuming such a fixed spatial configuration, we draw the value of the random variable h_x for every link. The Shannon rate is calculated for each receiver, and we count the number of success transmissions for each pair for a given rate threshold η. This process is repeated for sufficient number of iterations in order to get the rate meta-distribution. Network

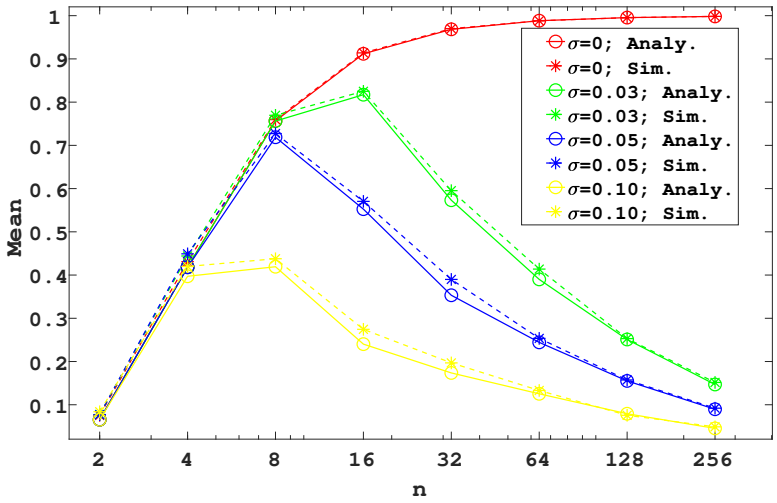

Figure 4.3: Mean of $P_s(\eta)$ as a function of n with misalignment.

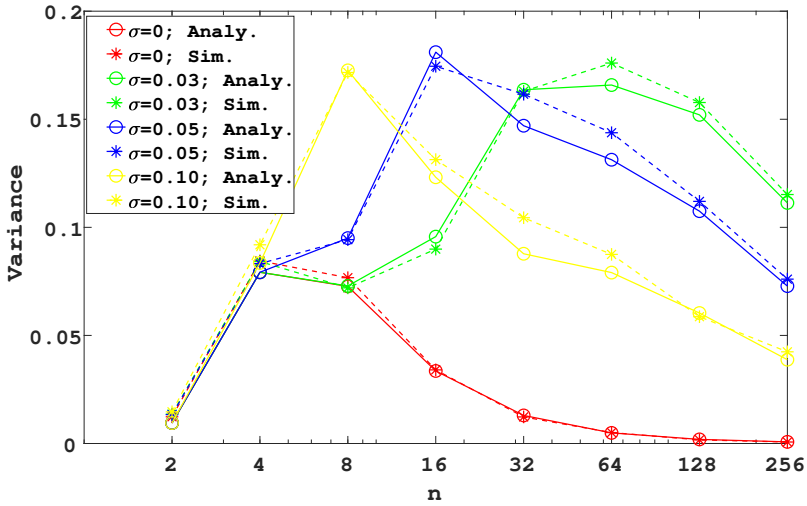

Figure 4.4: Variance of $P_s(\eta)$ as a function of n with misalignment.

parameters are as follows: $W = 1$ MHz, $\alpha = 3.5$, $r = 30$ m, $\lambda = 0.01$ m^{-2} and $\eta = 1$ Mbps. The standard deviation in Figure 4.6 is $\sigma = 0.05$.

Figure 4.3 shows the mean of $P_s(\eta)$ as a function of n, in presence of Gaussian misalignment. The solid curves show the analytical results derived from (4.15). The dotted curves are from the simulations results. The two sets of curves are very close. When there is no misalignment, the average of $P_s(\eta)$ is increasing with the number of antennas. This can be explained by the thinner beams which increase the useful received signal power while reducing interference. When there are misalignment errors, the coverage probability is decreasing with the error amplitude. Moreover, the average coverage probability is characterized by an optimal number of antennas.

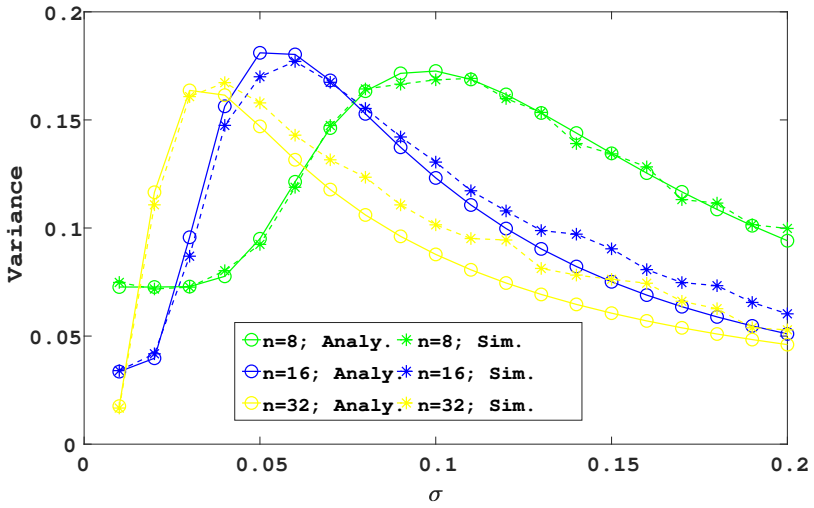

Figure 4.5: Variance of $P_s(\eta)$ as a function of σ with misalignment.

Thinner beams are indeed more prone to misalignment errors leading to a loss of coverage when the error is large. The optimal number of antennas is a decreasing function of the error magnitude due to this effect.

Figures 4.4 and 4.5 show the variance of P_s as a function of the number of antennas and of the error magnitude, respectively. The difference between the simulation and the analytical results is again relatively small. When σ is small, the variance is small because the coverage is good enough in most cases. On the contrary, most users cannot be covered when the error is strong, so the variance is also small. There is however an intermediate zone where sometimes users are connected, sometimes not, and the variance is relatively strong. This explains the bell shapes of the curves. The value of σ, which gives the maximum variance, gets smaller when the number of antennas increases. This is because the beam is thinner and we thus enter the intermediate interval with lower errors.

For a given value of the reliability threshold ϵ, we can interpret the meta distribution as follows: There is a proportion $1-F_{P_s(\eta)}(\epsilon)$ of users who meet the reliability requirement. The function $\epsilon \mapsto 1 - F_{P_s(\eta)}(\epsilon)$ is precisely the CCDF of $P_s(\eta)$, which is shown in Figure 4.6. The dotted curves are obtained by Monte Carlo simulations, and the solid curves are the beta approximation results.

First, note that the beta approximation is a sufficiently good approximation to analyze main performance trends. Curves are decreasing because, if the reliability threshold increases, there are less and less users meeting the requirement (see (4.9)). For a fixed threshold ϵ, if a curve is above another, this means that more users are

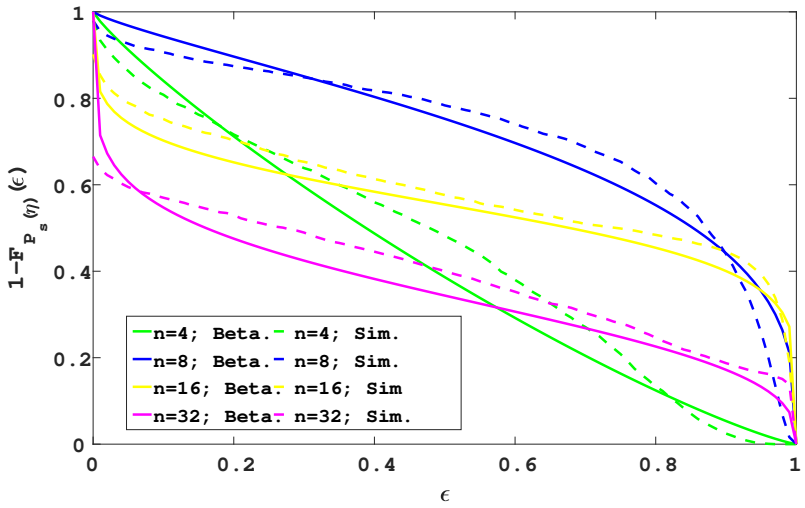

Figure 4.6: Meta distribution with misalignment.

meeting the reliability requirement; as a consequence, the higher is the curve, the more reliable is the network. Having this in mind, we see for example that $n = 8$ maximizes reliability for ϵ between 0 and 0.9 approximately, but then $n = 16$ is the best option. There is thus an optimal number of antennas which depends on the reliability threshold.

This also illustrates the fact that the best coverage does not always imply the best reliability. When $\sigma = 0.05$, Figure 4.3 shows that 4 antennas leads to a better average rate coverage than 32 antennas. However, according to Figure 4.6, we find that 32 antennas can cover more users if the reliability threshold is high enough. These two metrics can be combined together to evaluate the network performance comprehensively.

4.6 Conclusion

In this chapter, we study the rate meta-distribution in a mmWave D2D network with beamforming. Transmitters and receivers are both equipped with multiple antennas. The impacts of beam misalignment under a truncated Gaussian alignment error model are investigated. Our analytical and numerical results show a strong impact of beam misalignment which cannot be neglected in the analysis of coverage and when requiring a certain reliability. We show that there exists an optimal number of antennas that maximizes the (average) rate coverage probability. This optimal number depends on the error magnitude and the rate threshold. We also show

that there is an optimal number of antennas which maximizes the number of users satisfying a reliability requirement. Moreover, this optimal number is dependent on the required reliability.

Chapter 5

Beam management for mmWave URLLC D2D networks

In the previous chapter, we explored the effects of beam misalignment on the rate meta-distribution in mmWave D2D networks. Our findings revealed a significant degradation in coverage when misalignment is present. However, the misalignment was modeled only statistically, without discussing its specific sources. In this chapter, we will delve deeper into this issue by examining the beam alignment induced by the codebook. Specifically, we study a mmWave D2D network dedicated to URLLC, where users employ multiple antennas to perform beamforming. The packet transmission process is divided into two phases: a beam training phase, during which exhaustive beam sweeping is adopted, and a data transmission phase. The chapter investigates the misalignment error distribution resulting from an imperfect training phase, due to the finite codebooks resolution and the fast variation of the channel. For the data transmission phase, closed-form expressions for all the moments of the rate conditional coverage probability are derived, and the meta-distribution is approximated using the beta approximation. The study evaluates the overall network performance through the effective rate meta-distribution, which accounts for the training overhead and beam misalignment errors. The results show the detrimental impact of misalignment errors when URLLC requirements are stringent and highlight the trade-off between the training overhead and the gain brought by multiple antennas.

5.1 Introduction

To fully exploit the beamforming gain, the beam directions of D2D devices need to be steered towards desired directions through a process called beam training. The success of beam training depends on several factors, including the channel conditions, the training procedure, or the codebook design. Misalignment errors may thus occur, which can lead to a degradation of the data transmission performance [54], [57]. To address these challenges, our study proposes a theoretical analysis of the communication reliability in mmWave D2D networks in the context of URLLC. Our approach is based on stochastic geometry. It takes into account beam misalignment errors due to the beam training process when using mmWaves and the fundamental trade-off between training overhead and data transmission reliability.

Some papers investigate the effects of beam misalignment, however in an incomplete way. This is the case for example of [44], where the alignment errors are modelled using Gaussian or Uniform distributions and where only the *average* coverage probability is derived. In the previous chapter, we approximate the meta-distribution for the mmWave D2D network with imperfect beam alignment by considering a Gaussian distributed alignment error while assuming Rayleigh fading channels. These approaches need to be extended to Nakagami-M fading channels, which are better suited to the prominent LOS propagation of mmWaves and include both Rayleigh, Rician and more general fading distributions [58, Chap. 3]. They also need to be extended to realistic misalignment error models derived from the alignment procedure.

To better model a potential misalignment, several studies [59]–[63] investigate the probability of misalignment induced during the beam training process. These works assume an exhaustive search procedure, known as beam sweeping, to sequentially compare all possible transmitter-receiver beam directions. Specifically, the authors of [59], [60] study the impact of noise and derive upper and lower bounds for the misalignment probability. These studies are performed for a point-to-point transmission, while stochastic geometry allows for a system level analysis. Two papers are analysing beam misalignment in a cellular network context. Reference [62] studies the impact of user mobility, while the authors of [63] consider the potential beam misalignment due to the reuse of pilot signals by BSs. However, none of these works considers the effect of the codebook resolution, of the fast variation of the channel at mmWave frequencies and none of them studies the effective rate

meta-distribution, a useful metric for URLLC.

During the beam training process, there is a fundamental trade-off between training and data transmission: inadequate training may lead to poor channel estimation and thus to reduced data rate, while excessive training can result in disproportionate overhead. Several works have investigated the joint design of beam training and data transmission using stochastic geometry. For instance, the authors of [61], [63] show that narrowing the beam width can enhance throughput, but it can also prolong beam sweeping time during the initial association process. These works propose the notion of effective achievable rate to capture the training overhead and a Signal to Interference plus Noise Ratio (SINR) penalty for the training process. The former paper focuses on misalignment induced by interference, while the latter neglects misalignment. The reference [62] studies the overhead for beam handovers and misalignment under a user mobility model, but assumes that beam alignment can always be completed within a fixed amount of time, ignoring the different time constraints for beam sweeping with different beam widths and potential misalignment due to inadequate training. Furthermore, these studies assume a perfect codebook, where beams perfectly span the angular aperture without any hole or overlapping between the beams. In practice, however, the codebook resolution plays an important role in the magnitude of the misalignment error. Additionally, all these works focus solely on the average coverage probability of the network, while the study of the meta-distribution is required for understanding the network's performance in a URLLC context.

5.1.1 Contributions

We propose an analytical methodology based on stochastic geometry to study the communication reliability of mmWave D2D networks. The main contributions of the chapter are as follows.

- We propose closed-form formulas for the joint probability mass function of the antenna gains at the transmitter and the receiver resulting from the beam sweeping process, assuming any generic small-scale fading distribution, including Nakagami-M and any codebook resolution. In the literature, papers studying this problem ignore the effect of the varying small-scale fading and the influence of the codebook resolution [59]–[63].

- We derive closed-form formulas for the moments of the meta-distribution of

the effective rate from which we can derive the beta approximation. This meta-distribution allows us to obtain statistical latency guarantees for URLLC communications. In the literature, either authors ignore misalignment errors or do not provide a closed-form formula for the meta-distribution [61]–[63].

- Via numerical experiments, we highlight the trade-offs between training and data resources and between the number of antennas and misalignment errors. We are able to optimize the codebook size and the number of antennas. To the best of our knowledge, these trade-offs have not been studied in the literature using the meta-distribution while taking into account the codebook resolution.

The rest of this chapter is structured as follows: In section 5.2, we describe the system model for mmWave D2D networks with beamforming. In section 5.3, we present the beam sweeping process and study the effects of misalignment. Section 5.4 introduces several performance metrics, including the effective rate meta-distribution. We then provide mathematical expressions for these metrics in section 5.5. The numerical results are presented in section 5.6, followed by our conclusions in section 5.7.

5.2 System model

In this section, we introduce the network model and the codebook-based beamforming model.

5.2.1 Network model

Consider a mmWave D2D network as a classical bipolar network model, where the D2D transmitters form a homogeneous PPP Φ^T with intensity $\Lambda(\mathrm{d}x) = \lambda \times \mathrm{d}x$ in a 2-dimensional space $\mathbb{R}^2$ [16]. Each D2D transmitter is associated with a dedicated receiver and performs point-to-point data transmissions. The point process associated with the receivers is denoted by Φ^R. We assume that the D2D receivers are uniformly located on the circles around their dedicated transmitters, with a constant radius r. Such a process can be interpreted as a marked point process of Φ^T with independent random marks. Hence Φ^R is also a homogeneous PPP [15]. According to the Slivnyak-Meck theorem, the statistical characteristics do not change for a PPP if we add a typical point in a particular position, or more

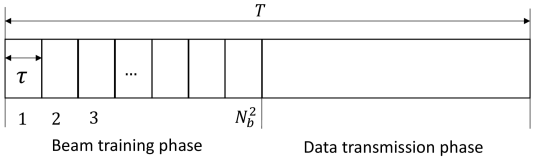

Figure 5.1: Time slot of duration T made of: (i) A beam training phase, which consists of N_b^2 mini-slots of duration τ; (ii) A data transmission phase.

formally, the reduced Palm distribution $\mathbb{P}_x^!(\cdot)$ of Φ is equal to the original distribution $\mathbb{P}(\Phi \in \cdot)$ [24]. For convenience, a typical receiver is assumed to be located at the origin and attempts to receive the data from the corresponding transmitter. In order to compensate for the propagation loss of mmWaves, we consider that D2D transmitters and receivers are equipped with ULA with N_a antenna elements, which allow directional transmissions [22], [43], [64]. Every ULA can be configured with a codebook, which is a finite set of N_b possible beams pointing in directions that divide $[0, 2\pi)$ into equal intervals. We assume that all users are synchronized and that time is divided into slots of duration T, see Figure 5.1. Each slot consists of a beam training phase and a data transmission phase. In the beam training phase, the transmitter and the receiver jointly train the beams from the pre-designed codebook to choose the best beam pair. The beam training phase is divided into N_b^2 mini-slots of duration τ, during which every beam pair is measured before choosing the optimal one. During the data transmission phase, users employ the beam pair that provided the highest signal strength during the first phase to send a data file of size L bits. In the context of URLLC, the time slot can be seen as a time budget for the transmission of a small packet that should be shared between beam training and data transmission.

5.2.2 Beamforming and channel model

The channel is modelled with a distance dependent path-loss and small-scale fading. For a typical receiver located at a distance r from a transmitter, the path-loss is modelled as $\ell(r) = Kr^{-\alpha}$, where α is the path-loss exponent and K is a constant depending on the path-loss reference distance and the carrier frequency [39]. The small scale fading coefficient h is modelled as a Nakagami-M fading, i.e., $h \sim \Gamma(M, \frac{1}{M})$ where Γ is the Gamma distribution with shape parameter M and rate parameter

$\frac{1}{M}$[58]. The special case $M = 1$ corresponds to Rayleigh fading. We denote $F(\cdot)$ and $f(\cdot)$ the Cumulative Distribution function (CDF) and the PDF of h, respectively. The equivalent channel matrix $\mathbf{H} \in \mathbb{C}^{N_a \times N_a}$, including the ULA responses, can be thus written as follows [13]:

$$\mathbf{H} = \sqrt{\ell(r)h}\mathbf{u}(\psi)\mathbf{v}^*(\xi) \tag{5.1}$$

where $\mathbf{u}(\psi) \in \mathbb{C}^{N_a \times 1}$ and $\mathbf{v}(\xi) \in \mathbb{C}^{N_a \times 1}$ are the array response vectors at the receiver side and the transmitter side, respectively, ψ is the Angle-of-Arrival (AoA) and ξ is the Angle-of-Departure (AoD) of the plane wave with respect to the antenna arrays axis. Taking the phase at the first antenna element as a reference, the array response vectors can be expressed as follows [63]:

$$\mathbf{u}(\psi) = [1, e^{j\frac{2\pi df_c}{c}\cos(\psi)}, e^{j\frac{2\pi df_c}{c}2\cos(\psi)}, ..., e^{j\frac{2\pi df_c}{c}(N_a-1)\cos(\psi)}]^{\mathrm{T}} \tag{5.2}$$

$$\mathbf{v}(\xi) = [1, e^{j\frac{2\pi df_c}{c}\cos(\xi)}, e^{j\frac{2\pi df_c}{c}2\cos(\xi)}, ..., e^{j\frac{2\pi df_c}{c}(N_a-1)\cos(\xi)}]^{\mathrm{T}} \tag{5.3}$$

where d is the distance between the adjacent antenna elements, f_c is the carrier frequency and c is the speed of light. Each device can steer its antenna bore-sight towards its desired direction. The receiver steers the beam in direction θ^R with respect to the antenna arrays axis using a combining vector $\mathbf{w}(\theta^R)$. The transmitter steers the beam in direction θ^T with respect to the antenna arrays axis using a beamforming vector $\mathbf{f}(\theta^T)$. We have [13], [43]:

$$\mathbf{w}(\theta^R) = [1, e^{-j\frac{2\pi df_c}{c}\cos(\theta^R)}, e^{-j\frac{2\pi df_c}{c}2\cos(\theta^R)}, ..., e^{-j\frac{2\pi df_c}{c}(N_a-1)\cos(\theta^R)}]^{\mathrm{T}} \tag{5.4}$$

$$\mathbf{f}(\theta^T) = \frac{1}{\sqrt{N_a}}[1, e^{-j\frac{2\pi df_c}{c}\cos(\theta^T)}, e^{-j\frac{2\pi df_c}{c}2\cos(\theta^T)}, ..., e^{-j\frac{2\pi df_c}{c}(N_a-1)\cos(\theta^T)}]^{\mathrm{T}} \tag{5.5}$$

where the $\frac{1}{\sqrt{N_a}}$ factor is to account for the power split among the N_a antenna elements. Ignoring for now interference, the received signal can be expressed as follows:

$$y = \mathbf{w}^*(\theta^R)\mathbf{H}\mathbf{f}(\theta^T)s + \mathbf{w}^*(\theta^R)\mathbf{z} \tag{5.6}$$

where s is the transmitted signal with average transmit power $\mathbb{E}[ss^*] = P$. The noise vector z follows a circularly-symmetric complex normal distribution $\mathbf{z} \sim \mathcal{CN}(\mathbf{0}, \sigma^2\mathbf{I})$ with average power $\sigma^2 = \mathcal{N}_0 W$, where W is the signal bandwidth and $\mathcal{N}_0$ is the Power Spectral Density (PSD) of thermal noise.

The beamforming vector codebook is defined as $\mathcal{C}^T = \{\mathbf{f}(\theta_m^T)\}_{m=1:N_b}$, where $\theta_m^T = \frac{2\pi(m-1)}{N_b}$ and N_b is the size of the codebook, i.e., the number of possible beam directions. Respectively, we denote the combining vector codebook as $\mathcal{C}^R =$

$\{\mathbf{w}(\theta_n^R)\}_{n=1:N_b}$, where $\theta_n^R = \frac{2\pi(n-1)}{N_b}$. Note that the sets $\{\theta_m^T\}_{m=1:N_b}$ and $\{\theta_n^R\}_{n=1:N_b}$ cover a full angle space of the transmitter and of the receiver respectively, with equal resolution $\theta_u = \frac{2\pi}{N_b}$. We denote $l = (m, n)$ a generic beamforming and combining vectors pair at transmitter and receiver sides, respectively. The small scale fading coefficients h are supposed to be independent and identically distributed (i.i.d.) for different beam pairs and between the training and the data transmission phases. This assumption is supported by the very short coherence time at high carrier frequencies. For example, assuming a speed of 10 km/h, the channel coherence time at 28 GHz is about 0.482 ms [9]. When the frequency is 71 GHz, the coherence time drops to 0.19 ms. These values are much shorter than a typical slot duration of 1 ms.

Note that the equivalent antenna gains can be expressed as $g^T(\xi, \theta^T) = |\mathbf{v}^*(\xi)\mathbf{f}(\theta^T)|^2$ and $g^R(\psi, \theta^R) = |\mathbf{w}^*(\theta^R)\mathbf{u}(\psi)|^2$ at the transmitter and at the receiver, respectively. For tractability reasons, we approximate the actual antenna pattern by the widely used "flat-top" model, particularly adapted to LoS propagation [46], [62], [63]. This model consists of a main beam of angular aperture ω and a side beam of width $2\pi - \omega$. More precisely, the antenna gain of a transmitter can be expressed as:

$$g^T(\xi, \theta^T) = \begin{cases} G_{max}^T, & 0 \leq |\xi - \theta^T| \leq \omega/2 \\ G_{min}^T, & \text{otherwise.} \end{cases} \tag{5.7}$$

Accordingly, the antenna gain of a receiver $g^R(\psi, \theta^R)$ has a main lobe of gain G_{max}^R within the same angular aperture ω around its boresight direction θ^R, and a sidelobe of gain G_{min}^R outside this range. The main beam lobe width ω can be interpreted as the Half Power Beam Width (HPBW) of the antenna pattern. The main beam gain is precisely the maximum gain of the ULA. The side beam gain is obtained by normalizing the total radiation power.

Lemma 17. *For a ULA with N_a antenna elements, the HPBW can be expressed as a function of N_a as follows:*

$$\omega(N_a) = 2\left(\frac{\pi}{2} - \arccos\frac{2.784}{N_a\pi}\right) \tag{5.8}$$

Furthermore, we have $G_{max}^T = N_a$, $G_{min}^T = \rho(N_a)$, $G_{max}^R = N_a^2$ and $G_{min}^R = N_a\rho(N_a)$, where

$$\rho(N_a) = \frac{\int_{-\pi}^{\pi} \frac{1}{N_a}\left|\frac{\sin(\frac{1}{2}N_a\pi\cos\theta)}{\sin(\frac{1}{2}\pi\cos\theta)}\right|^2 d\theta - N_a\omega(N_a)}{2\pi - \omega(N_a)} \tag{5.9}$$

Proof: The proof is similar to the proof in Appendix C, with the modification of replacing the power pattern g_e as a constant 1.

5.3 Beam training and misalignment

We present here the beam training process and study the effects of beam misalignment.

5.3.1 Beam sweeping

During the beam training phase, the devices adopt a beam sweeping strategy where the transmitter and the receiver jointly steer the beams successively in a set of directions by adopting the beamforming/combining vectors pair from the pre-defined codebooks presented in section 5.2.2. At every mini-slot of the training phase, the transmitter and its receiver choose a different beamforming and combining vectors pair $(f(\theta_m^T), w(\theta_n^R))$ from the codebooks $\mathcal{C}^T \times \mathcal{C}^R$, so that all pairs of vectors are measured. We denote $G_m^T = g^T(\xi, \theta_m^T)$ and $G_n^R = g^R(\psi, \theta_n^R)$ the transmitter and receiver antenna gains when the vectors pair $l = (m, n)$ is employed. The corresponding channel fading coefficient is denoted as h_l. The useful received signal when using the pair l is expressed as follows:

$$\mathcal{S}_l = P h_l G_m^T G_n^R \ell(r) \tag{5.10}$$

After sweeping over all the codebooks vectors pairs, the transmitter and its receiver select the beamforming/combining vectors pair that maximizes $\mathcal{S}_l$:

$$l^* = \underset{\substack{l=(m,n) \\ m,n\in[1:N_b]}}{\arg\max} \mathcal{S}_l \tag{5.11}$$

The chosen vectors pair $l^* = (m^*, n^*)$ is then employed by users during the subsequent data transmission phase. The pair l^* is the best one during the training phase. However, due to the variability of the channel, it is not necessary the best one during the data transmission phase.

5.3.2 Beam misalignment model

Beam misalignment may result from various phenomena like the device mobility, the resolution of the codebooks or the device phase errors [59], [60]. In this work,

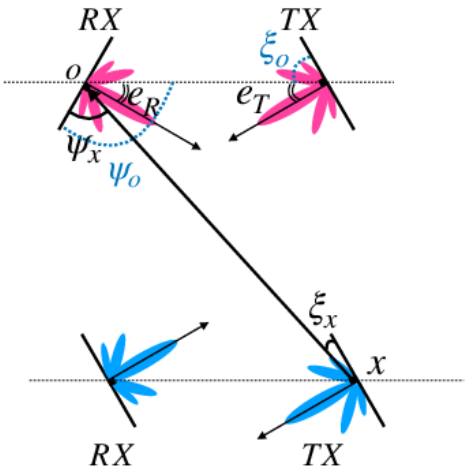

Figure 5.2: A D2D transmitter-receiver ('TX' and 'RX' in rose) at the origin o characterized by an AoD ψ_o and an AoA ξ_o. The alignment errors are denoted as e_T and e_R. An interfering D2D transmitter-receiver pair (in blue) is located in x and is characterized by an AoA ψ_x and an AoD ξ_x with respect to the rose D2D pair.

we consider the alignment errors induced during the training phase because of the codebook resolution and the channel variability. We assume the model shown in Figure 5.2. A link between a typical D2D transmitter-receiver pair (in rose) is characterized by an AoA ψ_o and an AoD ξ_o. The transmitter and the receiver point their beam in the directions θ_T and θ_R, respectively ($\theta_T = \theta_R = \pi/2$ in the figure). The link between the typical receiver ('RX' in rose) and another interfering D2D device ('TX' in blue) located in x has an AoA ψ_x and an AoD ξ_x. A misalignment occurs when the transmitter beam direction is different from the AoD or when the receiver beam direction is different from the AoA, i.e., when either $e_T = |\xi_o - \theta_T|$ or $e_R = |\psi_o - \theta_R|$ are non zero. At the transmitter side for example, the maximum antenna gain is achieved as long as $e_T < \omega/2$, see (5.7). The error e_T may result from the codebook resolution: as θ_T takes values in a finite set, it may not coincide with the AoD ξ_o. The error may also result from channel variability: due to the random variable h_l, the beam pair chosen during the training phase may not correspond to the best pair during the data transmission phase, see (5.10), (5.11). According to our network model, the AoD ξ_o and AoA ψ_o are uniformly distributed in $[0, 2\pi)$. Without loss of generality, we assume that $\xi_o \in [\theta_1^T - \frac{\theta_u}{2}, \theta_1^T + \frac{\theta_u}{2})$ and $\psi_o \in [\theta_1^R - \frac{\theta_u}{2}, \theta_1^R + \frac{\theta_u}{2})$, i.e., that the AoD and AoA correspond to the first value of the codebook.

5.3.3 Probability mass function of antenna gains

During the beam sweeping phase, a transmitter and a receiver antenna gain G_m^T and G_n^R are respectively observed when the beam pair $l = (m, n)$ is measured. These antenna gains are i.i.d. random variables across the mini-slots due to the random AoA and AoD. The Probability Mass Function (PMF) of these antenna gains depends on the codebook resolution θ_u, the codebook size N_b and the HPBW ω. We provide the PMF in the following lemma.

Lemma 18. *When $\omega \leq \theta_u$, the PMF of G_m^T can be expressed as follows:*

$$\mathbb{P}[G_m^T = G_{max}^T] = \begin{cases} \frac{\omega}{\theta_u} & \text{if } m = 1 \\ 0 & \text{if } m \neq 1 \end{cases} \tag{5.12}$$

$$\mathbb{P}[G_m^T = G_{min}^T] = 1 - \mathbb{P}[G_m^T = G_{max}^T] \tag{5.13}$$

The PMF of G_n^R have similar expressions as in (5.12) and (5.13), where index n is replaced by m. When $\omega > \theta_u$, the PMF of G_m^T and G_n^R can be expressed as follows:

$$\mathbb{P}[G_m^T = G_{max}^T] = \begin{cases} 1 & \text{if } 1 \leq m \leq \lfloor \frac{\omega-\theta_u}{2\theta_u} \rfloor + 1 \\ \frac{mod(\frac{\omega-\theta_u}{2}, \theta_u)}{\theta_u} & \text{if } m = \lfloor \frac{\omega-\theta_u}{2\theta_u} \rfloor + 2 \\ 0 & \text{if } \lfloor \frac{\omega-\theta_u}{2\theta_u} \rfloor + 3 \leq m \leq N_b - \lfloor \frac{\omega-\theta_u}{2\theta_u} \rfloor - 1 \\ \frac{mod(\frac{\omega-\theta_u}{2}, \theta_u)}{\theta_u} & \text{if } m = N_b - \lfloor \frac{\omega-\theta_u}{2\theta_u} \rfloor \\ 1 & \text{if } N_b + 1 - \lfloor \frac{\omega-\theta_u}{2\theta_u} \rfloor \leq m \leq N_b \end{cases} \tag{5.14}$$

$$\mathbb{P}[G_m^T = G_{min}^T] = 1 - P[G_m^T = G_{max}^T] \tag{5.15}$$

The PMF of G_n^R have similar expressions as in (5.14) and (5.15), where index n is replaced by m.

Proof: See Appendix E.

During the data transmission phase, the beam pair $l^* = (m^*, n^*)$ has been chosen. The observed antenna gains $G_{m^*}^T$ and $G_{n^*}^T$ thus depend on the measurements performed during the beam sweeping phase. The total antenna gain for a typical link is their product. We provide hereafter their joint PMF.

Lemma 19. *Let $\nu \in \mathcal{G}^T = \{G_{max}^T, G_{min}^T\}$ and $\kappa \in \mathcal{G}^R = \{G_{max}^R, G_{min}^R\}$ two possible values for the transmitter and receiver antenna gain, respectively. The joint*

probability $P[G^T_{m^*} = \nu, G^R_{n^*} = \kappa]$ *can be computed as follows:*

$$\mathbb{P}[G^T_{m^*} = \nu, G^R_{n^*} = \kappa] = \sum_{\substack{m\in[1:N_b] \\ n\in[1:N_b]}} \mathbb{P}[G^T_m = \nu, G^R_n = \kappa, l^* = (m,n)] \tag{5.16}$$

where

$$\begin{aligned} &\mathbb{P}[G^T_m = \nu, G^R_n = \kappa, l^* = (m,n)] \\ &= \sum_{\substack{(\nu_i,\kappa_j)\in\mathcal{G}^T\times\mathcal{G}^R \\ i\in[1:N_b]\setminus m,\, j\in[1:N_b]\setminus n}} \left\{ \mathbb{E}_h \left[\prod_{\substack{\bar{m}\in[1:N_b],\bar{n}\in[1:N_b] \\ (\bar{m},\bar{n})\neq(m,n) \\ \nu_m=\nu,\kappa_n=\kappa}} F\left(\frac{h\nu\kappa}{\nu_{\bar{m}}\kappa_{\bar{n}}}\right) \right] \mathbb{P}[G^T_m = \nu]\mathbb{P}[G^R_n = \kappa] \right. \\ &\qquad \left. \prod_{\substack{i\in[1:N_b]\setminus m \\ j\in[1:N_b]\setminus n}} \mathbb{P}[G^T_i = \nu_i]\mathbb{P}[G^R_j = \kappa_j] \right\} \end{aligned} \tag{5.17}$$

where h *is the channel fading coefficient with CDF* $F(\cdot)$ *and where the terms* $\mathbb{P}[G^T_i = \nu_i]$ *and* $\mathbb{P}[G^R_j = \kappa_j]$ *can be computed thanks to Lemma 18.*

Proof: See Appendix F.

If $\omega < \theta_u$, there is no overlap between adjacent beams. As per equation (5.12), if θ_u approaches ω, it becomes more likely for G^T_1 to reach its maximum value of G^T_{max}. On the other hand, when $\omega > \theta_u$, the antenna beam can cover multiple sectors of width θ_u. A smaller θ_u allows for more sectors to be covered, all of which will have maximum antenna gains. Considering these two facts, as θ_u decreases, the chosen beam pairs are more likely to achieve their maximum antenna gain according to Lemma 19.

5.4 Data transmission

We characterize in this section the data transmission performance in a URLLC context.

5.4.1 Effective achievable rate and delay

The transmission rate for a transmitter-receiver pair during the data transmission phase is approximated by the classical Shannon formula, where the interference is

considered as noise [58]. For a typical receiver at origin o and its associated transmitter as shown in figure 5.2, the *Transmission Rate* $\mathcal{R}$ during the data transmission phase is expressed as follows:

$$\mathcal{R} = W \log_2 \left(1 + \frac{P h_{x_o} G^T_{m^*} G^R_{n^*} \ell(r)}{\sum_{x \in \Phi \setminus x_o} P h_x g^R(\psi_x, \theta^R_{n^*}) g^T(\xi_x, \theta^T_x) \ell(|x|) + \mathcal{N}_0 W} \right) \tag{5.18}$$

where h_{x_o} and h_x are independent fading coefficients for the transmission and the interference link, respectively. The boresight direction of the interfering antenna is denoted as θ^T_x. The antenna gains $G^T_{m^*}$ and $G^R_{n^*}$ are random variables following the PMF in Lemma 19. During the data transmission phase, a user sends a data file using the beam pairs $l^* = (m^*, n^*)$ chosen during the beam training phase. In order to account for the fraction of the slot dedicated to beam training, we define the *Effective Achievable Rate* [62], [63]:

$$\widetilde{\mathcal{R}} = \left(1 - \frac{N_b^2 \tau}{T} \right)^+ \mathcal{R} \tag{5.19}$$

The *delay* D to transfer a data packet of length L consists of both the beam training delay and the data transmission delay:

$$D = N_b^2 \tau + \frac{L}{\mathcal{R}} \tag{5.20}$$

5.4.2 Effective rate conditional coverage probability

The *Rate Coverage Probability*, $p_c(\eta)$, is defined as the probability that the transmission rate for a typical transmitter-receiver link is greater than a threshold η in bits/s.

$$p_c(\eta) = \mathbb{P}(\mathcal{R} > \eta) \tag{5.21}$$

This metric can only characterize the spatial average coverage performance among different users. Users at different locations however perceive different channel conditions, so that the coverage probability is itself random across the links. The *Conditional Rate Coverage Probability*, $P_c(\eta)$, has thus been introduced in [18] to characterize the reliability for a typical user given a specific network topology realization:

$$P_c(\eta) \triangleq \mathbb{P}(\mathcal{R} > \eta | \Phi^T, \Phi^R) \tag{5.22}$$

The rate coverage probability in (5.21) is nothing else than its expectation with respect to the processes $\{\Phi^T, \Phi^R\}$. In the same way, we define the *Effective Rate*

Conditional Coverage Probability $\tilde{P}_c(\tilde{\eta})$, which is related to the effective achievable rate:

$$\tilde{P}_c(\tilde{\eta}) = \mathbb{P}\left(\widetilde{\mathcal{R}} > \tilde{\eta} | \Phi^T, \Phi^R\right) \tag{5.23}$$

where $\tilde{\eta}$ is the effective rate threshold.

We define the *Conditional Success Transmission Probability* as the probability that the delay D is smaller than the slot duration T for a typical D2D pair:

$$\mathbb{P}(D < T | \Phi^T, \Phi^R) = \mathbb{P}\left(\mathcal{R} > \frac{L}{T - N_b^2 \tau} | \Phi^T, \Phi^R\right) \tag{5.24}$$

$$= \mathbb{P}\left(\widetilde{\mathcal{R}} > \frac{L}{T} | \Phi^T, \Phi^R\right) \tag{5.25}$$

Equation (5.25) shows that when $\tilde{\eta} = \frac{L}{T}$, the effective conditional rate coverage probability is exactly the conditional success transmission probability to transfer a file of size L within a slot duration T. This is also equal to the rate coverage probability with $\eta = \frac{L}{T - N_b^2 \tau}$ during the data transmission phase, where $N_b^2 \tau \leq T$.

5.4.3 Effective rate meta-distribution

The meta-distribution is defined as the CCDF of the conditional coverage probability [18]. This metric provides the proportion of users whose coverage probability is above a certain threshold. It can thus be interpreted as a measure of the link reliability across the network. Similar to the definition in [18], [56], we define the *Rate Meta-distribution* to characterize the spatial distribution of the devices communications reliability:

$$\bar{F}_{P_c(\eta)}(\epsilon) \stackrel{\Delta}{=} \mathbb{P}^!(P_c(\eta) > \epsilon), \qquad \epsilon \in [0,1], \eta \in \mathbb{R}^+. \tag{5.26}$$

where $\mathbb{P}^!$ denotes the Palm measure of $\{\Phi^T, \Phi^R\}$. Respectively, this idea can be further extended to analysis the *Effective Rate Meta-distribution* as follows:

$$\bar{F}_{\tilde{P}_c(\tilde{\eta})}(\epsilon) \stackrel{\Delta}{=} \mathbb{P}^!(\tilde{P}_c(\tilde{\eta}) > \epsilon), \qquad \epsilon \in [0,1], \tilde{\eta} \in \mathbb{R}^+. \tag{5.27}$$

Users can successfully complete transmission within the time slot T if the effective achievable rate exceeds $\tilde{\eta} = \frac{L}{T}$. In such cases, the effective rate meta-distribution provides the proportion of users whose probability of successful transmission is greater than ϵ. Communication is considered reliable when a typical user's probability of achieving a transmission rate higher than $\tilde{\eta}$ is greater than ϵ. We call ϵ the *Reliability Threshold* of the network.

5.5 Rate meta-distribution with misalignment

This section provides mathematically tractable expressions for the rate meta-distribution. A common approach involves first the derivation of the moments of the conditional coverage probability, and then the application of either the Gil-Pélaez theorem or the beta approximation [18].

5.5.1 Moments of the conditional rate coverage probability

Theorem 20. *Consider a D2D network with the BF model introduced in section 5.2. The b-th moment of the conditional rate coverage probability* $M_b(\eta) = \mathbb{E}[(P_c(\eta))^b]$ *during the data transmission phase can be approximated as follows:*

$$M_b \simeq \sum_{k_1+\ldots+k_M=b} \binom{b}{k_1 \ldots k_M} \left(\prod_{m=1}^{M} \left(\binom{M}{m} (-1)^{m+1} \right)^{k_m} \right) \mathbb{E}_{G_o} \left[e^{-M\beta\eta' \frac{\mathcal{N}_0 W}{P G_o} \sum_{m=1}^{M} m k_m} e^{-\lambda Q(m,\eta',G_o)} \right] \tag{5.28}$$

where $\eta' = \frac{2^{\frac{\eta}{W}}-1}{\ell(r)}$, $\beta = [\Gamma(1+M)]^{-1/M}$. *The variable* $G_o = G^T_{m^*} G^R_{n^*}$ *is the total antenna gain of the typical transmitter-receiver link. The PMF of* G_o *can be obtained from Lemma 19. The function* $Q(m, \eta', G_o)$ *is defined as follows:*

$$\begin{aligned} & Q(m,\eta',G_o) \\ =& \frac{1}{2\pi}[\omega^2 A(m,\eta',G_o,G^T_{max}G^R_{max}) + \omega(2\pi-\omega)A(m,\eta',G_o,G^T_{max}G^R_{min}) \\ &+\omega(2\pi-\omega)A(m,\eta',G_o,G^T_{min}G^R_{max}) + (2\pi-\omega)^2 A(m,G_o,G^T_{min}G^R_{min})] \end{aligned} \tag{5.29}$$

where

$$A(m,\eta',G_o,G_x) = \lim_{T\to\infty} \frac{T^\delta \delta}{2} \int_0^1 \left(1 - \prod_{m=1}^{M} (1 + \frac{m\beta\eta' G_x}{G_o T t})^{-M k_m} \right) t^{\delta-1} dt \tag{5.30}$$

and $\delta = 2/\alpha$.

Proof: See Appendix G.

Corollary 3. *The first moment of the conditional coverage probability can be expressed as follows:*

$$M_1 \simeq \sum_{m=1}^{M} \binom{M}{m} (-1)^{m+1} \mathbb{E}_{G_o} \left[e^{-mM\beta\eta' \frac{\mathcal{N}_0 W}{P G_o}} e^{-\lambda Q(m,\eta',G_o)} \right] \tag{5.31}$$

where the expression of $Q(m,\eta',G_o)$ *is given by* (5.29). *The function* $A(m,\eta',G_o,G_x)$ *can be expressed as follows:*

$$A(m,\eta',G_o,G_x)=\lim_{T\to\infty}\frac{T^{\delta}\delta}{2}B(\delta,1)\sum_{n=1}^{M}\binom{M}{n}(-1)^{n+1}{}_2F_1(n,\delta,\delta+1;-\frac{G_oT}{m\beta\eta'G_x}) \tag{5.32}$$

where $B(\cdot)$ *denotes the Beta function and* ${}_2F_1(\cdot)$ *denotes the hypergeometric function [65].*

Proof: See Appendix H.

Corollary 4. *The second moment of the conditional coverage probability can be expressed as follows:*

$$\begin{aligned}M_2\simeq&\sum_{m=1}^{M}\left(\binom{M}{m}(-1)^{m+1}\right)^2\mathbb{E}_{G_o}\left[e^{-2mM\beta\eta'\frac{\mathcal{N}_0W}{PG_o}}e^{-\lambda Q_1(m,\eta',G_o)}\right]\\&+\sum_{i=1}^{M-1}\sum_{j=i+1}^{M}2\binom{M}{i}\binom{M}{j}(-1)^{i+j}\mathbb{E}_{G_o}\left[e^{-(i+j)M\beta\eta'\frac{\mathcal{N}_0W}{PG_o}}e^{-\lambda Q_2(m,\eta',G_o)}\right]\end{aligned} \tag{5.33}$$

Functions $Q_1(m,\eta',G_o)$ *and* $Q_2(i,j,\eta',G_o)$ *have similar expressions as in* (5.29), *where* $A(m,\eta',G_o,G_x)$ *are replaced by* $A_1(m,\eta',G_o,G_x)$ *and* $A_2(i,j,\eta',G_o,G_x)$ *respectively:*

$$A_1(m,\eta',G_o,G_x)=\lim_{T\to\infty}\frac{T^{\delta}\delta}{2}B(\delta,1)\sum_{n=1}^{2M}\binom{2M}{n}(-1)^{n+1}{}_2F_1(n,\delta,\delta+1;-\frac{G_oT}{m\beta\eta'G_x}) \tag{5.34}$$

$$A_2(i,j,\eta',G_o,G_x)=\lim_{T\to\infty}\frac{T^{\delta}\delta}{2}\int_0^1\left(1-(1+\frac{i\beta\eta'G_x}{G_oTt})^{-M}(1+\frac{j\beta\eta'G_x}{G_oTt})^{-M}\right)t^{\delta-1}dt \tag{5.35}$$

Proof: See appendix H.

Corollary 5. *To calculate the b-th moment of the effective conditional rate coverage probability* $\tilde{P}_c(\tilde{\eta})$ *in* (5.23), *we only need to replace* η *in Theorem 20 by* $\frac{T\tilde{\eta}}{T-N_b^2\tau}$, *where* $N_b^2\tau<T$.

5.5.2 Beta approximation

The numerical computation of the exact rate meta-distribution by using Gil-Pélaez theorem is often difficult. An alternative solution is to approximate it with a beta

distribution by matching the first and the second moment as follows:

$$\bar{F}_{P_c(\eta)}(\epsilon) = 1 - I_{\epsilon}\left(\frac{M_1 M_2 - M_1^2}{M_1^2 - M_2}, \frac{(1-M_1)(M_2-M_1)}{M_1^2 - M_2}\right) \tag{5.36}$$

where $I_{\epsilon}(\cdot)$ is the regularized incomplete beta function [46]. Similarly the effective rate meta-distribution $\bar{F}_{\tilde{P}_c(\tilde{\eta})}(\epsilon)$ can be approximated by using the first and second moment of $\tilde{P}_c(\tilde{\eta})$.

5.6 Numerical results

This section aims at verifying the accuracy of our analytical approximation through Monte Carlo simulations and providing insights for the design of mmWave URLLC D2D networks.

5.6.1 Simulation settings

Our simulation settings are close to the synchronization and initial access process parameters defined for 5G NR [66]. Our simulations assume a carrier frequency of $f_c = 28$ GHz and a transmission bandwidth of $W = 400$ MHz [67]. We assume a mini-slot duration of $\tau = 4.46$ μs, which is equivalent to one orthogonal frequency-division multiplexing (OFDM) symbol time with cyclic prefix, given a sub-carrier spacing of 240 kHz [67]. Inspired by URLLC requirements, we set $T = 1$ ms and $L = 32$ bytes [68]. Path-loss parameters are derived from the micro-cell scenario in [68]. The path-loss exponent is set to $\alpha = 2.3$ [39]; the constant path-gain K is calculated as the free space path loss (FSPL) at a reference distance of 1 meter, which is equal to $(\frac{c}{4\pi f_c})^2$, where c is the speed of light. The distance between a receiver and its associated transmitter is set to $r = 30$ m, with a transmission power of $P = 28$ dBm. The noise PSD is $\mathcal{N}_0 = -174$+NF dBm/Hz where the noise factor is set to NF $= 8$ dB. We assume a transmitter-receiver pair intensity of $\lambda = 0.001$ m^{-2} by default, i.e., the average distance between neighboring transmitter-receiver pairs is around 30 m. Parameters values are summarized in Tab. 5.1.

5.6.2 Impact of the number of antennas on the transmission rate

We investigate here the impact of the number of antennas on the data transmission rate while keeping the beam training codebook size fixed at $N_b = 15$. We set the

Table 5.1: System Parameters

Symbol	Description	Default values
W	Transmission bandwidth	400 MHz
P	Transmit power	28 dBm
$\mathcal{N}_0$	Thermal noise PSD	-166 dBm
r	The link distance between D2D users	30 m
f_c	Carrier frequency	28 GHz
K	FSPL at reference distance 1 m	$K = 7.2695e-07$
α	Path-loss exponent	$\alpha = 2.3$
T	Time slot duration	1 ms
τ	Mini-slot time duration	4.46 μs
L	File size	32 bytes
λ	D2D transmitter-receiver pairs density	0.001 m^{-2}

transmission rate threshold to $\eta = \frac{L}{T}$.

Figure 5.3 (a) and (b) show the mean and the variance of the conditional rate coverage probability $P_c(\eta)$ as a function of the number of antennas N_a. The green curves show the analytical results, see (5.28), while the red curves depict the simulation results. Dashed curves assume a perfect alignment of the transmitter and receiver beams, i.e., $G_o = G^T_{max} G^R_{max}$ always holds in equations. We first see that analysis and simulation results match very well: this confirms the accuracy of our approximation of the lower incomplete gamma function, see (G.3).

Figure 5.3 (a) shows that the mean of the rate conditional coverage probability is a monotonically increasing function of N_a when the beam alignment is perfect. This was expected since an increase in the number of antennas results in a stronger main lobe gain and a narrower beamwidth ω of the main lobe. These effects lead to a higher received power and a weaker interference when there are no alignment errors. However, when considering the beam misalignment due to the training phase, the performance may degrade. In Figure 5.3 (a), we see that the mean of the rate conditional coverage probability is first increasing and then decreasing with a maximum achieved for $N_a = 4$. Below this threshold, the amount of resources dedicated to training is sufficient and increasing the number of antennas also increases the joint antenna gain, leading in turn to better coverage. Beyond the optimal number of

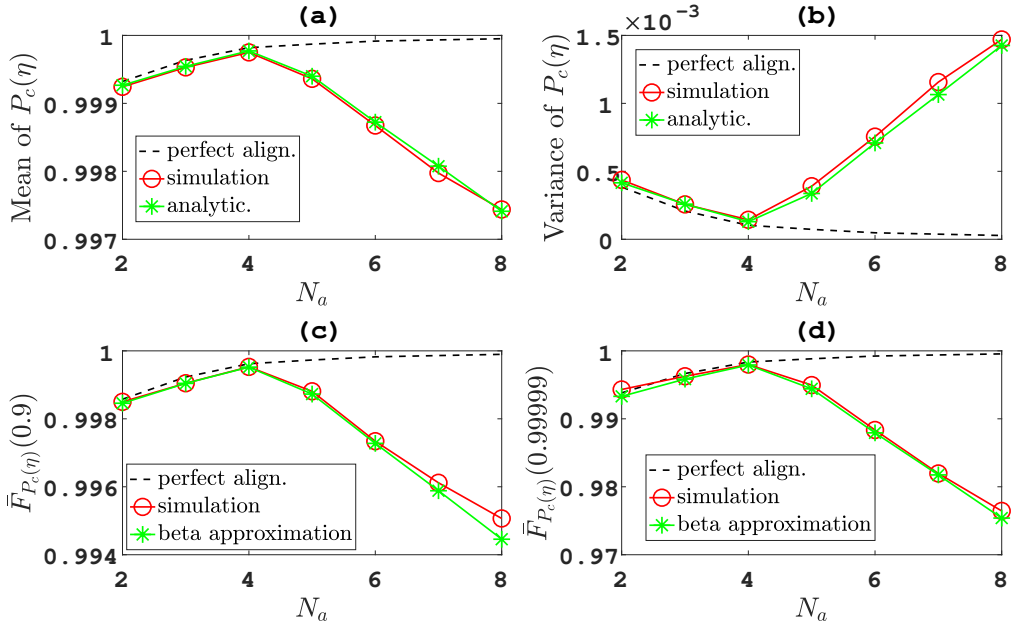

Figure 5.3: Mean (a) and variance (b) of the conditional rate coverage probability; Proportion of links that have a conditional rate coverage probability greater than a reliability threshold of 90% (c) or 99.999% (d), as a function of the number of antennas.

antennas however, the training phase is not sufficient for a good beam alignment: beams are thinner and even a small misalignment error leads to a rapid degradation of the coverage. This figure highlights the trade-off between the number of antennas and the rate coverage in the presence of beam misalignment, a phenomenon that is not captured by studies assuming perfect beam alignment.

Figure 5.3 (b) shows the variance of $P_c(\eta)$ as a function of N_a. When there is no misalignment, the variance is monotonically decreasing with the number of antennas. As N_a is increasing, the transmit power is indeed more and more precisely focused on the transmitter-receiver link, so that the interference created to other D2D pairs decreases; D2D transmissions are more and more independent on each other, so that the coverage performance is more homogeneous and the variance decreases. When misalignment errors are taken into account, the same trend is observed when the number of antennas is small because the training is sufficient to achieve a good alignment. On the contrary, when N_a grows, there are either very good communication conditions if beams manage to be aligned despite the poor training or very bad conditions when the error is significant. Thinner beams increase these differences, so that the variance increases.

For a given reliability threshold ϵ, we can interpret the meta distribution as the proportion $\bar{F}_{P_c(\eta)}(\epsilon)$ of users who meet the reliability requirement. In Figure 5.3 (c) and 5.3 (d), we compare the percentage of users who meet the reliability requirement assuming two reliability thresholds, namely $\epsilon = 0.9$ and $\epsilon = 0.99999$. The green curves in the figures depict the beta approximations for $\bar{F}_{P_c(\eta)}(\epsilon)$, while the red curves are obtained through simulation. The dashed curves is obtained from the beta approximation when the alignment is perfect. The figures demonstrate that the beta approximation is an accurate technique for analyzing the meta-distribution. The proportion of users meeting the reliability requirements follows the same trend as the mean of the conditional rate coverage probability for the same reasons: in absence of error, thinner beams provide enhanced signal strength, while in presence of errors, thinner beams are beneficial as long as the training resources are sufficient. There is thus an optimal number of antennas that maximizes the proportion of users meeting the reliability requirements. At last, changing the reliability threshold does not alter the performance trends, but it does impact the proportion of users that can satisfy the reliability constraint. For example, with 8 antennas, about 99.5% of the links can satisfy a reliability threshold of 90%, while only 97.5% of the links can achieve a more stringent reliability threshold of 99.999%.

5.6.3 Impact of the codebook size on the transmission rate

In addition to the number of antennas, the size of the training codebook, represented by the variable N_b, is another critical constraint that affects the network's performance. The transmission rate threshold is set to $\eta = \frac{L}{T}$. Figure 5.4 (a) and (b) show the mean and the variance of the rate conditional coverage probability $P_c(\eta)$ as a function of N_b for different numbers of antennas. The solid curves represent analytical results obtained from equation (5.28) while the dashed curves have been obtained from simulations. The straight dotted lines have been obtained with a perfect beam alignment. Here again, we see that analysis and simulations match very well. This confirms the tightness of our approximation.

In both figures, we observe that the curves accounting for misalignment errors converge to the curves assuming perfect alignment. As N_b increases, the codebook resolution θ_u decreases, so that the transmitter and the receiver have a finer estimation of the AoA and AoD. The probability of having an alignment error decreases and the magnitude of this error is also decreasing. In a nutshell, the higher N_b is,

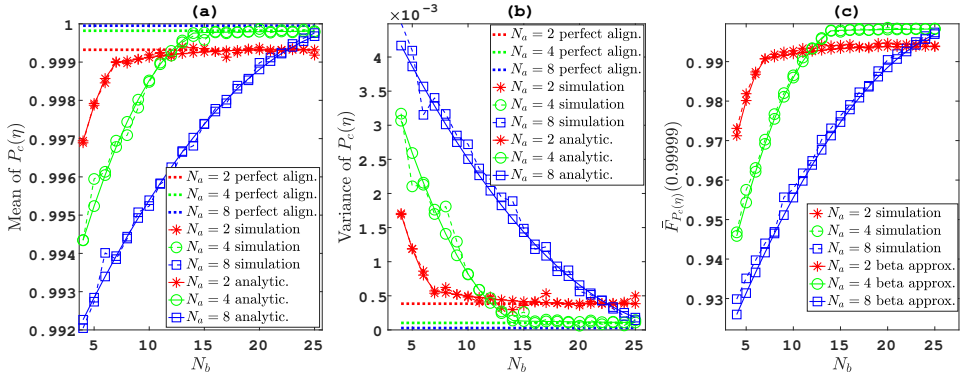

Figure 5.4: Mean (a) and variance (b) of the conditional rate coverage probability; Proportion of links that have a conditional rate coverage probability greater than a reliability threshold of 99.999% (c), as a function of the number of beams.

the more accurate the training period is. After some threshold, however, increasing N_b does not provide a significant gain on the performance since the beam resolution is much lower than the beam width. The figure also demonstrates that if N_a is large, $P_c(\eta)$ requires a larger N_b to approach its limit, as more antennas with thinner beam lobes require codebooks with a more precise resolution to perform beam alignment. At last, we see that the variance is decreasing with N_b and increasing with N_a. This can be explained by the fact that misalignment errors introduce variability in the communication conditions across the links.

Figure 5.4 (c) illustrates the percentage of D2D users whose rate conditional coverage probability $P_c(\eta)$ is larger than the reliability threshold of $\epsilon = 99.999\%$ as a function of N_b. The dashed curves show simulation results, while the solid curves are obtained using the beta approximation. Again, the close agreement between the curves suggests that the beta approximation is an accurate tool for analyzing the meta-distribution. These curves exhibit similar trends to the mean of $P_c(\eta)$, indicating that a longer training time can better align the beams and enable more users to have reliable communications. Increasing the number of antennas can ultimately guarantee more users to meet the reliability requirement, but it requires longer training time. For example, if we want to achieve a reliability of 99.999% for more than 99% of the users, then a training period with $N_b = 7$, 11, and 21 is required for $N_a = 2$, 4, and 8 antennas, respectively. However, it is impossible to have more than 99.5% of the users meeting the reliability requirement with only $N_a = 2$ antennas as the performance is saturating to a lower value, whatever the training period.

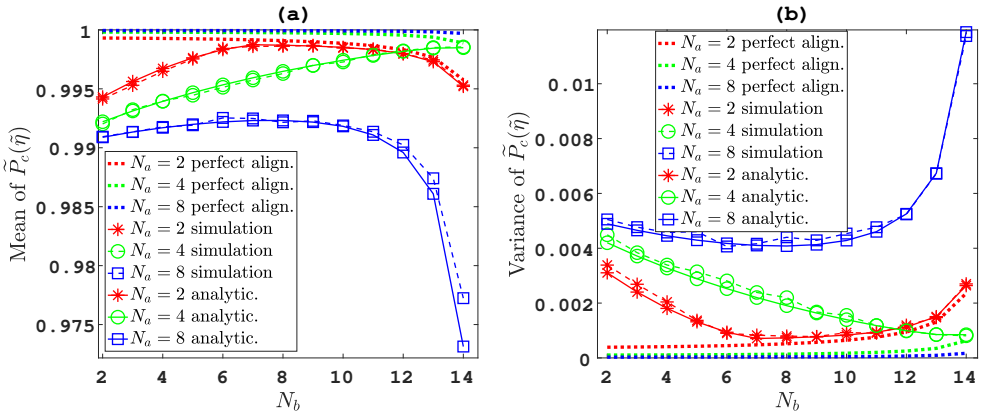

Figure 5.5: Mean (a) and variance (b) of the effective rate conditional coverage probability as a function of the number of beams.

5.6.4 Effective achievable rate analysis

The analysis presented so far focuses on the rate coverage probability during the data transmission phase. However, when taking into account the overhead of the beam training phase, the size of the beam training codebook is limited by the total time budget, resulting in $N_b \leq \lfloor \sqrt{\frac{T}{\tau}} \rfloor$. In this section, we study the effective achievable rate with an effective rate threshold of $\tilde{\eta} = \frac{L}{T}$.

Figure 5.5 (a) and (b) illustrate how the mean and the variance of the effective conditional rate coverage probability $\tilde{P}_c(\tilde{\eta})$ evolves with respect to N_b for different numbers of antennas. The solid curves represent analytical results obtained using the equations of Corollary 5, while the dashed curves depict simulation results. The dotted lines indicate the conditional rate coverage probability when there is no misalignment. We first observe that the mean is decreasing with N_b in the absence of errors. This is due to the lack of data resources when the training period becomes longer. Continuing with perfect alignment, the variance is increasing because interference is playing an increasing role as the transmission rate decreases. The various topological situations around every D2D pair create a certain variability in the signal quality and thus on the coverage.

In Figure 5.5 (a), we see that, in the presence of misalignment errors, curves are first increasing and then possibly decreasing. The reason lies in two conflicting effects: when N_b increases, the misalignment errors decrease while the amount of resources dedicated to data is reduced. If we look at Figure 5.4, we see that an almost perfect alignment is achieved for $N_b = 7$ and 14 for $N_a = 2$ and 4 antennas, respectively. This means that no improvement can be expected from the training

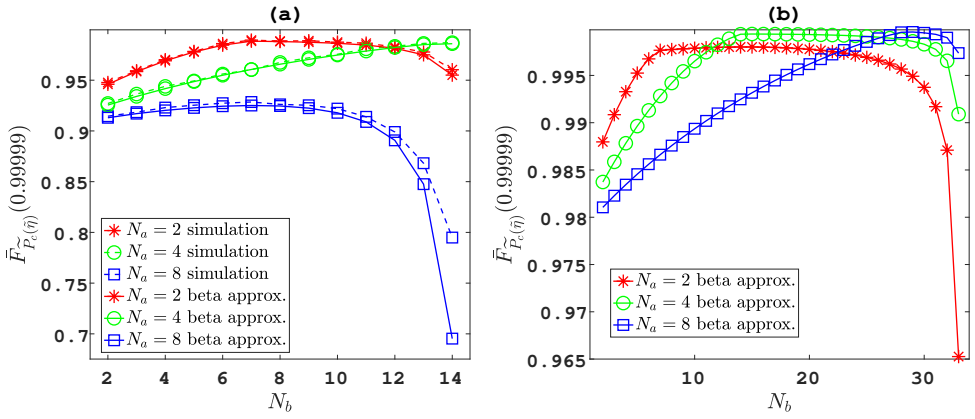

Figure 5.6: Proportion of links with an effective conditional rate coverage probability greater than the reliability thresholds 99.999% as a function of the number of beams for $T = 1$ ms (a) and $T = 5$ ms (b).

after these thresholds. This explains why the performance reaches its maximum at these values in Figure 5.5 (a). On the contrary, for $N_a = 8$ antennas, the training is far from perfect when $N_b = 14$. The training is not able to compensate for the lack of data resources. Overall, $N_a = 2$ and $N_b = 8$, or $N_a = 4$ and $N_b = 14$ offer the best performance, while $N_a = 8$ antennas are not able to recover from the errors with reasonable overhead.

By fixing N_b to a low value, e.g. $N_b = 4$, Figure 5.5 (a) shows that $\tilde{P}_c(\tilde{\eta})$ decreases as the number of antennas increases. This is due to the imprecise resolution of the codebook and a severe beam misalignment. With more antennas, the beam width is thinner and misalignment worsens. When $N_b = 14$ on the contrary, $\tilde{P}_c(\tilde{\eta})$ reaches its maximum with 4 antennas, which offer the best trade-off between signal quality achieved with beamforming and misalignment errors induced by an incomplete training.

The variance of $\tilde{P}_c(\tilde{\eta})$, as shown in Figure 5.5 (b), exhibits an opposite trend to the mean of $\tilde{P}_c(\tilde{\eta})$. Misalignment errors are a source of high variability in the link quality, especially when the beam is thin, because a small deviation with respect to the right direction induces a rapid loss in the beam gain. This explains why the variance decreases when the training becomes better. When the amount of resources dedicated to data decreases, only links with very good quality can reach the threshold. This quality is in turn very dependent on the interference situation around the D2D pair. Depending on the topology, we can thus see a variety of situations that is captured by an increasing variance.

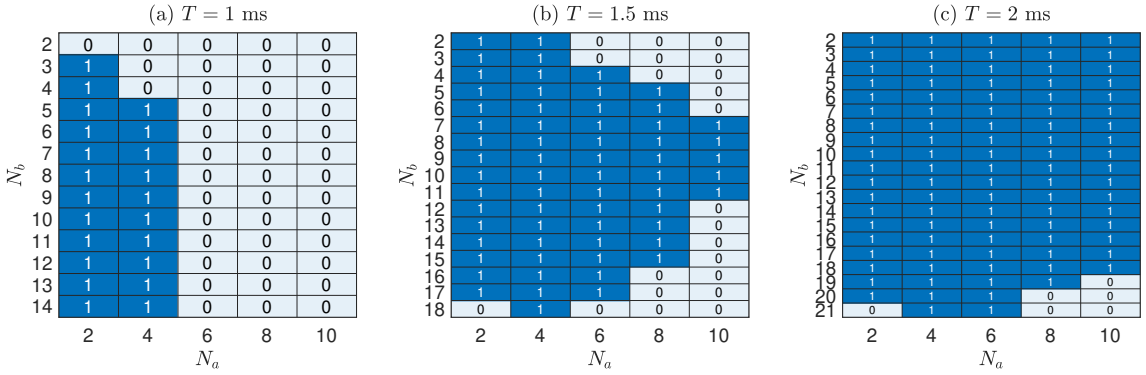

Figure 5.7: Feasibility of the URLLC requirement that 95% of the users communicate with 99.999% reliability and 1 (a), 1.5 (b), and 2 ms (c) latency [2] (feasible combinations in dark blue).

Figure 5.6 (a) shows the proportion of D2D users with an effective rate conditional coverage probability $\tilde{P}_c$ above the threshold $\epsilon = 99.999\%$ as a function of N_b for the different number of antennas. The proportion $\bar{F}_{\tilde{P}_c(\tilde{\eta})}(\epsilon)$ follows the same trend as the mean effective rate coverage probability, increasing with N_b when N_b is small and then dropping quickly when $N_b^2\tau$ approaches T. For a reliable URLLC network with low latency, a common requirement is that 95% of the users operate with 99.999% reliability and 1 ms latency [2]. According to Figure 5.6 (a), $N_a = 2$ always meets this strict constraint. When $N_a = 4$, N_b needs to be larger than 5 to ensure the reliability requirement. On the contrary, $N_a = 8$ antennas cannot achieve it.

However, increasing the number of antennas becomes a valid option if the delay requirement is relaxed. In Figure 5.6 (b), the slot duration is set to $T = 5$ ms. This lets more room for training and N_b can reach a higher value (here 33) on the x-axis. We see here how the optimal number of antennas varies with N_b. If N_b is small, it is better to use fewer antennas so that misalignment errors are less impactful. As N_b is increasing, it is more and more interesting to increase the number of antennas because we have enough time to train the beams, and consequently, the higher beam gains outperform the loss due to misalignment. For our studied scenario, the possible design choices in terms of the number of antennas and beams are summarized in Figure 5.7.

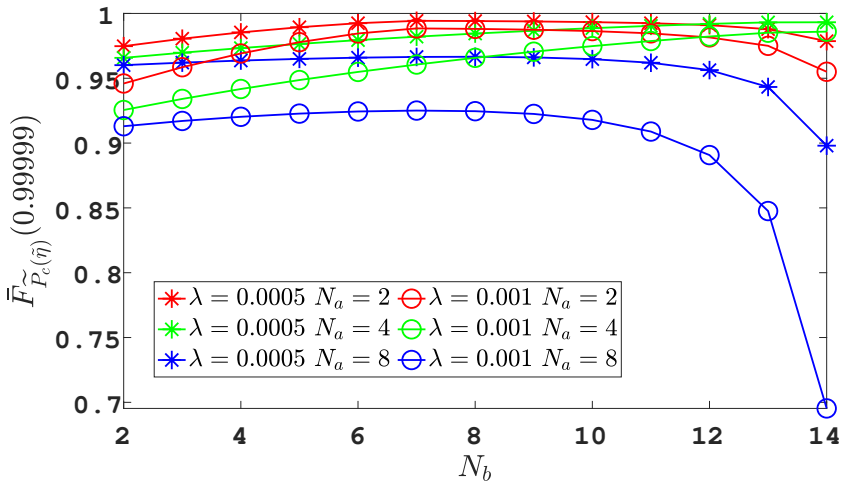

Figure 5.8: Proportion of links with an effective conditional rate coverage probability greater than a reliability threshold of 99.999% for the user densities $\lambda = 0.0005$ m^{-2} and $\lambda = 0.001$ m^{-2}.

5.6.5 Impact of user density

We investigate the impact of the user density in Figure 5.8 by comparing meta-distributions for $\lambda = 0.001$ m^{-2} and $\lambda = 0.0005$ m^{-2}. The figure shows that the user density does not influence the trends already observed for $\bar{F}_{\tilde{P}_c(\tilde{\eta})}(\epsilon)$ as a function of N_b or N_a. It shows that higher reliability can be achieved in the network with a lower user density thanks to the reduced interference. Our closed-form formulas allow the network designer to calculate the maximum allowed density for specific URLLC requirements.

5.7 Conclusion

In this chapter, we propose an analytical framework to investigate the impact of beam misalignment on mmWave URLLC D2D networks. First, the misalignment error distribution is evaluated based on the study of an imperfect exhaustive search approach. The imperfection of the beam sweeping procedure comes from the finite codebooks, the finite amount of resources dedicated to training and the high variability of the channel at high frequencies. We then derive mathematical expressions for the moments of the effective rate conditional coverage probability assuming Nakagami-M fading, and we approximate the effective rate meta-distribution using a beta approximation. Our results show that misalignment errors can be highly

detrimental if URLLC requirements are stringent. Misalignment errors not only reduce the joint beam gain but also introduces variability in the link quality that affects reliability. At last, our study highlights the trade-off between the training overhead and the number of antennas. Having fewer antennas is preferable when a very short delay is required with high reliability. In contrast, the potential gain of many antennas can be exploited when the delay constraint is relaxed.

Chapter 6

Conclusion and future works

This thesis explores the performance of mmWave D2D communication in future wireless networks. The mmWave D2D communication offers advantages such as abundant spectrum resources and expanded connectivity range. It can extend coverage and improve performance for traditional cellular networks. This technique is highly promising in the context of URLLC, as it provides fast and reliable transmissions. To overcome the high attenuation experienced in mmWave transmission, devices require multiple antennas and employ beamforming techniques to enhance signal strength and quality. This thesis proposes a tractable beamforming model for D2D communications based on the ULA, which can be analyzed from a stochastic geometry perspective. The success of beamforming requires beam training. Misalignment errors can occur within the training process, leading to a degradation of data transmission performance.

To address these challenges, our study primarily focuses on the theoretical analysis of mmWave D2D communication's performance in terms of latency, reliability, and coverage within the URLLC context. We employ stochastic geometry and queuing theory to evaluate the spatial and temporal variations in performance from two perspectives: the instantaneous average properties of the random network and the stability properties of a dynamic network with random service requests.

We investigate a dynamic D2D communication model as a spatial wireless birth-death network, where service requests are random in both time and space. Building on the previous findings of Sankararaman and Baccelli [20] regarding the stability condition of this network, we introduce directional antenna arrays for D2D users and study the stability performance with beamforming, where beam alignment can be imperfect. We evaluate the impacts of misalignment by assuming a statistical

alignment error distribution. Our contribution is establishing the stability region for the mmWave D2D network by considering both perfect and imperfect beam alignment. Our analytical and numerical results demonstrate that beamforming extends the stability region, and the critical arrival rate, also known as the stability threshold, increases with the number of antennas. However, in the presence of beam misalignment, the critical arrival rate can no longer increase without limit and has upper bounds related to the alignment errors' distributions.

For the instantaneous properties, we investigate the performance diversity among links in the mmWave D2D network. Different users located in different positions have distinct channel conditions and are subject to different interference. We analyze the reliability of different links by studying the meta-distribution for a D2D communication network with beamforming. We first evaluate the impacts of misalignment by assuming a statistical alignment error, similar to the dynamic case. We derive computationally tractable expressions of the conditional rate coverage probability's moments as a function of the number of antenna elements. Then, we approximate the meta-distribution using beta approximation methods. Our numerical simulations confirm our analytical results, indicating that the coverage performance can improve with an increase in the number of antenna elements. However, misalignment can cause a significant deterioration in coverage performance. There exists an optimal number of antenna elements that must be chosen to achieve the best coverage. Additionally, there is an optimal number of antennas that maximizes the number of users who satisfy the reliability constraints. This optimal value is a function of the reliability threshold.

Finally, we investigate the beam misalignment induced by the beam training method and the channel conditions. When considering an exhaustive beam sweeping method, the misalignment arises from finite codebooks, the finite amount of resources allocated to training, and the high variability of the channel at high frequencies. We derive the PMF of the beamforming gain using the expected beams chosen from the beam sweeping procedures. Furthermore, the alignment performance can improve with larger training overhead, which may, in turn, occupy too much time for data transmission. Our studies highlight the fundamental trade-off between training overhead and data transmission reliability. We introduce the effective rate conditional coverage probability by considering both overhead and misalignment, and we approximate the effective rate meta-distribution using a beta approximation. Our results demonstrate that misalignment errors not only reduce

the joint beam gain but also introduce variability in link quality that affects reliability. Having fewer antennas is preferable when a very short delay is required with high reliability. In contrast, the potential gain of many antennas can be exploited when the delay constraint is relaxed.

The future works involve many possibilities. In the short term, the following points could be studied:

- For the stationary case, the current beam sweeping method is time consuming. Future work can improve the model by considering more flexible and general beam training methods, such as hierarchical beam search. The beamforming in our current works is a simple analog case based on the phased array, which is not optimal when the link is not in LOS. We hope to study the network level performance with more advanced beamforming techniques, such as hybrid beamforming. More adaptive and effecient beam training methods need to be discussed for more advanced multi-antenna techniques.

- For the dynamic case, it is known that the configuration of devices' location at a time instant follows a stationary point process if the arrival rate of new users is not too high. But this is not a Poisson point process since there are clusters in this point process. The initial idea that devices adopt beamforming is that this can increase the SINR of each user. The impact of beamforming on the distribution of devices remains an interesting question to be answered. The coverage performance of this network under a stable state is expected to be investigated. Ideally we hope to find the spatial distribution of the expected sojourn time under a stable state.

- We should have more considerations in our future studies for the coherence time. On the one hand, higher spectrum faces sever Doppler effect and brings short channel coherence time. On the other hand, the channel coherence time can be reduced when beamforming is employed, see [69]. To fully account for this effect, we need to consider the spatial coherence and the beam coherence time, which indicate the general interval or average time to keep the same level of beamforming gain [69]. By considering coherence time, the independence among different links and different time slots is called into question, and the coverage meta-distribution needs to be reevaluated accordingly.

In the long term, investigating the effects of user mobility on the alignment performance and the coverage performance of the network would require more complex

studies. The future network would be a vast dynamic system with intense mobility. Recent works show that mobility can improve the network performance and reduce the variety of different users' quality of service in terms of the coverage [70], [71]. However, in a more realistic scenario, the D2D users' movement is limited by physical constraints like streets and architecture. So the Poisson linear process seems to be an ideal model to characterize the real world. It would be interesting to apply this model in further studies.

Appendix A

Proof of Theorem 14

This part is the proof of Theorem 14. To prove the theory, we apply the Miyazawa's rate conservative law (RCL) [72], which states that the average rates of increase should be equal to the rates of decrease for a stationary stochastic process. By applying RCL to the counting measure $\Phi_t(\mathbf{S})$, we get the relation:

$$\lambda|\mathbf{S}| = \lambda_d. \tag{A.1}$$

Where λ_d is the departure rate. Denote Φ_0 as the process when Φ_t is stable. By considering the total volume of data that visits the network, the RCL leads to:

$$\lambda|\mathbf{S}|L = \mathbb{E}\left[\sum_{x\in\Phi_0} R^{BF}(x,\Phi_0)\right] \tag{A.2}$$

Next we apply the RCL to the sum interference in the network, which is denoted as $\mathbf{I}_t^{BF} = \sum_{x\in\Phi_t} I^{BF}(x,\Phi_t)$. Let $\mathcal{I} = \mathbf{I}_{0+} - \mathbf{I}_0$ denotes the additional interference arisen by an arrival, and let $\mathcal{D} = \mathbf{I}_0 - \mathbf{I}_{0+}$ denotes the decrease of the interference arisen by a departure. Thus we get:

$$\lambda|\mathbf{S}|\mathbb{E}^{\uparrow}[\mathcal{I}] = \lambda_d\mathbb{E}^{\downarrow}[\mathcal{D}] \tag{A.3}$$

Where $\mathbb{E}^{\uparrow}$ and $\mathbb{E}^{\downarrow}$ are the palm probabilities at the time of arrival or departure. Combing (A.3) with (A.1), we know that:

$$\mathbb{E}^{\uparrow}[\mathcal{I}] = \mathbb{E}^{\downarrow}[\mathcal{D}] \tag{A.4}$$

By applying the Campbell's theory, we get:

$$\mathbb{E}^{\uparrow}[\mathcal{I}^{BF}] = 2\mathbb{E}[\sum_{x\in\Phi_0} G_{ox}^T G_{ox}^R P\ell(\|x\|)] \tag{A.5}$$

$$=2P\frac{\mathbb{E}[\Phi_0(\mathbf{S})]}{|\mathbf{S}|}\mathbb{E}[\int_{\mathbf{S}} G_{ox}^T G_{ox}^R \ell(\|x\|)dx] \tag{A.6}$$

Where G_{ox}^T and G_{ox}^R are the antenna gains between the receiver at origin and the interfering transmitter at x. Let $a^{BF} = \int_{\mathbf{S}} G_{ox}^T G_{ox}^R \ell(\|x\|)$. Since the position of interfering devices are uniformly distributed in the plane, and the antenna gain G_{ox}^T and G_{ox}^R are independent, we get the expression of $\mathbb{E}[\hat{a}^{BF}]$ in (3.12). For a stationary process, the departure rate λ_d follows the Papangelou's theorem [73]:

$$\lambda_d \mathbb{E}^{\downarrow}[\mathcal{D}] = \mathbb{E}[\lambda_d(0)\mathcal{D}] \tag{A.7}$$

Let $\mathbf{R}_0^{BF} = \sum_{x\in\Phi_0} R^{BF}(x,\Phi_0)$. We can then get the expression of $\mathbb{E}^{\downarrow}[\mathcal{D}]$ as follows:

$$\mathbb{E}^{\downarrow}[\mathcal{D}] = 2\mathbb{E}\left[\frac{\lambda_d(0)}{\lambda_d}\sum_{x\in\Phi_0}\frac{R^{BF}(x,\Phi_0)}{\mathbf{R}_0^{BF}} I^{BF}(x,\Phi_0)\right] \tag{A.8}$$

$$= 2\frac{\mathbb{E}[\sum_{x\in\Phi_0} R^{BF}(x,\Phi_0)I^{BF}(x,\Phi_0)]}{\mathbb{E}[\mathbf{R}_0^{BF}]} \tag{A.9}$$

$$= 2\frac{\mathbb{E}_{\Phi_0}^0[R^{BF}(0,\Phi_0)I^{BF}(0,\Phi_0)]}{\mathbb{E}[\mathbf{R}_0^{BF}]}\mathbb{E}[\Phi_0(\mathbf{S})] \tag{A.10}$$

Adapting (A.6) and (A.10) to (A.4), we get:

$$2P\frac{\mathbb{E}[\Phi_0(\mathbf{S})]}{|\mathbf{S}|}\mathbb{E}[a^{BF}] = \ 2\frac{\mathbb{E}_{\Phi_0}^0[R^{BF}(0,\Phi_0)I^{BF}(0,\Phi_0)]}{\mathbb{E}[\mathbf{R}_0^{BF}]}\mathbb{E}[\Phi_0(\mathbf{S})] \tag{A.11}$$

By applying (A.2) to (A.11), we obtain:

$$\lambda = \frac{\mathbb{E}_{\Phi_0}^0[R^{BF}(0,\Phi_0)I^{BF}(0,\Phi_0)]}{PL\mathbb{E}[a^{BF}]} \tag{A.12}$$

Given the definition of the transmission rate in (3.10), we have:

$$R^{BF}(0,\Phi_0)I^{BF}(0,\Phi_0) \leq \frac{PW g_a^T(\xi,\theta_0^T)g_a^T(\psi,\theta_0^R)\ell(r)}{\ln(2)} \tag{A.13}$$

Combing (A.12) and (A.13), we get the following inequality:

$$\lambda \leq \frac{W\mathbb{E}[g_a^T(\xi,\theta_0^T)]\mathbb{E}[g_a^T(\psi,\theta_0^R)]\ell(r)}{\ln(2)L\mathbb{E}[a^{BF}]}. \tag{A.14}$$

Appendix B

Miyazawa rate conservation law

Theorem 21. *(Miyazawa Conservation Principle [72]) Consider* $\{X(t)\}$, $t \in \mathbb{R}$ *as a bounded stationary real-valued stochastic process on* $(\mathbb{R}, \mathcal{B}(\mathbb{R}))$. *We assume that the sample path of* $X(t)$ *are continuous on the right and have limits on the left. This stochastic process is defined on* $(\Omega, \mathcal{F}, \mathbb{P})$.
Let N *be a stationary point process with a finite intensity* λ_N*(* $\mathbb{E}[N((0,1])] = \lambda_N$*), representing all the discontinuous epochs of* $X(t)$. N *is compatible with* θ_t. *We further assume that* $X(t)$ *has a right hand derivative* $X'(t)$ *for all* t, *and* N *is a counting process or simple point process (locally finite and positive). All discontinuous epoch of* $X(t)$ *are included in* N. $X^-(t) = X(t-) \equiv \lim_{\epsilon \to 0} X(t-\epsilon)$. *Then an elementary calculas leads, for all* $t > 0$,

$$X(t) = X(0) + \int_0^t X'(u)du + \int_0^t (X(u) - X(u-))N(du)$$

Assume either $\mathbb{E}(|X(0)|)$, $\mathbb{E}(|X'(0)|)$ *and* $\mathbb{E}_N(|X(0) - X(0-)|)$ *are finite. By the stationarity of* $X(t)$ *and the Fubini's theorem, we have the following formula after taking the expectation w.r.t* $\mathbb{P}$ *of both sides. Due to the* θ_t*-invariance of* P *we have.*

$$\int_0^t \mathbb{E}[X'(u)]du + \mathbb{E}\left[\int_0^t (X(u) - X(u-))Ndu\right] = 0$$

Where $\mathbb{E}[X'(u)] = \mathbb{E}[X'(0)]$. *By the definition of Palm probability we have.*

$$\mathbb{E}[X'(0)] + \lambda_N \mathbb{E}_N^0[X(0) - X(0-)] = 0$$

This formula is known as the rate conservative formula. It illustrates the facet that the average increased volume of rate equals to be the average decreased volume for a stationary process.

Appendix C

Simplified beamforming model

In this section, we express the two parameters ρ, ω as functions of the number of antenna elements n. The methods is based on [43]. A uniform linear array has n antenna elements aligned along the x-axis and are equally spaced with distance d. Consider a planar wave departing in (or arriving from) the direction θ with respect to the x-axis. The field pattern at every antenna element is denoted by $f_e(\theta)$, the power pattern is denoted by $g_e(\theta)$. Take the phase at the first antenna element as a reference. Considering the antennas at the transmitters part firstly, the combined far field pattern f_a of the array is obtained as:

$$f_a(\theta) = \frac{1}{\sqrt{n}} f_e(\theta) \sum_{i=1}^{n} a_i e^{j((i-1)kd\cos\theta)} \tag{C.1}$$

where $k = 2\pi/\lambda$ where λ is the wavelength and a_i is a phase offset applied at antenna element i. The $1/\sqrt{n}$ factor is to account for the power split among the n antenna elements at the transmission. Choosing $a_i = e^{-j((i-1)kd\cos\theta_0)}$, the power gain $g_a(\theta) = |f_a(\theta)|^2$ leads to:

$$g_a(\theta) = \frac{1}{n} g_e(\theta) \left| \frac{\sin(nk\frac{d}{2}(\cos\theta - \cos\theta_0))}{\sin(k\frac{d}{2}(\cos\theta - \cos\theta_0))} \right|^2 \tag{C.2}$$

The maximum array factor gain for the transmitter is achieved for $\theta = \theta_0$: the maximum array factor is n. If we assume a rectangular patch antenna, the antenna radiation pattern is hemispheric and has a directivity of 2 [43]. The power pattern is expressed as in (3.2). Hence we now assume $\theta_0 = \pi/2$ (boreside), $d = \lambda/2$. Finally the maximum gain of the transmitters antenna is $g_a(\theta_0) = g_e(\theta_0)n$. The HPBW of the array factor is obtained by solving the equation:

$$\frac{g_e}{n} \left| \frac{\sin(\frac{1}{2}n\pi\cos\theta)}{\sin(\frac{1}{2}\pi\cos\theta)} \right|^2 = \frac{g_e n}{2} \tag{C.3}$$

Using an approximation for the sine function for small arguments by approximating the denominator by $(\frac{1}{2}n\pi\cos\theta)^2$, we have to solve: $|\sin(x)/x|^2 = 1/2$. Numerically, we find: $x \approx 1.392$. So that the half power bandwidth width (HPBW) $\omega(n)$ of n transmitter antennas is:

$$\omega(n) \quad = \quad 2\left(\frac{\pi}{2} - \arccos\frac{2.784}{n\pi}\right) \approx \frac{1.7723}{n} \tag{C.4}$$

Let ρ be the minimum gain in the complementary sector. We equalize the approximate and exact radiated powers.

$$g_e n\omega(n) + \rho(\pi - \omega(n)) = K(n) \tag{C.5}$$

Then the transmitter antennas minimum gain is given by:

$$\rho \quad = \quad \frac{K(n) - g_e n\omega(n)}{\pi - \omega(n)} \tag{C.6}$$

where $K(n)$ is the total power gain of antennas half radiation region from $\theta = 0$ to $\theta = \pi$ shown by (C.2). For the receiver antenna, there is no need to divide the power to n parts. So the received signal is formed as follows:

$$f_a^{Rx}(\theta) \quad = \quad f_e(\theta)\sum_{i=1}^{n} a_i e^{j((i-1)kd\cos\theta)} \tag{C.7}$$

Now the power gain $g_a(\theta) = |f_a(\theta)|^2$ is:

$$g_a^{Rx}(\theta) \quad = \quad g_e(\theta)\left|\frac{\sin(nk\frac{d}{2}(\cos\theta - \cos\theta_0))}{\sin(k\frac{d}{2}(\cos\theta - \cos\theta_0))}\right|^2 \tag{C.8}$$

Similarly, the maximum array factor gain is achieved for $\theta = \theta_0$. We now assume $\theta_0 = \pi/2$ (broadside). Then the maximum gain is $g_a^{Rx}(\theta_0) = g_e n^2$. The HPBW for the receivers is obtained by solving the equation:

$$g_e\left|\frac{\sin(\frac{1}{2}n\pi\cos\theta)}{\sin(\frac{1}{2}\pi\cos\theta)}\right|^2 \quad = \quad \frac{g_e}{2}n^2 \tag{C.9}$$

The solution to (C.9) is the same as to (C.3). Hence ω does not distinguish between receiver and transmitter. But the minimum gain of the receiver is different because the total power gain $K(n)$ changes.

$$K(n) \quad = \quad \int_{-\pi}^{\pi} g_a^{Rx} d\theta \tag{C.10}$$

$$g_e n^2\omega(n) + G_{min}^{Rx}(\pi - \omega(n)) = K(n) \tag{C.11}$$

Thus the minimum gain of receiver's antenna has the value $G_{min}^{Rx} = n\rho$.

Appendix D

Proof of Theorem 16

Consider only the randomness of h_{x_0}. The conditional probability $\mathbb{P}(\mathcal{R} > \eta|\Phi^T, \Phi^R, h_x)$ is a constant for given configuration (Φ^T, Φ^R) and given value of h_x, for all $x \in \Phi^T \backslash x_o$. According to the definition of rate in (4.8), it follows:

$$\begin{aligned}
&\mathbb{P}(\mathcal{R} > \eta|\Phi^T, \Phi^R, h_x) \\
=&\mathbb{P}\left(h_{x_o} > \eta' \frac{\sum_{x\in\Phi^T\backslash x_o} P h_x G_x(\xi_x, \psi_x)\ell(|x|) + \mathcal{N}_0 W}{G_o(\xi_o, \psi_o)P}\right. \\
&\left.|\Phi^T, \Phi^R, h_x\right) \qquad \text{(D.1)} \\
=&\exp\left(-\eta' \frac{\sum_{x\in\Phi^T\backslash x_o} P h_x G_x(\xi_x, \psi_x)\ell(|x|) + \mathcal{N}_0 W}{G_o(\xi_o, \psi_o)P}\right) \qquad \text{(D.2)}
\end{aligned}$$

where $\eta' = \frac{2^{\frac{\eta}{W}}-1}{\ell(r)}$ and (D.3) comes from the fact that h_{x_0} is exponentially distributed with unit mean. The conditional rate coverage probability $P_s(\eta)$ can be written as follows:

$$\begin{aligned}
&P_s(\eta) = \mathbb{E}_{h_x}[\mathbb{P}(\mathcal{R} > \eta|\Phi^T, \Phi^R, h_x)] \\
=&\mathbb{E}_{h_x}\left[\exp\left(-\eta' \frac{\mathcal{N}_0 W}{P G_o(\xi_o, \psi_o)}\right) \prod_{x\in\Phi^T\backslash x_o} \exp\left(-\eta' \frac{G_x(\xi_x, \psi_x)}{G_o(\xi_o, \psi_o)} h_x \ell(|x|)\right)\right] \qquad \text{(D.3)} \\
=&\exp\left(-\eta' \frac{\mathcal{N}_0 W}{P G_o(\xi_o, \psi_o)}\right) \prod_{x\in\Phi^T\backslash x_o} \frac{G_o(\xi_o, \psi_o)}{\eta' G_x(\xi_x, \psi_x)\ell(|x|) + G_o(\xi_o, \psi_o)} \qquad \text{(D.4)}
\end{aligned}$$

We get (D.4) because the channels h_x, $x \in \Phi^T$ are supposed to be i.i.d.. Each follows an exponential distribution with unit mean. The b's moment of $P_s(\eta)$ is the expectation of $P_s(\eta)^b$ w.r.t. Φ^T and Φ^R:

$$M_b(\eta) = \mathbb{E}_{\Phi^T}\left[\mathbb{E}_{\Phi^R}\left[\left(\exp\left(-\eta'\frac{\mathcal{N}_0 W}{PG_o(\xi_o,\psi_o)}\right)\times \prod_{x\in\Phi^T\setminus x_o}\frac{G_o(\xi_o,\psi_o)}{\eta' G_x(\xi_x,\psi_x)\ell(|x|)+G_o(\xi_o,\psi_o)}\right)^b\right]\right] \tag{D.5}$$

$$= \mathcal{L}_N \times \mathbb{E}_{\Phi^T}\left[\prod_{x\in\Phi^T\setminus x_o}\mathbb{E}_{\xi_x}\left[\left(\frac{G_o(\xi_o,\psi_o)}{\eta' G_x(\xi_x,\psi_x)\ell(|x|)+G_o(\xi_o,\psi_o)}\right)^b\right]\right] \tag{D.6}$$

$$= \mathcal{L}_N \exp\left(-\lambda Q_b(\eta)\right) \tag{D.7}$$

where $\mathcal{L}_N = \exp\left(-b\eta'\frac{\mathcal{N}_0 W}{PG_o(\xi_o,\psi_o)}\right)$ and

$$Q_b(\eta) = \int_{\mathbb{R}^2}\left(1-\mathbb{E}_{\xi_x}\left[\left(\frac{G_o(\xi_o,\psi_o)}{\eta' G_x(\xi_x,\psi_x)\ell(|x|)+G_o(\xi_o,\psi_o)}\right)^b\right]\right)\mathrm{d}x \tag{D.8}$$

We get (D.6) because ψ_x and $|x|$ are deterministic values once Φ^R is fixed. The relative directions ξ_o and ψ_o within the typical pair are independent on Φ^T and Φ^R. The process Φ^R is a conditional random measure that depends both on Φ^T and $\{\xi_x\}$, $x \in \Phi^T$, where ξ_x for different $x \in \Phi^T$ are independent. So the expectation with respect to Φ^R in (D.5) can be replaced by the expectation with respect to ξ_x in (D.6). The equation (D.7) follows from the probability generation functional (PGFL) of a Poisson point process [24]. We then transform the integral part Q_b into polar form. Since $G_x(\xi_x,\psi_x) = 0$ when $-\pi < \psi_x < 0$, we get:

$$Q_b(\eta) = \int_0^\infty\int_0^\pi\left(1-\mathbb{E}_{\xi_x}\left[\left(\frac{G_o(\xi_o,\psi_o)}{\eta' G_x(\xi_x,\psi_x)\ell(v)+G_o(\xi_o,\psi_o)}\right)^b\right]\right)\mathrm{d}\psi_x v\mathrm{d}v \tag{D.9}$$

Remind that ξ_x is uniformly distributed in $[0, 2\pi]$. Given that $G_x(\xi_x,\psi_x) = 0$ when $\pi < \xi_x < 2\pi$, the integral Q_b has the following form:

$$Q_b(\eta) = \frac{1}{2\pi}\int_0^\infty\int_0^\pi\int_0^\pi\left(1-\left(1-\frac{\eta' G_x(\xi_x,\psi_x)\ell(v)}{\eta' G_x(\xi_x,\psi_x)\ell(v)+G_o(\xi_o,\psi_o)}\right)^b\right)v\mathrm{d}\xi_x\mathrm{d}\psi_x\mathrm{d}v \tag{D.10}$$

$$= \frac{1}{2\pi}\int_0^{\infty}\int_0^{\pi}\int_0^{\pi}\Big[1- \sum_{k=0}^{\infty}\binom{b}{n}\left(-\frac{\eta' G_x(\xi_x,\psi_x)\ell(v)}{\eta' G_x(\xi_x,\psi_x)\ell(v)+G_o(\xi_o,\psi_o)}\right)^n\Big] v\mathrm{d}\xi_x\mathrm{d}\psi_x\mathrm{d}v \tag{D.11}$$

where (D.11) comes from the binomial series.

$$Q_b(\eta) = \frac{1}{2\pi}\sum_{n=1}^{\infty}\binom{b}{n}(-1)^{n+1}\times \int_0^{\infty}\int_0^{\pi}\int_0^{\pi}\left(\frac{\eta' G_x(\xi_x,\psi_x)\ell(v)}{\eta' G_x(\xi_x,\psi_x)\ell(v)+G_o(\xi_o,\psi_o)}\right)^n v\mathrm{d}\xi_x\mathrm{d}\psi_x\mathrm{d}v \tag{D.12}$$

Let $u = v^{\alpha}$ and $\delta = 2/\alpha$. For $b \in \mathbb{C}$ we have :

$$Q_b(\eta) = \lim_{T\to\infty}\frac{\delta}{4\pi}\sum_{n=1}^{\infty}\binom{b}{n}(-1)^{n+1}\times \int_0^{T}\int_0^{\pi}\int_0^{\pi}\left(\frac{\eta' G_x(\xi_x,\psi_x)}{\eta' G_x(\xi_x,\psi_x)+G_o(\xi_o,\psi_o)u}\right)^n u^{\delta-1}\mathrm{d}\xi_x\mathrm{d}\psi_x\mathrm{d}u \tag{D.13}$$

By replacing u with $t = u/T$, we get:

$$Q_b(\eta) = \lim_{T\to\infty}\frac{T^{\delta}\delta}{4\pi}\sum_{n=1}^{\infty}\binom{b}{n}(-1)^{n+1}\times \int_0^{1}\int_0^{\pi}\int_0^{\pi}\left(\frac{\eta' G_x(\xi_x,\psi_x)}{\eta' G_x(\xi_x,\psi_x)+G_o(\xi_o,\psi_o)Tt}\right)^n r^{\delta-1}\mathrm{d}\xi_x\mathrm{d}\psi_x\mathrm{d}t \tag{D.14}$$

By adapting the definitions of $g_a^R(\psi_x,\theta_0^R)$ and $g_a^T(\xi_x,\theta_0^T)$, the gain G_x has three non-negative values G_1, G_2 and G_3 with probability p^2, $2p(1-p)$ and $(1-p)^2$. The notation Q_b can be then written as follows:

$$Q_b = \lim_{T\to\infty}\frac{T^{\delta}\delta\pi}{4}\sum_{n=1}^{\infty}\binom{b}{n}(-1)^{n+1}\int_0^{1}\left(\frac{p^2}{(1+\frac{G_o(\xi_o,\psi_o)tT}{G_1})^n}+ \frac{2(1-p)p}{(1+\frac{G_o(\xi_o,\psi_o)tT}{G_2})^n}+\frac{(1-p)^2}{(1+\frac{G_o(\xi_o,\psi_o)tT}{G_3})^n}\right)t^{\delta-1}\mathrm{d}t \tag{D.15}$$

The final expression in (4.12) is derived by replacing the integral parts into hypergeometric functions.

When there is misalignment, the additional misalignment of ξ_o or ψ_o doesn't impact the distributions of ξ_x nor ψ_x. Because ξ_x and ψ_x are all uniformly distributed with respect to independent transmitters at x. So the only factor that is impacted in (4.11) and (4.12) is G_o. We define $Q_b(G_o,\eta)$ as a function of G_o. It has the same expression as the right hand side of (4.12). According to the definition of G_o in (4.6)

and the definition of $g_a^R(\psi_o, \theta_0^R)$, $g_a^T(\xi_o, \theta_0^T)$, it is straightforward to give the PMF of G_o as follows:

$$G_o = \begin{cases} G_1 & p_{ma}^2 \\ G_2 & 2p_{ma}(p_{ef} - p_{ma}) \\ G_3 & (p_{ef} - p_{ma})^2 \\ 0 & else \end{cases} \tag{D.16}$$

Therefore when there is misalignment, the b's moment of $P_s(\eta)$ is the expectation of $P_s(\eta)^b$ with respect to Φ^T, Φ^R and also G_o. The expression (4.15) is obtained by calculating the expectation of formula (4.11) with respect to G_o.

Appendix E

Proof of Lemma 18

Receivers are uniformly distributed around their associated transmitters. The AoA ψ and AoD ξ are thus also uniformly distributed across in $[0, 2\pi)$. However, there exists only one unique beam pair (m', n') that can ensure $\xi \in [\theta^T_{m'} - \frac{\theta_u}{2}, \theta^T_{m'} + \frac{\theta_u}{2})$ and $\psi \in [\theta^R_{n'} - \frac{\theta_u}{2}, \theta^R_{n'} + \frac{\theta_u}{2})$, resulting in a uniform distribution of AoA and AoD in these two sectors. When $\omega \leq \theta_u$, the main lobe of the antennas can only cover the transmitter-receiver link if the beam pair (m', n') is chosen. The probability of covering the link is $\frac{\omega}{\theta_u}$ since the AoA/AoD is uniformly distributed in these sectors. If $\omega > \theta_u$, the main lobes at each transmitter and receiver side fully cover $2\lfloor \frac{\omega - \theta_u}{2\theta_u} \rfloor$ beam sectors of size θ_u. Therefore, the probability of the main lobes covering the transmitter-receiver link is 1 once m' and n' are among these fully covered sectors. There are two additional beam sectors that are only half-covered by the main lobe. Assuming that m' or n' are among these half-covered sectors, the AoD/AoA is uniformly distributed in beam sector m' or n'. Then the probability of the main lobe covering the transmitter-receiver link is $\frac{\mathrm{mod}(\frac{\omega - \theta_u}{2}, \theta_u)}{\theta_u}$.

Appendix F

Proof of Lemma 19

The joint PMF of $G^T_{m^*}$ and $G^R_{n^*}$ are calculated considering different optimal beam pairs, which leads to (5.16). The joint probability $\mathbb{P}[G^T_m = \nu, G^R_n = \kappa, l^* = (m,n)]$ can be expanded into $2^{2(N_b-1)}$ parts according to the joint distribution of $\{G^T_i\}_{i\neq m}$ and $\{G^R_j\}_{j\neq n}$:

$$\begin{aligned}
&\mathbb{P}[G^T_m = \nu, G^R_n = \kappa, l^* = (m,n)] \\
= &\sum_{\substack{(\nu_i,\kappa_j)\in\mathcal{G}^T\times\mathcal{G}^R \\ i\in[1:N_b]\setminus m,\, j\in[1:N_b]\setminus n}} \Big\{\mathbb{P}[l^* = (m,n)|G^T_m = \nu, G^R_n = \kappa, G^T_i = \nu_i, G^R_j = \kappa_j] \\
&\mathbb{P}[G^T_m = \nu, G^R_n = \kappa, G^T_i = \nu_i, G^R_j = \kappa_j]\Big\} \qquad \text{(F.1)}
\end{aligned}$$

Since the antenna gains G^T_i and G^R_j over different beam pairs are independent, the joint distribution of $\{G^T_i\}$ and $\{G^R_j\}$ can be expressed as follows:

$$\begin{aligned}
&\mathbb{P}[G^T_m = \nu, G^R_n = \kappa, \{G^T_i = \nu_i\}, \{G^R_j = \kappa_j\}] \\
&= \mathbb{P}[G^T_m = \nu]P[G^R_n = \kappa] \prod_{\substack{i\in[1:N_b]\setminus m \\ j\in[1:N_b]\setminus n}} \mathbb{P}[G^T_i = \nu_i]\mathbb{P}[G^R_j = \kappa_j] \qquad \text{(F.2)}
\end{aligned}$$

According to (5.11), the chosen beam pair is chosen by measuring the useful received power with different beam pairs. The conditional probability in (F.1) is the probability that the received signal gets the largest power over beam pair (m,n), which can be expressed as follows:

$$\begin{aligned}
&\mathbb{P}[l^* = (m,n)|G^T_m = \nu, G^R_n = \kappa, \{G^T_i = \nu_i\}, \{G^R_j = \kappa_j\}] \\
&= \mathbb{E}_h \prod_{\substack{\bar{m}\in[1:N_b],\bar{n}\in[1:N_b] \\ (\bar{m},\bar{n})\neq(m,n) \\ \nu_m=\nu,\kappa_n=\kappa}} \mathbb{P}[h\nu\kappa > h_{(\bar{m},\bar{n})}\nu_{\bar{m}}\kappa_{\bar{n}}|h] \qquad \text{(F.3)}
\end{aligned}$$

$$= \mathbb{E}_h \prod_{\substack{\bar{m}\in[1:N_b],\bar{n}\in[1:N_b] \\ (\bar{m},\bar{n})\neq(m,n) \\ \nu_m=\nu,\kappa_n=\kappa}} F\left(\frac{h\nu\kappa}{\nu_{\bar{m}}\kappa_{\bar{n}}}\right) \tag{F.4}$$

The CDF of gamma distribution is expressed as $F(x) = \frac{1}{\Gamma(M)}\gamma(M, Mx)$. In order to reduce the calculation complexity, the lower incomplete gamma function $\gamma(\cdot)$ can be approximated by $\gamma(n, x) = (n-1)!\left(1 - e^{-x}\sum_{k=0}^{n-1}\frac{x^k}{k!}\right)$ [74].

Appendix G

Proof of Theorem 20

Consider only the randomness of h_{x_0}. The conditional probability $\mathbb{P}(\mathcal{R} > \eta|\Phi^T, \Phi^R, h_x)$ is a constant for a given configuration (Φ^T, Φ^R) and a given value of h_x, for all $x \in \Phi^T \backslash x_o$. According to the definition of the rate in (5.18), we have:

$$\begin{aligned}
&\mathbb{P}(\mathcal{R} > \eta|\Phi^T, \Phi^R, h_{x_o}) \\
&= \mathbb{P}\left(h_{x_o} > (2^{\frac{\eta}{W}} - 1)\frac{\sum_{x\in\Phi^T\backslash x_o} Ph_xG_x\ell(|x|) + \mathcal{N}_0W}{G_oP\ell(r)}|\Phi^T, \Phi^R, h_x,\right) && \text{(G.1)} \\
&= 1 - \frac{1}{\Gamma(M)}\gamma(M, M\eta'\frac{\sum_{x\in\Phi^T} PG_xh_x\ell(|x|) + \mathcal{N}_0W}{PG_o}) && \text{(G.2)} \\
&\simeq 1 - (1 - e^{-\beta M\eta'\frac{\sum_{x\in\Phi^T} PG_xh_x\ell(|x|)+\mathcal{N}_0W}{PG_o}})^M && \text{(G.3)} \\
&= \sum_{m=1}^{M}\binom{M}{m}(-1)^{m+1}e^{-\frac{mM\beta\eta'\mathcal{N}_0W}{PG_o}}\prod_{x\in\Phi^T} e^{-m\beta M\eta'\frac{G_xh_x\ell(|x|)}{G_o}} && \text{(G.4)}
\end{aligned}$$

Where $\eta' = \frac{2^{\frac{\eta}{W}}-1}{\ell(r)}$ and $\gamma(\cdot)$ refers to the lower incomplete gamma function. The equation (G.2) comes from the fact that h_{x_o} is a gamma distributed variable. The approximation (G.3) is obtained by adapting the following tight inequality [75]:

$$(1 - e^{-\beta Mx})^M < \frac{1}{\Gamma(M)}\gamma(M, Mx) \tag{G.5}$$

The rate conditional coverage can be obtained by averaging the probability $\mathbb{P}(\mathcal{R} > \eta|\Phi^T, \Phi^R, h_{x_o})$ with respect to h_x, $x \in \Phi$. The coefficients $\{h_x\}_{x\in\Phi}$ are i.i.d. with Gamma distribution. Thus we have the following formulas:

$$\begin{aligned}
P_c(\eta) &= \sum_{m=1}^{M}\binom{M}{m}(-1)^{m+1}e^{-\frac{mM\beta\eta'\mathcal{N}_0W}{PG_o}}\prod_{x\in\Phi^T}\mathbb{E}_{h_x}\left[e^{-m\beta M\eta'\frac{G_x\ell(|x|)}{G_o}h_x}\right] && \text{(G.6)} \\
&= \sum_{m=1}^{M}\binom{M}{m}(-1)^{m+1}e^{-\frac{mM\beta\eta'\mathcal{N}_0W}{PG_o}}\prod_{x\in\Phi^T}\frac{1}{(1 + \frac{m\beta\eta'G_x\ell(|x|)}{G_o})^M} && \text{(G.7)}
\end{aligned}$$

The b's moment of $P_c(\eta)$ is the expectation of $P_c(\eta)^b$ w.r.t. Φ^T, Φ^R and the antenna gain G_o. By using the multinomial theorem[76], it can be expressed as follows:

$$M_b = \sum_{k_1+k_2+\ldots+k_M=b} \binom{b}{k_1 \ldots k_M} \times \mathbb{E} \prod_{m=1}^{M} \left(\binom{M}{m} (-1)^{m+1} e^{-\frac{mM\beta\eta'\mathcal{N}_0 W}{PG_o}} \prod_{x\in\Phi^T} \frac{1}{(1+\frac{m\beta\eta' G_x \ell(|x|)}{G_o})^M} \right)^{k_m} \tag{G.8}$$

$$= \sum_{k_1+k_2+\ldots+k_M=b} \binom{b}{k_1 \ldots k_M} \left(\prod_{m=1}^{M} \left(\binom{M}{m} (-1)^{m+1} \right)^{k_m} \right) \mathbb{E}_{G_o} \left[e^{-M\beta\eta'\frac{\mathcal{N}_0 W}{PG_o}\sum_{m=1}^{M} m k_m} \times \mathbb{E}_{\Phi^T} \prod_{x\in\Phi^T} \mathbb{E}_{\Phi^R} \prod_{m=1}^{M} (1+\frac{m\beta\eta' G_x \ell(|x|)}{G_o})^{-M k_m} \right] \tag{G.9}$$

The process Φ^R is a conditional random measure that depends both on Φ^T and $\{\xi_x\}$, $x \in \Phi^T$, where ξ_x for different $x \in \Phi^T$ are independent. So the expectation with respect to Φ^R in (G.9) can be replaced by the expectation with respect to ξ_x shown as follows:

$$\mathbb{E}_{\Phi^T} \left[\prod_{\Phi^T} \mathbb{E}_{\Phi^R} \left[\prod_{m=1}^{M} (1+\frac{m\beta\eta' G_x \ell(|x|)}{G_o})^{-M k_m} \right] \right] = \exp\left(-\lambda \int_{\mathbb{R}^2} 1 - \mathbb{E}_{\xi_x} \left[\prod_{m=1}^{M} (1+\frac{m\beta\eta' G_x \ell(|x|)}{G_o})^{-M k_m} \right] \mathrm{d}x \right) \tag{G.10}$$

The integral part in equation (G.10) follows from the probability generation functional (PGFL) of a Poisson point process [24]. We then denote this integral part as $Q(m, \eta', G_o)$ and transform it into polar form. Since ψ_x is uniformly distributed in $[0, 2\pi)$, we get:

$$Q(m, \eta', G_o) = \int_{\mathbb{R}^2} 1 - \mathbb{E}_{\xi_x} \left[\prod_{m=1}^{M} (1+\frac{m\beta\eta' G_x \ell(|x|)}{G_o})^{-M k_m} \right] \mathrm{d}x \tag{G.11}$$

$$= \int_0^\infty \int_{-\pi}^{\pi} 1 - \frac{1}{2\pi} \int_{-\pi}^{\pi} \prod_{m=1}^{M} (1+\frac{m\beta\eta' G_x \ell(|v|)}{G_o})^{-M k_m} \mathrm{d}\xi_x v \mathrm{d}\psi_x \mathrm{d}v \tag{G.12}$$

$$= \frac{1}{2\pi} \int_{-\pi}^{\pi} \int_{-\pi}^{\pi} \int_0^\infty \left(1 - \prod_{m=1}^{M} (1+\frac{m\beta\eta' G_x \ell(|v|)}{G_o})^{-M k_m} \right) v \mathrm{d}v \mathrm{d}\xi_x \mathrm{d}\psi_x \tag{G.13}$$

We then let $A(m, \eta', G_o, G_x)$ denote the following function:

$$A(m, \eta', G_o, G_x) = \int_0^\infty \left(1 - \prod_{m=1}^{M} (1+\frac{m\beta\eta' G_x \ell(|v|)}{G_o})^{-M k_m} \right) v \mathrm{d}v \tag{G.14}$$

Because the angles ξ_x and ψ_x are all uniformly distributed in $[0, 2\pi)$ and the antenna gain G_x is the product of $g^T(\xi_x, \theta_x^T)$ and $g^R(\psi_x, \theta_x^T)$, where θ_x^T and θ_x^R are also uniformly distributed, we get (5.29). Let $u = v^\alpha$ and $\delta = 2/\alpha$ we get:

$$A(m, \eta', G_o, G_x) = \lim_{T\to\infty} \delta/2 \int_0^T \left(1 - \prod_{m=1}^{M} (1 + \frac{m\beta\eta' G_x}{G_o u})^{-Mk_m}\right) u^{\delta-1} \mathrm{d}u \qquad \text{(G.15)}$$

By replacing u with $t = u/T$, we get:

$$A(m, \eta', G_o, G_x) = \lim_{T\to\infty} \frac{T^\delta \delta}{2} \int_0^1 \left(1 - \prod_{m=1}^{M} (1 + \frac{m\beta\eta' G_x}{G_o T t})^{-Mk_m}\right) t^{\delta-1} \mathrm{d}t \qquad \text{(G.16)}$$

Appendix H

Proof of Corollary 4 and 5

First Moment

According to (5.28) in Theorem 20, the first moment of the rate conditional coverage probability can be expressed as (5.31) when $b = 1$. The function $A(m, \eta', G_o, G_x)$ can be then expressed as follows:

$$A(m,\eta',G_o,G_x) = \lim_{T\to\infty} \frac{T^\delta \delta}{2} \int_0^1 \left(1 - (1 + \frac{m\beta\eta' G_x}{G_o T t})^{-M}\right) t^{\delta-1} \mathrm{d}t \tag{H.1}$$

$$= \lim_{T\to\infty} \frac{T^\delta \delta}{2} \int_0^1 \left(1 - (1 - \frac{1}{1 + \frac{G_o T t}{m\beta\eta' G_x}})^{M}\right) t^{\delta-1} \mathrm{d}t \tag{H.2}$$

By using the binomial theorem, it can be further expressed as:

$$A(m,\eta',G_o,G_x) = \lim_{T\to\infty} \frac{T^\delta \delta}{2} \sum_{n=1}^{M} \binom{M}{n} (-1)^{n+1} \int_0^1 \left(1 + \frac{G_o T t}{m\beta\eta' G_x}\right)^{-n} t^{\delta-1} \mathrm{d}t \tag{H.3}$$

The final (5.32) is derived by replacing the integral parts by hypergeometric functions [65].

Second Moment

When $b = 2$, the set $\{k_1, ..., k_M\}$ in (5.28) can either be $\{2, 0, ..., 0\}$ or $\{1, 1, 0, ..., 0\}$. According to (5.28), the second moment of the rate conditional coverage probability can be expressed as in (5.33), where Q_1 and Q_2 can be expressed as follows:

$$\begin{aligned} &Q_1(m,\eta',G_o) \\ =&\frac{1}{2\pi}[\omega^2 A_1(m,\eta',G_o,G^T_{max}G^R_{max}) + \omega(2\pi-\omega)A_1(m,\eta',G_o,G^T_{max}G^R_{min}) \\ &+\omega(2\pi-\omega)A_1(m,\eta',G_o,G^T_{min}G^R_{max}) + (2\pi-\omega)^2 A_1(m,G_o,G^T_{min}G^R_{min})] \end{aligned} \tag{H.4}$$

$$
\begin{aligned}
&Q_2(i,j,\eta',G_o) \\
=&\frac{1}{2\pi}[\omega^2 A_2(i,j,\eta',G_o,G^T_{max}G^R_{max})+\omega(2\pi-\omega)A_2(i,j,\eta',G_o,G^T_{max}G^R_{min}) \\
&+\omega(2\pi-\omega)A_2(i,j,\eta',G_o,G^T_{min}G^R_{max})+(2\pi-\omega)^2 A_2(i,j,G_o,G^T_{min}G^R_{min})]
\end{aligned} \tag{H.5}
$$

The functions $A_1(m,\eta',G_o,G_x)$ can be derived as follows:

$$
A_1(m,\eta',G_o,G_x)=\lim_{T\to\infty}\frac{T^\delta\delta}{2}\int_0^1\left(1-(1+\frac{m\beta\eta'G_x}{G_oTt})^{-2M}\right)t^{\delta-1}\mathrm{d}t \tag{H.6}
$$

Equation (5.34) is derived by using hypergeometric functions. The expression of $A_2(i,j,\eta',G_o,G_x)$ in (5.35) is derived by setting $k_i=1$, $k_j=1$ and $k_n=0$ for all $n\neq i$ and $n\neq j$.

Bibliography

[1] W. Jiang, B. Han, M. A. Habibi, and H. D. Schotten, "The road towards 6G: A comprehensive survey," *IEEE Open Journal of the Communications Society*, vol. 2, pp. 334–366, 2021.

[2] 3GPP, "Study on physical layer enhancements for NR ultra-reliable and low latency case (URLLC)," 3rd Generation Partnership Project (3GPP), Tech. Rep. 38.824, 2019, Version 16.0.

[3] L. Song, D. Niyato, Z. Han, and E. Hossain, *Wireless device-to-device communications and networks*. Cambridge University Press, 2015, ISBN: 1107063574.

[4] K. Venugopal, M. C. Valenti, and R. W. Heath, "Device-to-Device millimeter wave communications: Interference, coverage, rate, and finite topologies," *IEEE Transactions on Wireless Communications*, vol. 15, no. 9, pp. 6175–6188, 2016.

[5] N. Bahadori, N. Namvar, B. Kelley, and A. Homaifar, "Device-to-Device communications in the millimeter wave band: A novel distributed mechanism," in *2018 Wireless Telecommunications Symposium (WTS)*, IEEE, 2018, pp. 1–6.

[6] R. Wang, N. Deng, and H. Wei, "Towards a deep analysis of millimeter wave D2D underlaid cellular networks," *IEEE Transactions on Communications*, vol. 69, no. 10, pp. 6545–6560, 2021.

[7] E. Turgut and M. C. Gursoy, "Uplink performance analysis in d2d-enabled millimeter-wave cellular networks with clustered users," *IEEE Transactions on Wireless Communications*, vol. 18, no. 2, pp. 1085–1100, 2019. DOI: 10.1109/TWC.2018.2889755.

[8] R. Liu, G. Yu, J. Yuan, and G. Y. Li, "Resource management for millimeter-wave ultra-reliable and low-latency communications," *IEEE Trans. on Communications*, vol. 69, no. 2, pp. 1094–1108, 2020.

[9] D. Tse and P. Viswanath, *Fundamentals of wireless communication*. Cambridge university press, 2005.

[10] S. Kutty and D. Sen, "Beamforming for millimeter wave communications: An inclusive survey," *IEEE Communications Surveys & Tutorials*, vol. 18, no. 2, pp. 949–973, 2015.

[11] Y. Ni, S. Jin, W. Xu, Y. Wang, M. Matthaiou, and H. Zhu, "Beamforming and interference cancellation for D2D communication underlaying cellular networks," *IEEE Transactions on Communications*, vol. 64, no. 2, pp. 832–846, 2015.

[12] J. Mirza, G. Zheng, K.-K. Wong, and S. Saleem, "Joint beamforming and power optimization for D2D underlaying cellular networks," *IEEE Transactions on Vehicular Technology*, vol. 67, no. 9, pp. 8324–8335, 2018.

[13] H. Asplund, D. Astely, P. von Butovitsch, *et al.*, *Advanced Antenna Systems for 5G Network Deployments: Bridging the Gap Between Theory and Practice*. Academic Press, 2020.

[14] P. Popovski, Č. Stefanović, J. J. Nielsen, *et al.*, "Wireless access in ultra-reliable low-latency communication (urllc)," *IEEE Transactions on Communications*, vol. 67, no. 8, pp. 5783–5801, 2019.

[15] F. Baccelli and B. Błaszczyszyn, *Stochastic geometry and wireless networks*. Now Publishers Inc, 2009, vol. 1.

[16] M. Haenggi, *Stochastic geometry for wireless networks*. Cambridge University Press, 2012.

[17] A. H. Sakr and E. Hossain, "Cognitive and energy harvesting-based D2D communication in cellular networks: Stochastic geometry modeling and analysis," *IEEE Trans. on Communications*, vol. 63, no. 5, pp. 1867–1880, 2015.

[18] M. Haenggi, "The meta distribution of the SIR in Poisson bipolar and cellular networks," *IEEE Transactions on Wireless Communications*, vol. 15, no. 4, pp. 2577–2589, 2015.

[19] F. P. Kelly, *Reversibility and stochastic networks*. Cambridge University Press, 2011.

[20] A. Sankararaman and F. Baccelli, "Spatial birth–death wireless networks," *IEEE Transactions on Information Theory*, vol. 63, no. 6, pp. 3964–3982, 2017.

[21] C. Preston, "Spatial birth and death processes," *Advances in applied probability*, vol. 7, no. 3, pp. 465–466, 1975.

[22] J. D. Kraus and R. J. Marhefka, *Antenna for all applications*. McGraw-Hill, 2002.

[23] D. Stoyan, W. S. Kendall, S. N. Chiu, and J. Mecke, *Stochastic geometry and its applications*. John Wiley & Sons, 2013.

[24] F. Baccelli, B. Błaszczyszyn, and M. Karray, *Random measures, point processes, and stochastic geometry*, 2020.

[25] X. Yu, Q. Cui, Y. Wang, N. Li, X. Tao, and M. Valkama, "Stochastic geometry based analysis for heterogeneous networks: A perspective on meta distribution," *Science China Information Sciences*, vol. 63, pp. 1–21, 2020.

[26] J. Gil-Pelaez, "Note on the inversion theorem," *Biometrika*, vol. 38, no. 3-4, pp. 481–482, 1951.

[27] M. Haenggi, "Efficient calculation of meta distributions and the performance of user percentiles," *IEEE Wireless Communications Letters*, vol. 7, no. 6, pp. 982–985, 2018.

[28] S. Guruacharya and E. Hossain, "Approximation of meta distribution and its moments for poisson cellular networks," *IEEE Wireless Communications Letters*, vol. 7, no. 6, pp. 1074–1077, 2018.

[29] S. Wang and M. Di Renzo, "On the meta distribution in spatially correlated non-poisson cellular networks," *EURASIP Journal on Wireless Communications and Networking*, vol. 2019, no. 1, pp. 1–11, 2019.

[30] S. Karlin and J. McGregor, "The classification of birth and death processes," *Transactions of the American Mathematical Society*, vol. 86, no. 2, pp. 366–400, 1957.

[31] J. Møller, "On the rate of convergence of spatial birth-and-death processes," *Annals of the Institute of Statistical Mathematics*, vol. 41, no. 3, pp. 565–581, 1989.

[32] A. Asadi, Q. Wang, and V. Mancuso, "A survey on device-to-device communication in cellular networks," *IEEE Communications Surveys & Tutorials*, vol. 16, no. 4, pp. 1801–1819, 2014.

[33] F. Jameel, Z. Hamid, F. Jabeen, S. Zeadally, and M. A. Javed, "A survey of device-to-device communications: Research issues and challenges," *IEEE Communications Surveys & Tutorials*, vol. 20, no. 3, pp. 2133–2168, 2018.

[34] X. Lin, J. G. Andrews, A. Ghosh, and R. Ratasuk, "An overview of 3GPP device-to-device proximity services," *IEEE Communications Magazine*, vol. 52, no. 4, pp. 40–48, 2014.

[35] S. Chen, J. Hu, Y. Shi, *et al.*, "Vehicle-to-everything (V2X) services supported by lte-based systems and 5g," *IEEE Communications Standards Magazine*, vol. 1, no. 2, pp. 70–76, 2017.

[36] M. H. C. Garcia, A. Molina-Galan, M. Boban, *et al.*, "A tutorial on 5G NR V2X communications," *IEEE Communications Surveys & Tutorials*, vol. 23, no. 3, pp. 1972–2026, 2021.

[37] 3GPP, "User equipment (UE) radio transmission and reception," 3rd Generation Partnership Project (3GPP), Tech. Rep. 38.101, 2022, Version 17.

[38] S. Sun, G. R. MacCartney, and T. S. Rappaport, "Millimeter-wave distance-dependent large-scale propagation measurements and path loss models for outdoor and indoor 5g systems," in *2016 10th European Conference on Antennas and Propagation (EuCAP)*, IEEE, 2016, pp. 1–5.

[39] Y. Xing and T. S. Rappaport, "Millimeter wave and terahertz urban microcell propagation measurements and models," *IEEE Communications Letters*, vol. 25, no. 12, pp. 3755–3759, 2021.

[40] R. W. Heath, N. González-Prelcic, S. Rangan, W. Roh, and A. M. Sayeed, "An overview of signal processing techniques for millimeter wave mimo systems," *IEEE Journal of Selected Topics in Signal Processing*, vol. 10, no. 3, pp. 436–453, 2016.

[41] I. Ahmed, H. Khammari, A. Shahid, *et al.*, "A survey on hybrid beamforming techniques in 5g: Architecture and system model perspectives," *IEEE Communications Surveys & Tutorials*, vol. 20, no. 4, pp. 3060–3097, 2018.

[42] O. El Ayach, S. Rajagopal, S. Abu-Surra, Z. Pi, and R. W. Heath, "Spatially sparse precoding in millimeter wave mimo systems," *IEEE transactions on wireless communications*, vol. 13, no. 3, pp. 1499–1513, 2014.

[43] H. J. Visser, *Array and phased array antenna basics*. John Wiley & Sons, 2006.

[44] M. Wang, C. Zhang, X. Chen, and S. Tang, "Performance analysis of millimeter wave wireless power transfer with imperfect beam alignment," *IEEE Trans. on Vehicular Technology*, vol. 70, no. 3, pp. 2605–2618, 2021.

[45] M. S. Zia, D. M. Blough, and M. A. Weitnauer, "Coverage in millimeter-wave networks with SNR-dependent beam alignment errors," in *2020 IEEE 91st Vehicular Technology Conference (VTC2020-Spring)*, IEEE, 2020, pp. 1–5.

[46] N. Deng and M. Haenggi, "A fine-grained analysis of millimeter-wave device-to-device networks," *IEEE Transactions on Communications*, vol. 65, no. 11, pp. 4940–4954, 2017.

[47] M. Salehi, A. Mohammadi, and M. Haenggi, "Analysis of D2D underlaid cellular networks: SIR meta distribution and mean local delay," *IEEE Transactions on Communications*, vol. 65, no. 7, pp. 2904–2916, 2017.

[48] X. Lu, M. Salehi, M. Haenggi, E. Hossain, and H. Jiang, "Stochastic geometry analysis of spatial-temporal performance in wireless networks: A tutorial," *IEEE Communications Surveys Tutorials*, pp. 1–1, 2021.

[49] P. D. Mankar, M. A. Abd-Elmagid, and H. S. Dhillon, "Spatial distribution of the mean peak age of information in wireless networks," *IEEE Transactions on Wireless Communications*, vol. 20, no. 7, pp. 4465–4479, 2021.

[50] R. Rao and A. Ephremides, "On the stability of interacting queues in a multiple-access system," *IEEE Transactions on Information Theory*, vol. 34, no. 5, pp. 918–930, 1988.

[51] N. L. Johnson, S. Kotz, and N. Balakrishnan, *Continuous Univariate Distributions, Volume 1, 2nd Edition*. John Wiley and Sons, 1994, ISBN: 978-0-471-58495-7.

[52] A. AlAmmouri, J. G. Andrews, and F. Baccelli, *Stability and metastability of traffic dynamics in uplink random access networks*, 2020. arXiv: 1906.04683 [cs.IT].

[53] M. Cheng, J.-B. Wang, Y. Wu, X.-G. Xia, K.-K. Wong, and M. Lin, "Coverage analysis for millimeter wave cellular networks with imperfect beam alignment," *IEEE Transactions on Vehicular Technology*, vol. 67, no. 9, pp. 8302–8314, 2018.

[54] J. Wildman, P. H. J. Nardelli, M. Latva-aho, and S. Weber, "On the joint impact of beamwidth and orientation error on throughput in directional wireless poisson networks," *IEEE Transactions on Wireless Communications*, vol. 13, no. 12, pp. 7072–7085, 2014.

[55] N. Bahadori, N. Namvar, B. Kelley, and A. Homaifar, "Device-to-Device communications in millimeter wave band: Impact of beam alignment error," in *2019 Wireless Telecommunications Symposium (WTS)*, IEEE, 2019, pp. 1–6.

[56] N. Deng and M. Haenggi, "The energy and rate meta distributions in wirelessly powered d2d networks," *IEEE Journal on Selected Areas in Communications*, vol. 37, no. 2, pp. 269–282, 2018.

[57] M. Rebato, J. Park, P. Popovski, E. De Carvalho, and M. Zorzi, "Stochastic geometric coverage analysis in mmwave cellular networks with realistic channel and antenna radiation models," *IEEE Trans. on Communications*, vol. 67, no. 5, pp. 3736–3752, 2019.

[58] A. Goldsmith, *Wireless communications*. Cambridge university press, 2005.

[59] S. Hur, T. Kim, D. J. Love, J. V. Krogmeier, T. A. Thomas, and A. Ghosh, "Millimeter wave beamforming for wireless backhaul and access in small cell networks," *IEEE Trans. on communications*, vol. 61, no. 10, pp. 4391–4403, 2013.

[60] C. Liu, M. Li, S. V. Hanly, I. B. Collings, and P. Whiting, "Millimeter wave beam alignment: Large deviations analysis and design insights," *IEEE journal on selected areas in communications*, vol. 35, no. 7, pp. 1619–1631, 2017.

[61] Y. Li, J. G. Andrews, F. Baccelli, T. D. Novlan, and C. J. Zhang, "Design and analysis of initial access in millimeter wave cellular networks," *IEEE Trans. on Wireless Communications*, vol. 16, no. 10, pp. 6409–6425, 2017.

[62] S. S. Kalamkar, F. Baccelli, F. M. Abinader, A. S. M. Fani, and L. G. U. Garcia, "Beam management in 5G: A stochastic geometry analysis," *IEEE Trans. on Wireless Communications*, vol. 21, no. 4, pp. 2275–2290, 2021.

[63] A. Alkhateeb, Y.-H. Nam, M. S. Rahman, J. Zhang, and R. W. Heath, "Initial beam association in millimeter wave cellular systems: Analysis and design insights," *IEEE Trans. on Wireless Communications*, vol. 16, no. 5, pp. 2807–2821, 2017.

[64] C. A. Balanis, *Antenna theory: analysis and design*. John wiley & sons, 2015.

[65] I. S. Gradshteyn and I. M. Ryzhik, *Table of integrals, series, and products*. Academic press, 2014.

[66] 3GPP, "Study on New Radio (NR) access technology," 3rd Generation Partnership Project (3GPP), Tech. Rep. 38.912, 2017, Version 14.0.

[67] M. Giordani, M. Polese, A. Roy, D. Castor, and M. Zorzi, "A tutorial on beam management for 3GPP NR at mmwave frequencies," *IEEE Communications Surveys & Tutorials*, vol. 21, no. 1, pp. 173–196, 2018.

[68] T.-K. Le, U. Salim, and F. Kaltenberger, "An overview of physical layer design for Ultra-Reliable Low-Latency Communications in 3GPP releases 15, 16, and 17," *IEEE Access*, vol. 9, pp. 433–444, 2020.

[69] V. Va, J. Choi, and R. W. Heath, "The impact of beamwidth on temporal channel variation in vehicular channels and its implications," *IEEE Transactions on Vehicular Technology*, vol. 66, no. 6, pp. 5014–5029, 2016.

[70] N. S. Ramesan and F. Baccelli, "How wireless queues benefit from motion: An analysis of the continuum between zero and infinite mobility," *IEEE Transactions on Wireless Communications*, vol. 20, no. 12, pp. 8149–8162, 2021.

[71] X. Tang, X. Xu, and M. Haenggi, "Meta distribution of the SIR in moving networks," *IEEE Transactions on Communications*, vol. 68, no. 6, pp. 3614–3626, 2020.

[72] M. Miyazawa, "Rate conservation laws: A survey," *Queueing Systems*, vol. 15, pp. 1–58, 1994.

[73] F. Baccelli and P. Bremaud, *Elements of Queueing Theory: Palm Martingale Calculus and Stochastic Recurrences*. Springer, 2003.

[74] H. S. Wall, *Analytic theory of continued fractions*. Courier Dover Publications, 2018.

[75] H. Alzer, "On some inequalities for the incomplete gamma function," *Mathematics of Computation*, vol. 66, no. 218, pp. 771–778, 1997.

[76] E. A. Bender and S. G. Williamson, *Foundations of combinatorics with applications*. Courier Corporation, 2013.

ECOLE
DOCTORALE

Titre : Évaluation des performances et allocation des ressources dans les réseaux terminal à terminal à ondes millimétriques avec formation de faisceaux

Mots clés : communications terminal à terminal, formation de faisceaux, géométrie stochastique, URLLC, désalignement

Résumé : La communication de terminal à terminal (D2D) est une technologie clé pour les futurs réseaux sans fil. Elle permet aux appareils de communiquer directement, sans avoir besoin d'une infrastructure cellulaire. La communication en ondes millimétriques (mmWave) utilise des fréquences radio de haute fréquence. Elle offre des bandes passantes très larges, ce qui permet des transmissions rapides et fiables. Cependant, les fréquences mmWave ont une atténuation élevée, ce qui nécessite que les appareils aient plusieurs antennes et utilisent la formation de faisceau. La formation de faisceau nécessite un alignement précis des faisceaux, et les erreurs d'alignement peuvent entraîner une dégradation des performances de transmission. Dans notre étude, nous nous concentrons sur l'analyse théorique des performances de la communication D2D en mmW dans le contexte des communications très fiables et à très faible latence, dites URLLC. Nous utilisons la géométrie stochastique et la théorie des files d'attente pour évaluer les variations spatiales et temporelles des performances selon deux perspectives différentes. D'une part, nous examinons les propriétés moyennes instantanées du réseau aléatoire, et d'autre part, nous étudions les conditions de stabilité d'un réseau dynamique avec des demandes de service aléatoires. Pour les propriétés dynamiques, nous nous concentrons sur la condition de stabilité du réseau D2D en introduisant des réseaux d'antennes directionnelles pour les utilisateurs D2D. Le réseau est modélisé sur la base d'un processus spatial de naissance et de mort. Pour les propriétés instantanées, nous nous soucions principalement de la méta-distribution comme une métrique qui tient compte de la distribution spatiale de la probabilité de couverture. Nous dérivons une expression de la méta-distribution du débit effectif comme une garantie de latence statistique pour les communications URLLC, en considérant à la fois les coûts d'apprentissage et le désalignement pour un réseau D2D avec formation de faisceaux. Enfin, nous proposons des méthodes pour choisir le nombre optimal d'antennes et pour allouer des ressources pour la formation des faisceaux.

Title : Performance evaluation and resource allocation in millimeter waves device-to-device networks with beamforming

Keywords : D2D communications, beamforming, stochastic geometry, URLLC, misalignement

Abstract : Device-to-Device (D2D) communication is a key technology for future wireless networks, allowing devices to communicate directly without relying on a cellular infrastructure. Millimeter wave (mmWave) communication utilizes high-frequency radio, providing very large bandwidths for fast and reliable D2D transmissions. However, mmWave frequencies have high attenuation, requiring devices to have multiple antennas and perform beamforming. The success of beamforming requires beam training. The beam misalignment can impact the performance of the network. To address these challenges, our study focuses on the theoretical analysis of the performance of mmWave D2D communications within the context of Ultra-Reliable Low Latency Communications (URLLC). We use stochastic geometry and queuing theory to evaluate both spatial and temporal variations in performance from two different perspectives: the instantaneous average properties of the random network and the global stability properties of a dynamic network with random service requests. For the dynamic properties, we focus on the stability condition of D2D network by introducing directional antennas arrays for the D2D users. The network is modeled based on a spatial birth-death process. For the instantaneous properties, we mainly care about the meta-distribution of the network, which is a metric that accounts for the spatial distribution of coverage probability. We derive the meta-distribution of the effective rate as a statistical latency guarantee for URLLC communications, by considering both the training overhead and misalignment for a D2D network with beamforming. At last, we propose methods to choose the optimal number of antennas and to allocate resource for beam training.

Institut Polytechnique de Paris
91120 Palaiseau, France